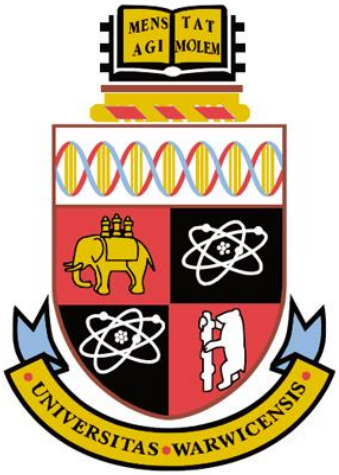

Terahertz Communications at the Nanoscale

by

Zhichao Rong

Thesis

Submitted to the University of Warwick

for the degree of

Doctor of Philosophy

School of Engineering

October 2017

Contents

List of Figures

List of Tables

Acknowledgements

I would like to express my deepest gratitude to my supervisors, Dr Mark S. Leeson and Dr Matthew D. Higgins for giving me the great opportunity to work under their guidance, and for their continual support and patience during my Ph.D. study. I would like to particularly thank Dr Mark S. Leeson, for his trust and encouragement during my tough times. I am also thankful to him for helping me to steadily progress in the successful completion of this thesis.

I would also like to thank the panel members of the School of Engineering at the University of Warwick throughout my Ph.D. study, their insightful comments and suggestions have helped me to achieve solid research objectives towards this thesis.

My sincere thanks go to all the former and current members of Communication Networks Laboratory and Communication Systems Laboratory, especially Dr Yi Lu, for their support and the friendship established since the beginning. I also express my thanks to my friends, Richard, Bessie, Ryan, and Guannan for their companion and comfort during my hard time in the UK and also Kaka, James, Jesse, Robin, Zhechi, for their remotely care and support.

Above all, I wish to express my gratitude to my family, especially my parents, my wife, my sister and Suning, whose endless love, trust, support, and encouragement gave me the confidence and motivated me to continue.

Declaration

This thesis is submitted in partial fulfilment for the degree of Doctor of Philosophy under the regulations set out by the Graduate School at the University of Warwick. I herewith declare that this thesis contains my own research performed under the supervision of Dr Mark S. Leeson and Dr Matthew D. Higgins, without the assistance of third parties, unless stated otherwise. No part of this thesis was previously published or submitted for a degree at any other universities.

List of Publications

Published:

- Z. Rong, M. S. Leeson, M. D. Higgins, "Relay-assisted nanoscale communication in the THz band", *Micro & Nano Letters.* 12, 373–376, 2017.
- Z. Rong, M. S. Leeson, M. D. Higgins, Y. Lu, "Simultaneous wireless information and power transfer for AF relaying nanonetworks in the Terahertz Band", *Nano Communication Networks.* 14, 1–8, 2017.
- Z. Rong, M. S. Leeson, M. D. Higgins, Y. Lu, "Nano-Rectenna Powered Body-Centric Nanonetworks in the Terahertz Band", *Healthcare Technology Letters.* 2018. (In Press)

To be submitted:

- Z. Rong, M. S. Leeson, M. D. Higgins, Y. Lu, "Rate-Energy Trade-off Analysis of SWIPT for Nanonetworks",

Abstract

Nanotechnology reduces the sizes of devices to a scale of hundreds of nanometres. The integration of such nano-sized entities equipped with fundamental functional units enables the development of nanosensors. These offer the prospect of the development of new tools to discover novel events at the nanoscale. To enlarge the capabilities of individual nanosensors, a number of them can be interconnected to establish nanosensor based networks, namely nanonetworks. These will empower new applications in many fields, such as healthcare, military, and environmental monitoring, and so on. The miniatured size of nanoantennas and their properties lead to communications within nanonetworks within the Terahertz (THz) band (0.1 – 10 THz). The objective of this thesis is to improve the system performance of graphene-enabled EM nanonetworks in this THz Band. Firstly, the channel model for THz waves is studied, and the path loss, channel noise and channel capacity for the THz band are analysed. Secondly, a novel three-terminal relaying protocol for nanonetworks is proposed and its performance is numerically investigated. Both amplify-and-forward (AF) and decode-and-forward (DF) relaying modes are studied. Thirdly, a new nano-rectenna based energy harvesting system is developed to power nanosensors within nanonetworks. The results obtained indicate the great potential and advantage of nano-rectennas. Fourthly, a simultaneous wireless information and power transfer system for nanonetworks in the THz Band is proposed. An amplify and forward (AF) relaying nanonetwork in this band is investigated. The performance of the system based on both time-switching and power-splitting protocols is numerically analysed.

Nomenclature

3D	Three-dimensional
AF	Amplify-and-Forward
BER	Bit Error Rate
BPSK	Binary Phase Shift Keying
CDF	Cumulative density function
CNTs	Carbon Nanotubes
CR	Cognitive Radio
CSI	Channel State Information
DBPSK	Differential Binary Phase Shift Keying
DF	Decode-and Forward
ECC	Error Correction Code
EM	Electromagnetic
FSPL	Free-Space spreading (Path) Loss
GNRs	Graphene Nanoribbons
HITRAN	High-resolution TRANsmission
ICT	Information and Communication Technology
IoT	Internet of Things
IoNT	Internet of Nano-things
IoBNT	Internet of Bio-Nano Things
IoMNT	Internet of Multimedia Nano Things
ISI	Inter-Symbol Interference
LOS	Light-of-Sight
MC	Molecular Communications
MEMS	Micro-electromechanical systems
MI	Mutual Information
MIM	Metal-Insulator-Metal
MIMO	Multiple-Input Multiple-Output
MRC	Maximal Ratio Combining

NEMS	Nano-Electro-Mechanical Systems
NLOS	Non-Light-of-Sight
OFDM	Orthogonal Frequency Division Multiplexing
OOK	On-off Keying
P2P	Point to point
R_X	Receiver
SNR	Signal-to-Noise Ratio
SINR	Signal-to-Interference-Noise Ratio
SIMO	Single-Input-Multiple-Output
SISO	Single-Input-Single-Output
SPP	Surface Plasmon Polariton
SSD	Self-Switching Device
SWIPT	Simultaneous Wireless Information and Power Transfer
THz	Terahertz
T_X	Transmitter
WNSN	Wireless Nanosensor Network

List of Symbols

A_{eff}	The effective area of the antenna
A^u	The amplitude of signal transmitted from u to the destination
B	Bandwidth
c	The speed of light in a vacuum
C	Channel capacity
C_{cap}	The capacitance of the ultra-nanocapacitor
C_D	The capacitance of the diode
C_t	The total Capacitance per unit length of Graphene
d	Transmission distance between T_X and R_X
d_0	Distance between S to R, R to D and S to D.
E_h	The harvested energy
f	Frequency
f_0	Centre frequency of the antenna
f_c	The cut-off frequency of a rectenna
f_i	Centre frequency of the i_{th} sub-band
$g_{S,R}, g_{S,D}, g_{R,D}$	The channel coefficients in the SR, SD and RD link
$H(f)$	The transfer function of the channel frequency response
$H_{abs}(f)$	The transfer function of molecular absorption loss
$H_{spread}(f)$	The transfer function of spreading loss
h, h_c	The impulse response of the THz channel
h_a^{Tx}, h_a^{Rx}	The impulse response of transmission and reception antennas
$h_{S,R}, h_{R,D}, h_{S,D}$	The impulse response of the SR, SD and RD channel
I	Current

J	Total number of sub channel allocated for information transfer
$k(f)$	The absorption coefficient
k_B	The Boltzmann constant
$k^q(f)$	The absorption coefficient of the gas q in the air
K	Total number of sub channel allocated for energy harvesting
l_p	The resonance length of plasmonic antennas
L	Total Path Loss
L_{spread}	The free space spreading loss
L_{abs}	The molecular absorption loss
$L_{S,R},\ L_{S,D}, L_{R,D}$	The path loss in the SR, SD and RD link
$\mathcal{L}_t$	The total inductance per unit length of Graphene
m	Number of parity check bits of Hamming codes
M	Total number of sub channels
n_D, n_R	The noise terms at the relay and destination.
$n_{S,R}, n_{S,D}, n_{R,D}$	The noise terms within the SR, SD and RD paths.
$n'_{R,D}$	The equivalent noise terms within RD path.
$N(f)$	The total noise power spectral density
$\mathcal{N}_I$	The overall interference
N_0	The total noise power
N_{0D}, N_{0R}	The total noise power at the relay, destination
N_I	The variance of interference
$N_{S,D}, N_{S,R}, N_{R,D}$	The total noise power within SD, SR and RD link
$p(x_1)$	The probability of sending a pulse
p_0	The reference pressure
p_i, p_j, p_k	The transmit power allocated to the $i_{th}, j_{th}, and\ k_{th}$ sub channel
p_{sys}	The system pressure
p_{out}	The outage probability
P	The total transmitted power

P_{in}	The input EM wave power
P_{out}	The output power of the rectenna
P_r	The transmitted power of the relay
P_s	The transmitted power from source
Q^q	Number of molecules per unit volume (molecules m^{-3}) of gas q
R	The information rate
R_a	The resistance of the antenna
R_d	The rectifier differential resistance
R_G	Equivalent resistance of the nano-generators
R_{rec}	The rectenna's equivalent resistance
R_{th}	The threshold transmission rate
$\mathfrak{R}_I$	The instantaneous throughput
$\mathfrak{R}_{DL}$	The delay-limited throughput
S	The power spectral density for the propagated signal
$S(f_i)$	The power spectral density for the propagated signal in the i_{th} sub-band
T	System Temperature
T_0	Reference temperature
T_{mol}	The molecular noise temperature
T_{STP}	The standard temperature at standard pressure
U	Number of nanosensors
v_{SPP}	The propagation speed of SPP wave along Graphene plasmonic antenna
V_{ac}	The input AC voltage
V_{bias}	The bias voltage
V_D	The DC voltage generated from the rectenna
V_G	The power source of the nano-generator
V_{opt}	The AC output voltage of the antenna
x_S	Signal from source
y_{AF}	The amplified signal at the relay node

$y_D, y_{R,D}$	The received signal from the relay at the destination
$y_R, y_{S,R}$	The received signal at the relay node
$y_{S,D}$	The received signal at the destination from source
y	The combined signal at the destination
y_i	The signal for i_{th} path
α	The time-switching fraction
$\alpha_1^{AF}, \alpha_2^{AF}$	The parameters the maximal ratio combining for AF relaying
α_1^{DF} α_2^{DF}	The parameters the maximal ratio combining for DF relaying
α_i	The parameters the maximal ratio combining for i_{th} path
β	The amplifying gain
γ	The MRC output SINR at the destination
γ_0	Cut-off value of water-filling power allocation scheme
$\gamma_{S,D}$,$\gamma_{S,R,D}$	The SINR at the destination from SD and SRD link.
γ_{th}	The threshold SNR
Γ	The confinement factor
Δf	Bandwidth of the sub-band
ε	The emissivity of the medium
$\bar{\mathcal{E}}$	The average BER
$\mathcal{E}_0$	The threshold BER
$\mathcal{E}_j$	BER of the j_{th} channel
η	The energy conversion efficiency factor
η_a	The absorption efficiency of the antenna
η_c	The coupling efficiency of the rectenna
ζ	The ratio of the symbol duration to the pulse duration
κ_i , κ_j	The information rate of the i_{th}, j_{th} channel
λ	Wavelength of EM wave in free-space
λ_0	Wavelength of the incident wave in antenna
λ_{SPP}	Wavelength of SPP wave in free-space

μ_1, μ_2, μ_3	Largrange multipliers
ξ	The ratio of the second to the first derivative of the current
ρ	The power fraction factor
σ^q	The absorption cross-section ($\mathrm{m}^2\ (\mathrm{molecule})^{-1}$) of gas q
σ_R^2, σ_D^2	The variances of the overall AWGN in sub channels
ς	The energy conversion factor
τ	The transmittance of the medium
φ_i	The phase shift of the signal

Chapter 1
Introduction

1.1 Background

Nanotechnology is expected to advance the continuing technological revolution driven by engineering and science in many fields. It is enabling the development of devices on a scale ranging from one to a few hundred nanometres [1]. Novel devices at the nanoscale provide an opportunity to equip any environment or set of objects with a plethora of molecular-scale sensors. The most fundamental nano-sized devices are called nano-machines. These are devices fabricated at a size of around 1 to 100 nanometres enabling very simple tasks being conducted at the nanoscale. The concept of nanotechnology was first expounded by Richard Feynman in his famous speech in 1959 [2], where he described a vision of how humans would manufacture more and more tiny and powerful miniaturized devices. Later, nanotechnology was defined as the processing of materials at the scale of one molecule or one atom, i.e. separation, consolidation and deformation [3]. The definition was then explored further by Drexler during the 1980s in [4], where he suggested that nano-machines could self-replicate with the aid of computer control rather than being operated by humans. After that, nanotechnology advancements began to accelerate from the early 2000s so that

now, it has provided new methods for engineers to monitor and control events at a scale of one atom or one molecule.

Nanosensors are one of the most promising applications of nanotechnology [5], [6]. A nanosensor of the order of a few nanometres offers the advantages of the unique properties of nanomaterials to discover novel events at the nanoscale. For instance, nanosensors can detect very tiny variations i.e. one in a billion and the existence of abnormalities in human tissues such as a virus or a harmful bacterium [7]. Nevertheless, individual nanosensors can only perform the very simple tasks and the detection ranges covered by individual nanosensors are limited to their near environment. Coordination and information sharing among these nanosensors can expand their abilities and operating range, which leads towards the development of upcoming nanosensor networks [8], creating new applications of nanotechnology in the medical, environmental and military fields [9]. The formation of nanosensor networks will massively enlarge the cover ranges and conduct information exchange and processing among each nanosensor.

It is quite challenging to develop nanosensors that are capable of executing activities autonomously. According to [9], the size of a nanosensor integrated with different functional components is around 10 to 100 μm^2, which is able to perform fundamental activities such as local actuation and basic computation. As is reported in [1], three different approaches for developing nanosensors have been proposed, i.e. the top-down approach, the bottom-up approach, and the bio-hybrid approach. For example, with the aid of latest manufacturing techniques, such as the 45 nm lithographic manufacturing process [10] and the micro-contact printing process [11], nanosensors can be developed by downscaling existing micro-scale devices. In [12],

Nano-Electro-Mechanical Systems (NEMS) have been developed using the top-down approach. The bottom-up approach is a molecular manufacturing process which builds nanosensors using individual molecules [13]. Recently, molecular nanosensor devices such as molecular switches and shuttles have been designed based on interlocked of molecules [14]. The bio-hybrid method is based on the application of biological nanosensors, which are those biological architectures found in cells and other living organisms [15]. These existing biological nanosensor devices equipped with fundamental functions such as sensing, actuating and data storing can be used as the basic nano-bio-components to develop more complex nanosensors. For instance, a biological nanomotor has been developed using the bio-hybrid approach [16]. Therefore, those nanosensors manufactured using the top-down approach are namely physical nanosensors, otherwise, the other two approaches are used to develop biomolecular nanosensor.

1.2 Communication Paradigms among Nanosensors

Despite the substantial progress in nanotechnology in the last decade, the application potential of a single nanosensor is quite limited [9], as the size of such nanosensors is estimated to be in the range of approximately hundreds of nanometres to tens of micrometres. Communication among nanosensors is capable of expanding their abilities to accomplish considerably more complex tasks by means of information sharing and cooperation [9], [17]. It has led to increasing interest in the interconnection of such nanoscale devices with established macroscale networks to form nanosensor networks. The resulting nanonetworks will boost the range of applications of nanotechnology bringing new opportunities in a range of diverse fields in Information

and Communication Technology (ICT) [1]. However, a nanonetwork is not a mere downscaled version of a conventional network; on the contrary, classical communication paradigms need to undergo a profound revision before being applied to this new scenario. To date, there are several nanoscale communication schemes have been proposed, e.g. acoustic, molecular and electromagnetic [1], [9], [18]–[20]. Amongst them, molecular communication and electromagnetic communication are the two most promising paradigms.

In the following paragraphs, the two communication alternatives are briefly reviewed.

1.2.1 Molecular Communications

In molecular communication (MC), transceivers decode and encode information using molecules during the process of transmission and reception [1]. Due to the operation domain and size, it is easy to integrate molecular transceivers and other functional components into nanosensor devices. In the operation of MC, transceivers will release specific molecules as the reaction to some other molecules when receiving system orders or executing some processing tasks [1]. These molecular nano devices can be developed either from reengineering biological organisms such as cells and bacteria or from artificial nano components [21], [22]. The biological cells can be mapped as typical nanosensor devices as seen in Figure 1-1 according to [23]. They comprise the following:

- **Processing & Control Unit:** genetic instructions are stored in the DNA molecules of the cell, where DNA molecules encode and generate protein molecules acting as control and processing instructions, respectively.

- **Memory Unit: a** variety of molecules in the cell's cytoplasm are synthesized following DNA instructions, therefore, the cytoplasm of the cell acts as the memory unit of the biological nanosensor device.
- **Power Unit:** there are many kinds of molecules and structures in the cell can generate energy, i.e. triphosphate, chloroplasts, and mitochondrion.
- **Sensing and Actuation Unit:** there exist various chemical receptors inside the cell, which can identify external molecules and response to the ambient stimuli i.e. light and pressure. Hence, they are acting as sensors. The sensing signal then makes the moving components such as flagella, pili, and cilia do the corresponding reactions.
- **Communication Unit:** the gap junction of the cell can exchange information with outside which acts as a communication unit.

Moreover, there are three different propagation schemes in MC [22], [24], i.e. walkway based MC [25], flow-based MC [22] and diffusion-based MC [26]. In the first of these, molecules propagate through pre-designed pathways, where molecular motors are used to transport them. While in flow-based MC, molecules propagate via a fluidic medium, in which the propagation paths are constrained. Diffusion-based MC relies on the autonomous diffusion of molecules, i.e. molecules diffuse spontaneously in the medium.

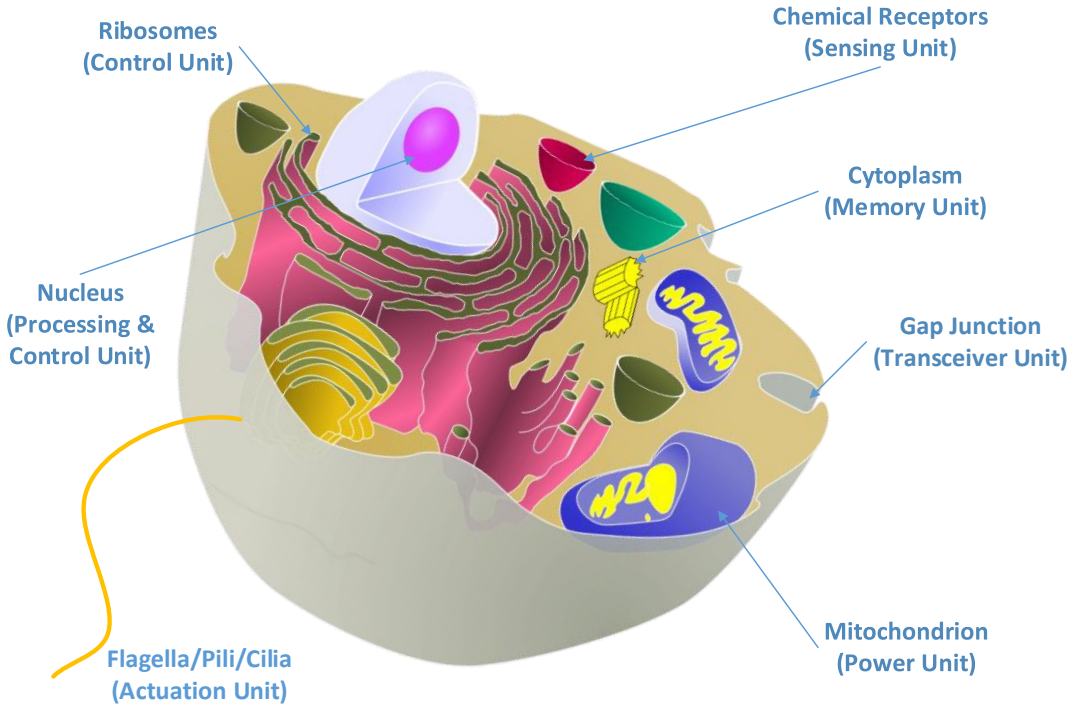

Figure 1-1 The architecture of a biological cell as a nanosensor device (adapted from [23]).

1.2.2 Electromagnetic Communications

The realization of nanonetworks via communications among nanosensors by means of electromagnetic (EM) waves is another promising paradigm. EM communications can provide much higher data transmission speeds than MC.

Recent advanced nanomaterials such as graphene have opened the door to the manufacturing of vital components for nanosensors [27]–[30]. Therefore, some novel communication paradigms have been developed recently, e.g. graphene-based wireless communication [9] [31]. Based on [9], a conceptual architecture of an EM-

based nanosensor device is shown in Figure 1-2. The EM-based nanosensors are similar to but not just downscaled versions of the micro and macro sensors reported in [32]. They are developed based on the top-down approach with the use of graphene and carbon nanotubes (CNTs) [33], [34]. The outstanding physical and electrical properties of graphene and its derivatives i.e. CNTs and graphene nanoribbons (GNRs) have enabled the development of many kinds of nanoscale components [35]. As seen in Figure 1-2, the EM-based nanosensor devices are the integration of several nano-components with specific functions.

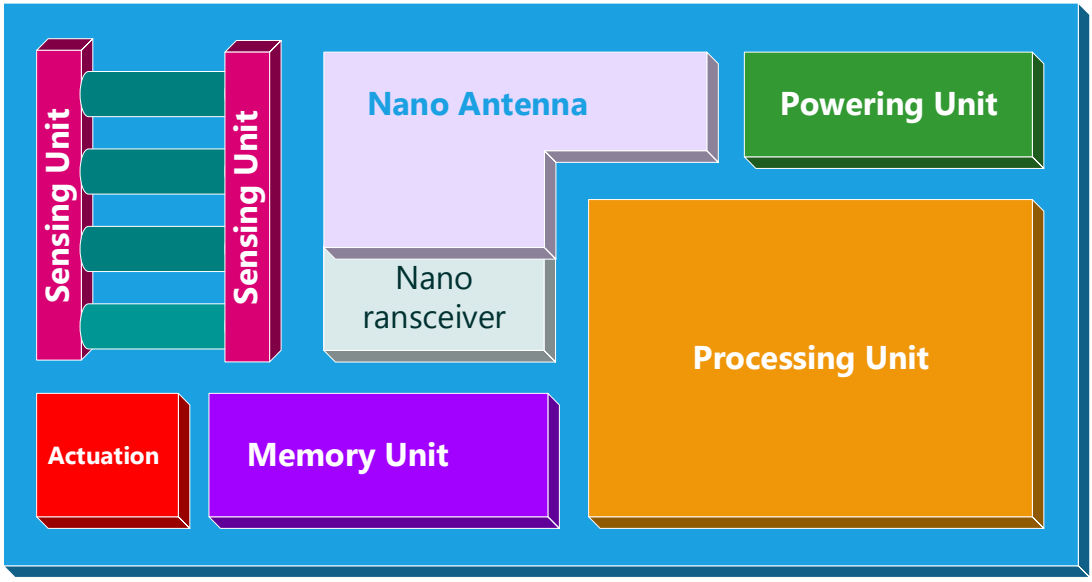

Figure 1-2 A conceptual architecture of an EM-based nanosensor device

- **Processing Unit**: nano processors can be fabricated using FET transistors based on CNTs and GNRs. Recently, thin GNR enabled transistors have been developed according to [36]. These transistors are just 10×1 carbon atoms which can operate at very high frequency. Therefore, nano processors can be developed by integrating a number of these GNR-enabled FET transistors.
- **Memory Unit**: nano memories are being made possible by novel manufacturing techniques using of nanomaterials. The nano memory reported in [37] allows

single bit storage using just a single atom. Otherwise, the conceptual magnetic atomic nano memories can also store a single bit using a single atom [38], [39]. Therefore, the total storage capacity of a nano memory is determined by its size. These conceptual nano memories are very promising in developing the nanosensor device.

- **Power Unit**: again, due to the size constraints of nano components, new kinds of nano-sized batteries are required for nanosensors [40], [41]. In addition, wireless energy harvesting techniques at the nanoscale are also encouraging candidates. For instance, an ultrasound-driven energy harvesting system which adopts piezoelectric technology in nanowires has been proposed to convert vibration into electricity [42]–[47]. Alternatively, energy harvesting relying on nano-rectennas is a very promising approach to power nanosensors, which absorbs EM waves and then converts to electricity [48]. The harvested energy is stored in nano batteries and then supplied to the system dynamically. The energy harvesting rate and the energy storage capacity in the nano battery are determined by the dimensions of the corresponding nano components.
- **Sensing & Actuation Unit:** Nanosensors made from GNRs, CNTs and other nanomaterials have been developed [5], [49]–[52]. Despite their tiny sizes, these sensors are capable of detecting the presence and concentration of chemical compounds; to monitor and measure the physical properties of objects at nanoscale, and to identify the presence of virus, bacteria or illness on cells. Their small sizes and unique properties equip nanosensors with more accurate sensing capabilities and higher efficiencies. Moreover, nanosensors are able to interact

with ambient via nano actuators and some CNTs based nano-actuators have been designed [6].

- **Communication Unit**: communications among nanosensors are facilitated by the realization of nano-sized antennas and transceivers. Limited by the extremely small size of nano-components, the length of a nanoantenna should be constrained within several micrometres. However, there are doubts concerning the feasibility of scaling down current metallic antennas, mainly because the resonant frequency would be extremely high [1], [53]. For the expected size of nanosensor devices, the frequency radiated by their antennas would be in the optical range, resulting in a very large channel attenuation that might render wireless communication at the nanoscale infeasible. In order to overcome this limitation, graphene-based miniaturized antennas [27], [31], [54]–[57] have been investigated, enabling the implementation of wireless communications among nanosensors. Graphene presents very good conditions for the propagation of Surface Plasmon Polariton (SPP) waves which allow graphene-based antennas with a few μm to resonate in the terahertz (THz) band (0.1 -10 THz), at a frequency up to two orders of magnitude lower than a metallic antenna of the same size [29], [57]. Received signals at the nanoantennas will then be processed through nano transceivers. As the envisioned operating frequencies of nanoantennas are in the THz band (shown in Figure 1-3), nano transceivers should consequently resonate at those frequencies. Recently, graphene-based nano transceivers have been proposed in [29], which opens the door to wireless EM communications among nanosensors in the THz band.

The research of this thesis focuses on EM communication of nanonetworks in the THz band.

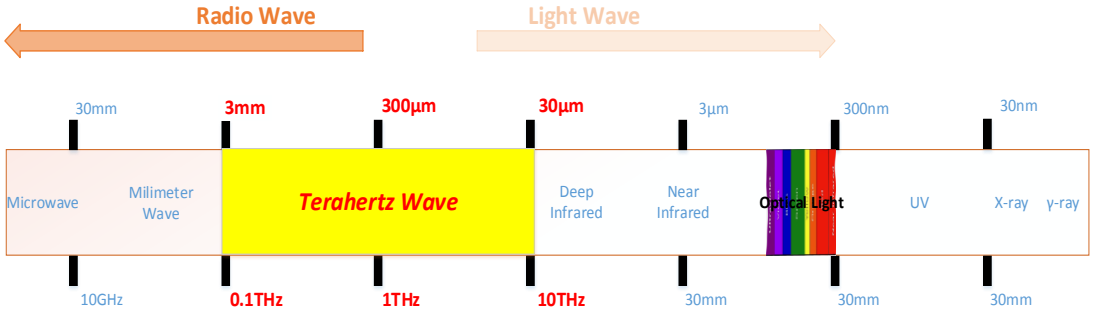

Figure 1-3 THz Band (0.1-10 THz) in the EM spectrum.

1.3 Architecture of Nanonetworks and Applications

As mentioned above, the term nanonetwork refers to the interconnection of a quantity of nanosensors by the means of new communication schemes. The unique properties of nanosensors and nanonetworks enable many types of applications in various areas and different scenarios.

1.3.1 Internet of Nano-things

Recent advancements in the Internet of Things (IoT) have attracted increasing attention from researchers [58]. In the IoT, a larger number of objects and sensors can interact and establish widespread networks. Meanwhile, at the nanoscale dimension, the development of nanotechnology enables the interconnection of nanosensors embedded in various of objects to form the Internet of Nano-things (IoNT) [17], [35]. In an IoNT system, a number of nanosensors equipped with fundamental computing and communication abilities can be distributed in the environment for data processing

and exchange in the monitoring system. The application of the IoNT will be extensive in prediction, especially in healthcare, military and environmental applications [59]. For example, in Figure 1-4 an interconnected office is illustrated, nanosensors are embedded in every individual object and enable all objects to be connected online permanently. The users can thus access and monitor all their items.

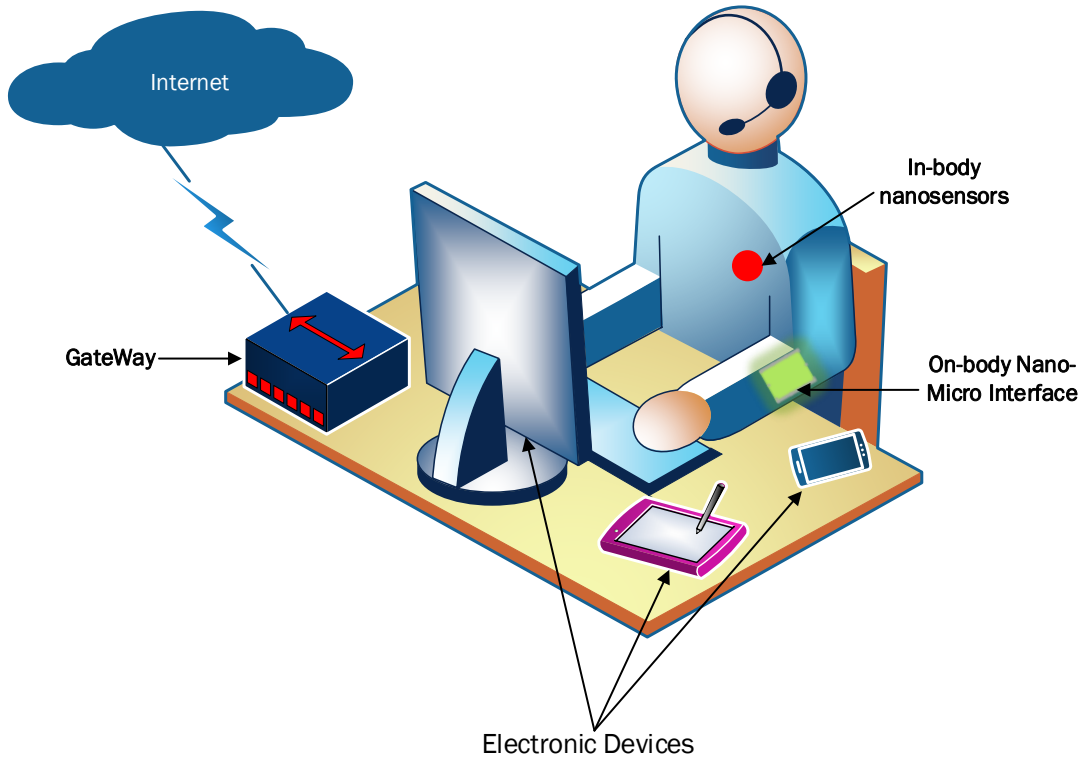

Figure 1-4 The Conceptual Architecture of the Internet of Nano Things

Likewise, an evolved edition of the IoNT has been proposed recently, namely the Internet of Bio-Nano Things (IoBNT) [23]. As seen in Figure 1-5, biology and nanotechnology have been combined in an IoBNT system, where intra-body nanosensors are based on biological nanodevices and the bio-cyber interface connects the intra MC nanonetwork with the outside internet. Furthermore, the Internet of

Multimedia Nano Things (IoMNT) [60] is another advancement of the IoNT, which integrates nanosensors with some multimedia units such as nano cameras and nano phones.

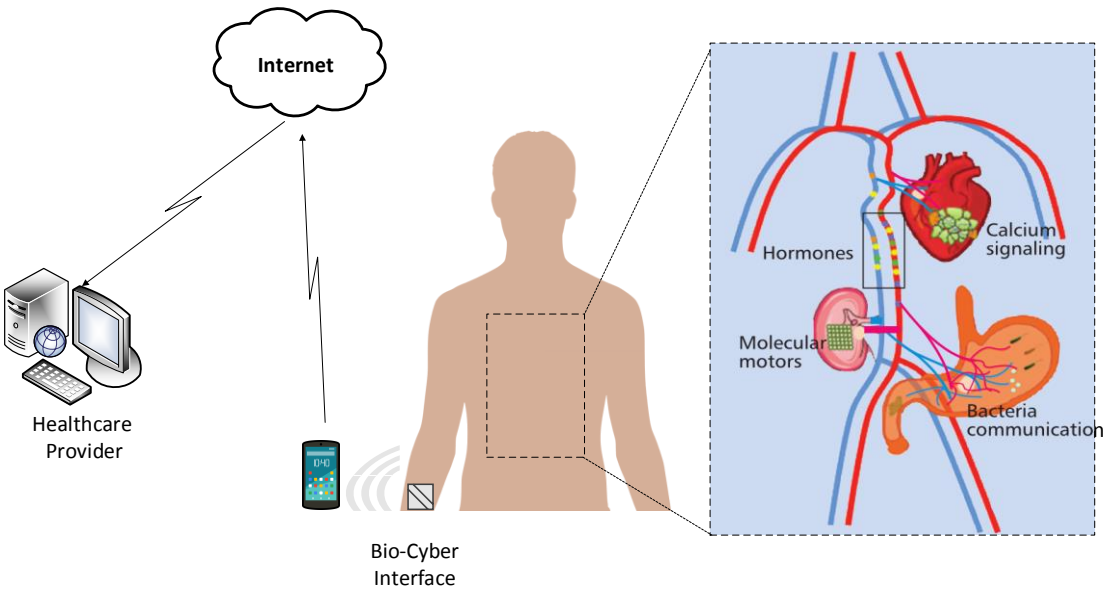

Figure 1-5 The Conceptual Architecture of the Internet of Bio-Nano Things [23].

1.3.2 Biomedical Applications

One of the most encouraging applications of nanonetworks is in the realm of biomedical systems and healthcare. By taking advantage of the small size of nanosensors, nanonetworks can address many limitations that exist in the traditional medical systems. Biomedical nanonetworks can extensively facilitate health monitoring, drug delivery, and other biomedical solutions [1]. For instance, nanosensors may be distributed inside and outside human body to monitor the concentrations of various chemicals such as sodium and glucose [61]. Moreover, the distribution of many nanosensors around the body forms a Wireless Body Area Nanonetwork (shown Figure 1-6), in which the nanosensors collect a patient's relevant

health data. A portable or wearable medical device such as a smart watch acts as the wireless nano-micro interface between the nanosensors and a micro gateway such as a smartphone or a medical device. The gateway obtains all the health data and forwards them to the healthcare centre via the internet.

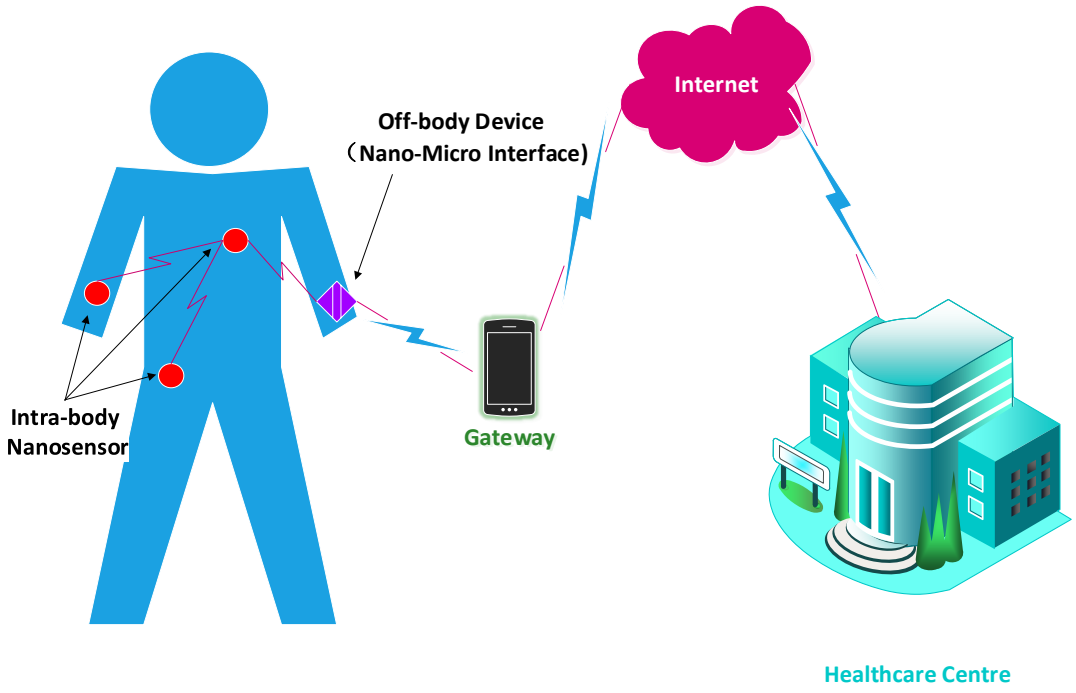

Figure 1-6 Wireless Nanonetworks for Healthcare Monitoring

1.3.3 Environmental Monitoring

Variations of environmental conditions can be better investigated through the detection of composition and concentration of chemical substances released by plants [62]. Figure 1-7 illustrates the application of nanonetworks in plant monitoring [63]. In the system, a large number of nanosensors are distributed pervasively on the leaves of the plants, where they catch the chemical substances released by the plants. The raw data collected by the nanosensors are forwarded to the nearest nano-micro interface device which then sends them to the micro gateway. Environmentalists can therefore

access the data through the internet remotely. In addition, the communication between nanosensors and nano-micro interfaces is based on an adaptable THz channel, where the transmission frequency can be selected dynamically to enhance the performance of the network throughputs.

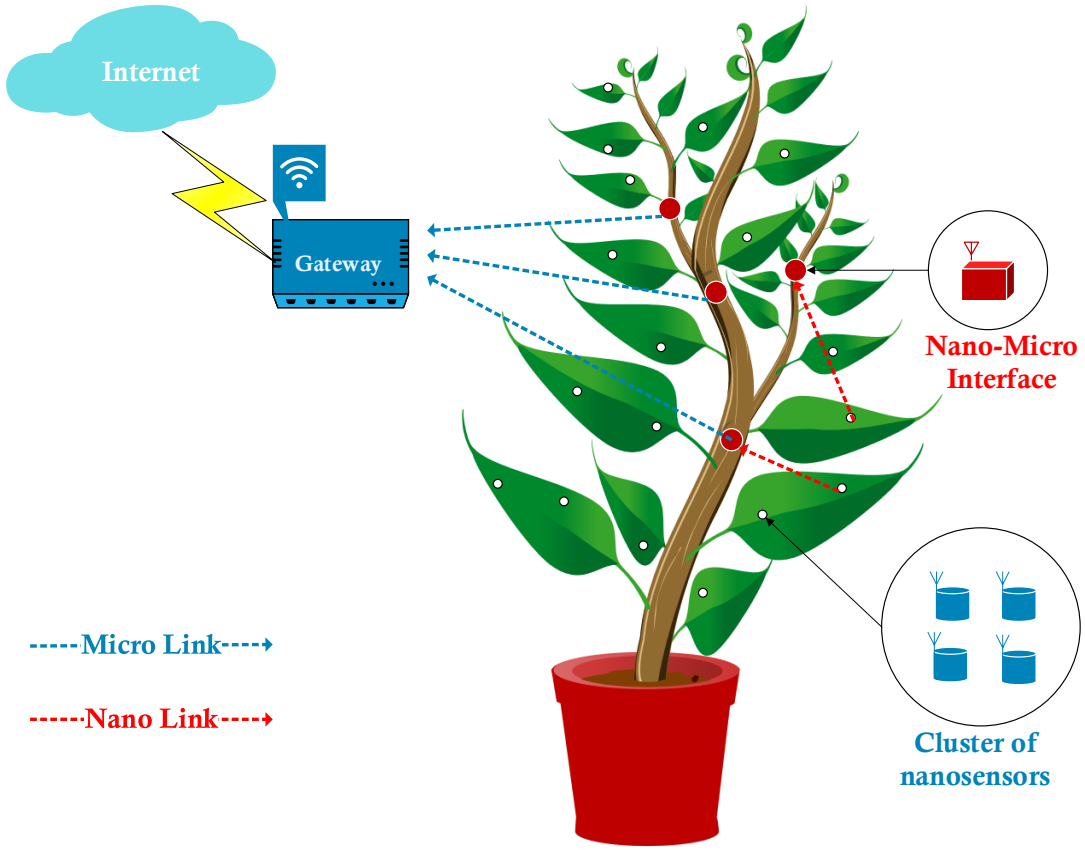

Figure 1-7 Structure of a nanonetwork as the application of plant monitoring [63].

Although EM nanonetworks are envisioned to be applied widely in many new scenarios and to provide unprecedented benefits to daily life, there are inevitable challenges in their implementation.

1.4 Challenges in THz Nanonetworks Analysis

The miniature size, as well as the very high radiation frequency of nanosensors, imposes many difficulties on the feasibility of THz communication nanonetworks. There are many challenges in realizing such a novel networking scheme along with a new communication paradigm which will require new solutions and reengineering some well-established concepts in traditional communication and network theory. The challenges range from the development of new nanoscale antennas to the description of the THz channel in which the nanoscale antennas will operate and the design of specific communication mechanisms for nanosensors including channel coding, data modulation and so on. Moreover, the extremely small size of nanodevices imposes substantial challenges on the implementation of the power unit.

1.5 Motivations

The development of nanoscale communications in the THz band is not an intentional choice but the very tiny size of nanosensors and the specific characteristics of graphene-based nanoantennas determine their communications in this band. Recently, research on THz communications in nanonetworks has been more and more prosperous. On the one hand, the very small size of nanodevices enables unprecedented and advanced applications of nanotechnology in many fields. On the other, realizing nanonetworks in the THz band is still a big challenge. The promising prospect of nanonetworks motivates further investigations in this area to overcome all the aforementioned challenges and to facilitate the reliability and performance in every aspect of nanonetworks.

Due to the high frequency and the presence of molecular absorption, an EM wave suffers fierce path loss in the THz band. Moreover, the frequency-selective channel introduces molecular absorption noise which is non-white. As a result of these, the transmission ranges and performance within nanonetworks are very limited. Motivated by these limitations, new communication protocols are required, such as the configuration of nanoscale relaying channels to form cooperative communications among nanosensors (presented in Chapter 3).

Moreover, energy consumption is another big concern for nanonetworks, again due to the very small size, the energy storage capacity in a nano battery is quite limited, which in consequence limits the capability of the communication units. To overcome this bottleneck and liberate the potential of nanonetworks, novel system powering and energy management solutions are needed. Motivated by this, some novel energy harvesting schemes have been proposed, amongst them, the nano-rectenna based energy harvesting system is a very promising approach (presented in Chapter 4).

1.6 Objectives

The main objective of this thesis is to improve the system performance of graphene-enabled EM nanonetworks in the THz Band (0.1-10 THz). The starting point is the description of THz channel and the evaluation of the channel capacity and system performance. Based on the channel model, a three-terminal relaying protocol for nanonetworks is investigated to enhance the transmission distance and performance. In addition, a wireless energy harvesting system is developed to study the energy bottleneck of the nanonetworks. Moreover, a wireless information and power transfer scheme for nanonetworks is proposed to provide another solution to self-powering nanosensors in nanonetworks.

Details of the methods developed within each topic to address the objective are given in the following section.

1.7 Thesis Contributions

It is believed that significant contributions have been made to research in Terahertz Communications and Nanoscale Communications. Firstly, based on the channel model developed in [64], a three-terminal relaying system on the THz band is established for the first time. In contrast to the original channel model, which considers the molecular absorption as thermal loss, in the proposed relaying model the energy loss from molecular absorption is considered as a re-radiation signal and follows a Rayleigh distribution. Another contribution of the thesis is to develop an effective energy harvesting model for nanosensor networks based on Nano-rectennas. With the concern of energy and size constraints within nanosensors, the Nano-rectenna systems enable powering nanosensors wirelessly and offer better performance than existing systems. Further to that, Nano-rectennas share the same signal which conveys only information in other systems. By jointly designing information transfer and energy harvesting in the same system, the EM wave is split. The resulting system is the third contribution of the thesis, in which the power-splitting and time-switching protocols are firstly applied in the THz channel. The THz SWIPT system provides a promising solution to powering nanosensors within nanonetworks. Moreover, the novel channel-splitting protocol proposed in the thesis is another contribution, the new SWIPT protocol is proposed with the consideration of the unique peculiarities of the THz band,

in which an energy and information rate trade-off is optimally achieved. Furthermore, an adaptive power allocation scheme is utilised in the new system.

1.8 Thesis Outline

The structure of the thesis is presented as follows:

Chapter 2: Terahertz Communication Channel Model for Nanonetworks.

In this chapter, the THz channel model for nanonetworks is studied. A review of the related works on THz channel modelling is provided. The characterization of the propagation channel is given. The most significant factor that impact the THz communication i.e. molecular absorption is described. The contribution in this chapter is:

- A literature review on recent research on the THz band and nanoscale communications from the perspectives of different operation scenarios with the corresponding applications.
- The path loss and noise calculation models are presented, the channel capacity of the channel is derived.

Chapter 3: Relay-Assisted Nanoscale Communication in the Terahertz Band.

In this chapter, a three-terminal relaying protocol for THz band communication at the nanoscale is investigated. The performance of the protocol is measured regarding the bit error rate (BER) output. The details for this chapter are:

- For the first time, a possible configuration for a nanoscale THz relaying scheme is introduced.

- Two relaying protocols namely Amplify-and-Forward (AF) and Decode-and Forward (DF) are studied. Maximal Ratio Combining (MRC) method is used to combine the signals at the destination.
- The benefits of the two relaying protocols regarding to the predicted BER of the proposed scheme is derived.

Chapter 4: Energy Harvesting for Body-Centric Nanonetworks in the THz Band Based on Nano-Rectennas

Here, a novel energy harvesting system for nanonetworks with application in healthcare is proposed. The details of the chapter are:

- A novel nano-rectenna based energy harvesting system is proposed for body-centric nanonetworks in the THz band. As a result, a wireless powered body-centric nanonetwork is also proposed.
- Nano-rectennas based on CNTs, graphene and other materials are considered.
- The output power generated by the nano-rectenna is calculated and compared with the power required for nanosensors to communicate in the THz band.
- Performance is measured and compared with the existed piezoelectric-based nano-generator regarding the output power and voltage etc.

Chapter 5: Simultaneous Wireless Information and Power Transfer for AF Relaying Nanonetworks in the Terahertz Band.

In this chapter, simultaneous wireless information and power transfer (SWIPT) nanonetworks in the THz Band is proposed. The details of this chapter are:

- For the first time, the SWIPT system being applied in the nanoscale communication in the THz band.
- AF relaying protocol is applied in the system.

- Two energy and information distribution protocols namely time-switching and power-splitting are investigated in the chapter.
- The optimal time switching fraction and power splitting ratio that achieve the maximal throughput at the destination are derived including both the instantaneous and the time-delayed throughputs.

Chapter 6: Energy Trade off Analysis of SWIPT System in the THz Band.

In this chapter, the power splitting protocol for a SWIPT system in the THz band is proposed. In particular:

- Different power allocation schemes are analyzed in the chapter, i.e. water-filling, equal power and adaptive power allocation.
- The rate-energy trade-off analysis is given in the chapter.

Chapter 7: Conclusions and Future Research. To conclude, a summary of this thesis with an overview of the future research topics in this area is presented.

Chapter 2
Terahertz Communication Channel Model for Nanonetworks

In spite of the considerable strides made in research on nanotechnology, communication among nanodevices is still a significant technical obstacle. Mature schemes in conventional communications are not suitable for nanonetworks without profound modifications. Limitations exist in size, energy consumption and complexity of current transceivers designed for radio frequency and optical communications meaning that the feasibility of downscaled nano-sized devices for electromagnetic communication (EM) at the nanoscale is doubtful [65]. Motivated by those limitations, new materials need to be developed for novel devices of much reduced size. The most impressive and promising material is Graphene, which is just one-atom-thick [34]. Along with its derivatives such as GNRs and CNTs, the unique properties discovered in graphene have opened a door to the development of nanodevices, i.e. nanoantennas, nanosensors, nano transceivers and nano batteries [66]. Therefore, the frequency band of operation for graphene-based nanonetworks is determined by EM radiation properties of this pioneer material and its derivatives. Previous work suggests that the THz Band (0.1-10.0 THz) is a promising operating frequency range for EM communications among nanoscale transceivers. In this chapter, an EM propagation model for wireless communication among nano-transceivers in the THz band is presented.

2.1 Introduction

As the EM wave propagates through the medium from the transmitter (Tx) towards the receiver (Rx), its characteristics vary. Many factors can result in these changes such as the composition of the medium, the distribution and concentration of the constituents, the distance and the existence of obstacles between Tx and Rx, the frequency of the transmitted EM wave and so forth. The term channel model refers to a model which is able to predict the behaviour of a propagation channel with respect to the transmitted signal [67]. The major tasks in assembling a channel model are to calculate path loss and noise, as well as scattering loss and multipath fading. The profile of the received signal at Rx can therefore be predicted based on the given channel model. Traditional channel models usually focus on aspects including path loss, multipath fading, diffraction, and shadowing [68], [69] but in the THz band, different subjects have to be considered in the channel such as molecular absorption. Therefore, new a channel model for wireless communication among nanodevices in the THz band needs to be developed.

The rest of the chapter is organized as follows: Section 2.2 reviews the properties of graphene and the graphene based nanoantennas. Section 2.3 reviews the related research in recent years on THz channel modelling. In Section 2.4, the THz channel model is presented and the channel capacity is analysed. Finally, in section 2.5, the conclusion of the chapter is given.

2.2 Graphene-based Nanoantenna

The development of nanosized antennas for nano transceivers will be the first mission to deploy the EM communication among nanodevices. The reduction in size of antennas made from traditional materials (i.e. metals) to the level of several nanometres would imply operation at extremely high frequencies, up to hundreds of THz [27]. The unique properties of Graphene have enabled the implementation of EM communication among nanodevices. One of the most important properties is that of tuneable conductivity. It enables the propagation of SPP waves on Graphene [70], [71]. According to [72], [73], the conductivity of Graphene can be modelled based on the Kubo formula. In [73], the authors analytically proved that the conductivity determines the wave vector of the SPP waves and, thus, determines the propagation properties of these waves. In turn, the conductivity of Graphene is determined by its structure and Fermi energy. Therefore, by means of doping or electrostatic bias the SPP flow properties can be tuned by the conductivity.

According to classical antenna theory, the propagation speed of electrical current waves along antennas is at the light speed in vacuum i.e. c_0. In contrast, due to the conductivity of graphene, the travelling speed of the electrical current wave along a Graphene-based plasmonic antenna is at the speed of the SPP wave [73]. The propagation speeds of SPP waves are much lower than the speed of EM waves in vacuum. Therefore, the wavelength of an SPP wave is smaller than the wavelength of EM waves in free space ($\lambda_{SPP} < \lambda$). The ratio $\Gamma = \lambda/\lambda_{SPP}$ is defined as the confinement factor which dominated by the plasmonic material [74]. For a plasmonic antenna, its resonance length is expressed as $l_p \approx \lambda_{SPP}/2 = \lambda/2\Gamma$ [74], and the confinement factor for graphene is usually between 10 to 100. These graphene-based

nanoantennas make the resonant frequency about two orders below the value of traditional antennas [27], [29], [75]. This opens the door to nanoscale communication with EM waves. According to [27], [29], [75], the operating frequency of graphene-based nanonetworks is in the THz band above.

Moreover, wave propagation at the nanoscale is mainly dominated by two quantum effects in graphene, i.e. either the kinetic inductance or the quantum capacitances [76]. This is because when analysing the transmission line properties of GNR, the propagation speed of SPP waves is determined by the total inductance $\mathcal{L}_t$ and the total capacitance $\mathcal{C}_t$ per unit length of the Graphene plasmonic antenna [73], given that $v_{SPP} = \frac{1}{\sqrt{\mathcal{L}_t \mathcal{C}_t}}$. The total inductance is the sum of total kinetic inductance and the magnetic inductance, the total capacitance is the parallel equivalent of the quantum capacitance and the electrostatic capacitance. More details are given in [27] and [73]. As mentioned previously, the properties of SPP waves motivate the development of Graphene plasmonic nanoantennas operating in the THz band.

2.3 Related Work

Most of the existing channel models for THz bands aim to characterize communication among transceivers with distances as far as several metres [77]–[81], however, EM waves suffer severe path loss over such propagation distances. This is because of the effect of molecular absorption, which reduces the entire THz band to just a few smaller bandwidth windows. As a result, most of the current research on either channel modelling or device development is concentrated on frequencies around 300 GHz which is the available transmission window defined by molecular absorption [82]–

[87]. For the purpose of communication among nanodevices within nanonetworks and considering the very short communication range of nano- transceivers, a nanonetwork channel model for in the entire THz band needs to be developed. Therefore, in this thesis, the focus is only on a THz propagation model for transmission within a range of 1 metre.

Jornet and Akyldiz firstly proposed a free-space THz channel model for communications below one metre in 2010 [27]. In [64], they briefly described the proposed model, introduced the concept of molecular absorption and gave the calculation methods to obtain the molecular absorption noise and the path loss. For THz free-space transmission, the molecular absorption loss is considered to be caused by air molecules only in [64], where water vapour is the major contributor attenuating the propagation signal in free-space. The model is mainly developed for Light-of-Sight (LOS) communications. However, it can be modified to adapt to different media consisting of a variety of gases with different concentrations and compositions.

Based on this model, Afsharinejad et al. [62], [63], [88]–[90], proposed a path loss model for communications in vegetation, where they addressed the signal attenuation due to the absorption of both air molecules and plant leaves. The characteristics of the plants were considered as the main factors such as the distribution and the thickness of the plant leaves. As a result, the absorption coefficients in the model were modified to include the integration of absorption coefficients due to air molecules and due to leaves. Moreover, the model also put scattering loss and shadowing fading into consideration.

Federici et al. [91] investigated the effect of weather on the outdoor THz propagation channel. The authors emphasised the impact of atmospheric gases and

airborne particulates i.e. water vapour, oxygen, dust, fog, clouds, and rain on attenuating the THz signal. The work theoretically analysed the attenuation impacts of atmospheric gases and airborne particulates and validated this with measurements. In [92], Kokkoniemi et al. have also proposed an improvement THz channel model for LOS communications where the impact of particle scattering on the THz communication was studied. The study showed that particle scattering redirects part of the LOS energy which results in additional loss to the LOS communications along the channel. Although the particle scattering reduces the LOS signal as does the molecular absorption, the multiple scattering behaviours enable the Tx signal to arrive at the Rx, which exhibits Non-Light-of-Sight (NLOS) communication. Moreover, NLOS propagation also introduces delays to the system besides the degradation in signal power. Therefore, in [93], the authors have improved their model in both the frequency and the time domains in order to take NLOS propagation delay into account. The extended work presented in [94] revises the multiple scattering models [93] by putting commercially available particles into consideration which makes the model more realistic. Others have also studied the LOS and NLOS model in the THz band [95], which addresses that molecular absorption and spreading loss cause high path-loss for LOS components while high reflections exist for NLOS components. Llatster et al. have also proposed a THz model in both frequency and time domains in [96] where the impact of molecular absorption on short-range communication channels has been investigated [96].

To date, there are many THz models aiming to capture multipath propagation but most focus on 300GHz [80], [85], [97]–[100]. In [101], Han et al. have developed a precise multi-ray THz propagation model in the cases of both LOS and NLOS using

ray-tracing techniques. Moreover, the proposed model also considers the reflection, scattering, and refraction communication paths. It is presented theoretically with experimental validation and an in-depth study of THz channel peculiarities is conducted based on the model. According to the numerical results provided, the performance of communications in the THz band can be improved by using multi-carrier and distance-adaptive transmissions. In [95], [98], [99], the authors have also used a ray-tracing approach. For example, in [99] a realistic multipath THz wave propagation simulation in an office environment is conducted. With ray-tracing techniques, the THz wave can be modelled very precisely because of the quasi-optically propagation of THz waves and their ultra-narrow wavelength in the THz band.

Most of the channel models developed so far are focused on transmission in a gaseous medium, however, the potential application of nanonetworks in biomedical situations envisions the signal propagation through human tissues and blood. In order to analyse the feasibility of such an application of EM communication nanonetworks, investigation of THz propagation behaviour in materials other than gaseous is needed [102].

To date, there is much research that has been conducted in the area of healthcare or biomedical applications. Most of this is based on RF and microwave frequencies [103]–[110]. On account of the unique characteristics of THz channel, these research achievements cannot be used in THz nanonetworks. In [111], Yang et al. have proposed a very fundamental path loss model for short range communications through the human body. The study assumes that blood and fat are the key components which can affect path loss in the channel. According to the results given, due to the

higher water concentration, blood impacts more on signal degradation than fat. Moreover, in contrast to the impact of water molecules in free space transmission on attenuation, the effect of blood and fat on signal degradation does not varying across the THz band. Later in [112], a numerical analysis on the absorption loss at 1 THz for signals travelling through fat tissue is given. It is found that the absorption loss is not significantly large for transmission distances within a few millimetres. Since water is the maximum component of the human body and is the most significant factor attenuating the THz transmission signal, a comparative investigation between path loss in pure water and in salt (NaCl) water has been given in [113]. According to the results, the former contributes more attenuation in THz propagation loss than the latter. As an improvement work, a very detailed THz channel model for body-centric nanonetworks is presented in [59]. The proposed path loss model is based on [64], which modifies the channel model for free space to be suitable for THz transmission through human tissues and blood. In the paper, the authors theoretically study the impact of human tissue and blood on absorbing the THz signal and validate the results with measurements. It is found that reflection between fat and skin does not cause significant loss. Furthermore, the paper has also provided a channel capacity model for the body-centric nanonetworks, the calculation results show that femtosecond pulses can offer high transmission distances and data rates.

In [114], Zarepour et al. study the THz channel within human lungs which is the basis of a THz Wireless Nanosensor Network (WNSN) [9], [115], [116]. The proposed THz channel will be used to transmit the data measured by the WNSN inside human lungs to the internet. It is shown that the absorption coefficient of the THz channel varies periodically along with patient's respiration. Moreover, the study finds

that THz absorption varies in relation to the ‘sweet spot’ in patient’s respiration which is the spot enables the lowest THz absorption values. The authors have also presented an estimation algorithm for the THz periodic channel. Based on this algorithm they claim that the estimation accuracy of the period of the THz channel and the sweet spots is 98.5%. Furthermore, an analysis of frequency-dependent absorption for the entire THz channel is conducted in the paper. The analysed results reveal that the impact of a patient’s respiration cycle varies across the entire frequency band. Particularly, a subchannel with 20 GHz bandwidth (0.1¬0.12 THz) is impacted the least.

The application of WNSNs in the healthcare area has attracted significant interest; besides the channel modelling proposed in [114], Javed and Naqvi [117], present a path loss model for long distance THz transmission. It is assumed that the location of the WNSN’s control centre is outside the body while the nanosensors are distributed inside the body. When considering the effect of molecular shadowing, the authors assume that both the air and body components make the major contribution to it. The THz signal in the long-distance model is attenuated randomly by the molecular absorption, while the molecular absorption is determined by two kinds of media, i.e. air and the human body. For molecular absorption contributions from the air, water vapour is found to be the most significant factor, the concentration of water vapour can vary from different areas and weather conditions and is reported to be from 1% to 5%. While for attenuation caused by the human body, different parts all contribute to it, for example, bones, muscles, blood, fat, skin and so on. As attenuation caused by water molecules is the most significant compared with the others, the molecular absorption coefficient for the human body is therefore reshaped as the combined absorption coefficients of the concentration of water molecules in different parts of

the body (Table 2-1). Both the short and medium communication distances are investigated in the developed model through the air, the human body and hybrid medium (air and the human body), respectively. The results given reveal that the high concentration of water molecules inside the human body results in a high level of path loss in the THz WNSN channel through the human body.

Table 2-1 Average concentration of water in different human parts (Adapted from [117])

Body Parts	% in body	% water
Bones	15	22
Muscles	38	75
Blood	8	83
Skin	16	72
Fat	20	12
others	3	-

In [118], Guo et al. have developed a THz channel model for intra-body optical communication nanonetworks. With the aid of plasmonic nanoantennas, the proposed model operates in the optical window i.e. 400 – 750 THz. The body is comprised of many kinds of elements, such as molecules and cells which have different EM properties. Thus, the proposed channel model considers the molecular absorption that accounts from various types of molecules and scattering contributed by different kinds of cells. Then the impact of both a single cell and a number of cells on the propagation of THz waves is analysed. For the perspective of a single cell, scattering effect and

absorption are analysed by modelling the cell as a multi-layer ball shape. Then the scattering effect due to multiple cells is modelled using a chain model and three-dimensional (3D) models. Based on the proposed model, the simulation results indicate that the scattering from cells has a major impact on the propagation of the THz wave. Compared with this, the contribution from molecular absorption is neglected. These observations suggest that EM communication at lower bands would be a better choice.

2.4 Channel Modelling of EM Propagation in the THz Band

In this section, the EM propagation model for wireless communication among nanodevices in the THz band is presented. As an EM wave propagates, its power reduces as the channel is traversed due to path loss and noise. In the THz channel, molecular absorption is the most important factor which introduces path loss and random noise. In this thesis, the propagation model used in the THz band is based on that of Jornet and Akyildiz [64], [119], where the total path loss in the THz channel is given as:

$$L(f,d) = L_{spread}(f,d)\,L_{abs}(f,d) \tag{2.1}$$

where L_{spread} refers to the free space spreading loss and L_{abs} represents the molecular absorption loss.

2.4.1 Free Space Spreading Loss

The free-space spreading (path) loss (FSPL) is the attenuation of the signal energy when an EM wave propagates through a LOS path in free space. For an isotropic antenna, the FSPL can be obtained based on the Friis equation as:

$$L_{spread}\left(f_0, d\right) = \left(\frac{4\pi f_0 d}{c}\right)^2 \tag{2.2}$$

where f_0 is the centre frequency, d is the transmission distance and c is the speed of light in a vacuum.

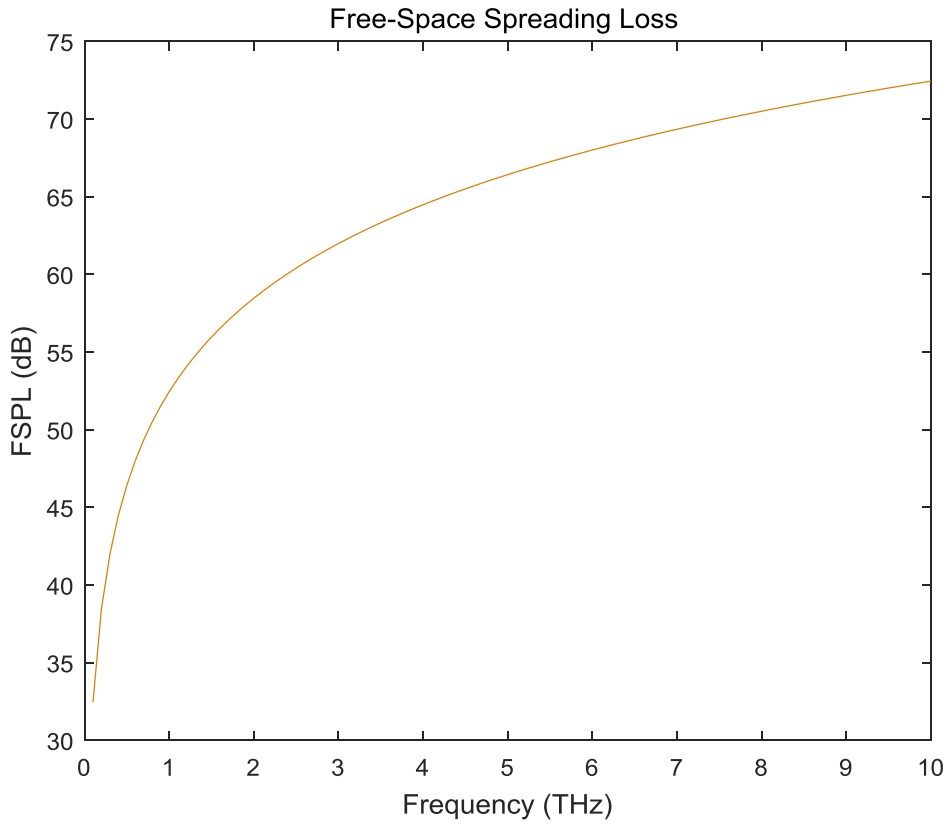

Figure 2-1 The Free-Space Spreading Loss for a signal travels in the THz channel for a propagation distance of 0.01 m.

According to (3.2), it can be seen from that the FSPL depends on the transmission frequency and distance. Figure 2-1 is the plot of FSPL over the THz (0.1-10THz) band for a transmission distance of 0.01m.

2.4.2 Absorption Loss

As an EM wave travels along a standard medium, several molecules existing in the medium are excited to vibrating at certain frequencies in the THz band. The vibration of these molecules results in energy loss of the EM wave. This is the so-called molecular absorption loss. The molecular absorption is determined by the transmittance of the medium τ, which is:

$$\tau = e^{-k(f)d}. \tag{2.3}$$

Therefore, according to the Beer-Lambert law, the molecular absorption loss is given as:

$$L_{abs}(f_0, d) = \frac{1}{\tau} = e^{k(f_0)d} \tag{2.4}$$

where $k(f)$ is the absorption coefficient of the transmission medium i.e. air [9]. The medium absorption coefficient is the parameter that describes how much the signal loss in the medium in a certain frequency and a unit of distance. It is determined by many factors, such as the content and the electrical properties of each compositions within the medium. As is seen from (2.4), the molecular absorption loss depends on the absorption coefficient. Moreover, for transmission in air, the absorption coefficient is given as:

$$k(f) = \sum_q k^q(f) \tag{2.5}$$

where $k^q(f)$ stands for the absorption coefficient of the gas q in the air, i.e. water vapor, oxygen and nitrogen. Therefore, the absorption coefficient of air can be written as:

$$k(f) = \sum_q \frac{p}{p_0} \frac{T_{STP}}{T} Q^q \sigma^q(f) \tag{2.6}$$

where p is the system pressure, p_0 is the reference pressure, T_{STP} represents the standard temperature, Q^q refers to the number of molecules per unit volume (molecules m^{-3}) of gas q and σ^q is the absorption cross-section (m^2 $(molecule)^{-1}$) of gas q. The values of Q^q and σ^q can be obtained using the data provided in the HITRAN (High resolution TRANsmission) molecular absorption database [120]. Figure 2-2 gives an example of molecular absorption coefficient for water vapour as the function of the frequency [64]. It is known that, water vapour contributes the majority to the total absorption of the air. More details are given by Jornet and Akyildiz in [64].

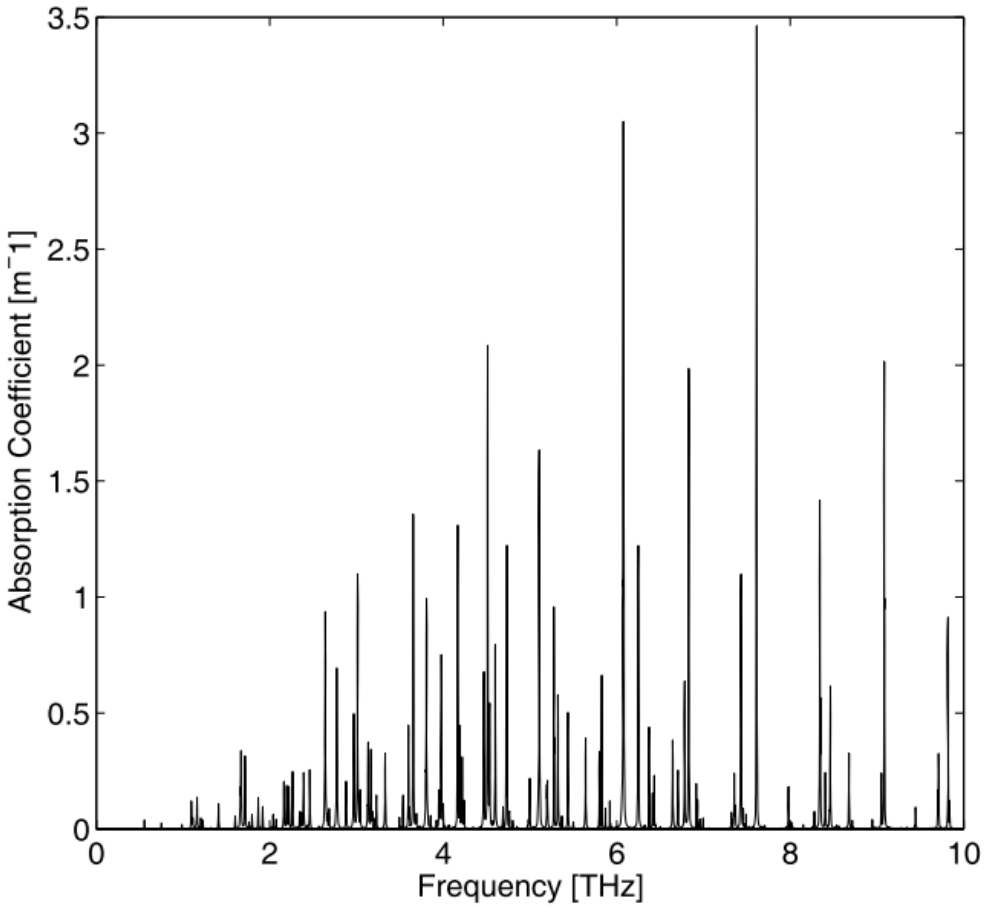

Figure 2-2 Molecular absorption coefficient for water vapour as the function of the frequency [64].

2.4.3 Wave Propagation

The propagation of the wave is characterized by the THz channel response. The transfer function of the channel frequency response H is given as [121]:

$$H(f,d) = H_{abs}(f,d) H_{spread}(f,d) \tag{2.7}$$

where H_{abs} and H_{spread} are the transfer functions of molecular absorption loss and spreading loss respectively, given by

$$H_{abs}(f,d) = \sqrt{\frac{1}{L_{abs}}} = \sqrt{\frac{1}{e^{k(f)d}}} = e^{\left(-\frac{1}{2}k(f)d\right)} \tag{2.8}$$

and

$$H_{spread}(f,d)=\left(\frac{c}{4\pi d f_0}\right)e^{\left(-i2\pi f\frac{d}{c}\right)} \tag{2.9}$$

where f_0 is the centre frequency of the antenna. In this thesis, it is assumed that the power is radiated spherically and spreads with distance. The antenna used to detect the signal power is isotropic broadband which has an effective area of

$$A_{eff}=\frac{\lambda_0}{4\pi} \tag{2.10}$$

with $\lambda_0 = {}^{c}/_{f_0}$.

The impulse response of the THz channel is, therefore, the inverse Fourier transformation of the channel frequency response,

$$h(t,d)=\mathcal{F}^{-1}\left\{H(f,d)\right\} \tag{2.11}$$

2.4.4 Absorption Noise

According to [121] , the system noise in the THz channel is contributed by two sources: thermal and molecular with the latter forming the main contributor [64]. The total noise power spectral density $N(f)$ can be calculated as the Boltzmann constant $k_B$multiplied by the total noise temperature:

$$N(f,d)=k_B\left[T_{sys}+T_{mol}(f,d)\right]\approx k_B T_{mol}(f,d) \tag{2.12}$$

where T_{sys} is the system temperature and T_{mol} is the molecular noise temperature. The molecular noise temperature can be expressed as follows [64]:

$$T_{mol}(f,d)=T_0\varepsilon=T_0(1-\tau)=T_0\left(1-e^{-k(f)d}\right) \tag{2.13}$$

where T_0 is the standard temperature, ε is known as the emissivity of the medium, τ is the transmittance of the medium given in (2.3) and k represents the medium absorption coefficient given in (2.5).

Therefore, the noise power at the receiver is given by :

$$P_{RX}(f,d) = \int_{BW} N(f,d)\,df \approx \int_{BW} T_{mol}(f,d)\,df \tag{2.14}$$

2.4.5 Channel Capacity

For a communication channel with Gaussian noise, the channel capacity can be calculated using the Shannon-Hartley theorem [122]:

$$C = B\log_2\left(1+\frac{S}{N}\right) \tag{2.15}$$

where C is the channel capacity, B denotes the channel bandwidth, S represents received signal power, N is the average noise power over the channel and S/N stands for the Signal-to-Nosie ratio (SNR).

The THz propagation channel is highly frequency-selective while the noise contributed by molecular absorption is non-white [122]. Therefore, the capacity of the THz band can be obtained by dividing the entire bandwidth into small sub-bands which are narrow enough to ensure each sub-channel be non-selective and the noise be white. The i_{th} sub-band has a centre frequency of f_i and a bandwidth of Δf , (i= 1, 2, 3….). Thus, by rewriting (2.12) the channel capacity can be obtained using,

$$C(d) = \sum_i \Delta f \log_2\left(1+\frac{S(f_i)}{L(f_i,d)N(f_i,d)}\right)df \tag{2.16}$$

where d is the signal propagation distance, $S(f_i)$ denotes the power spectral density for the propagated signal in the i_{th} sub-band.

For example, in Figure 2-3, the 0.5 to 1.5 THz band is divided into 10 sub-bands with sub-bandwidth of 0.1 THz.

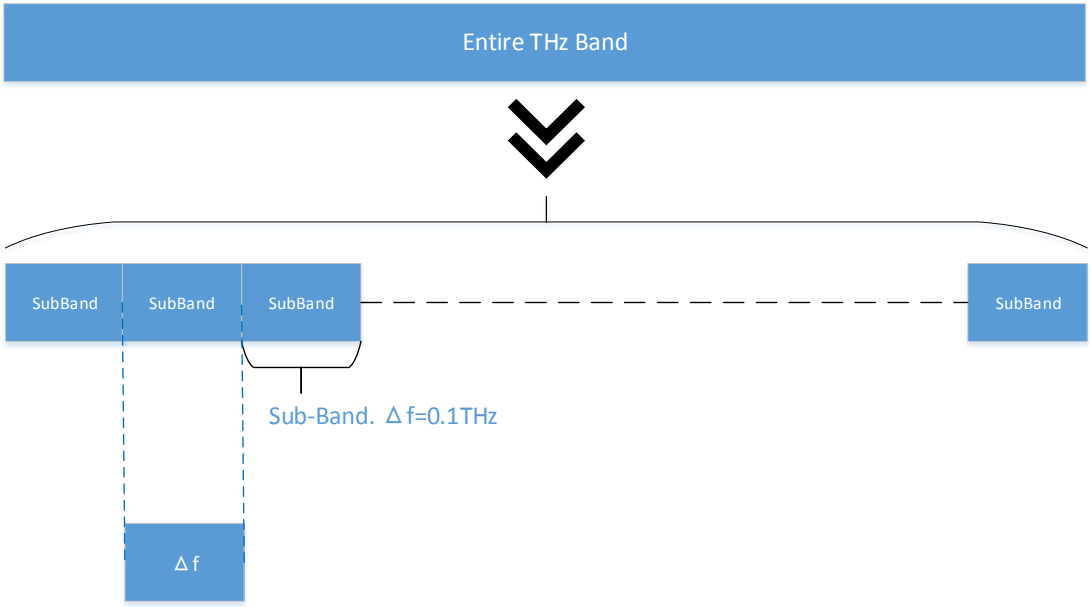

Figure 2-3 Dividing the entire band into small sub-bands

As is shown in Figure 2-4, the path loss varies with the change of both wave frequency and transmission distance with the trend being a growing path loss with both of these. However, as the molecular absorption coefficients vary sharply in some frequencies, absorption loss may change dramatically with increasing frequency. According to the result shown in Figure 2-4, absorption loss decreases at around 1.4 THz which results in a reduction of the total path loss from 1.4 THz to 1.5 THz. Similarly, molecular absorption noise temperature grows with increasing frequency and distance but shows a similar decrease past 1.4 THz as seen in Figure 2-5. The noise temperature finally reaches the reference temperature when the transmission distance is around 6 millimetres. Correspondingly, the SNR has the same trend as is shown in Figure 2-6.

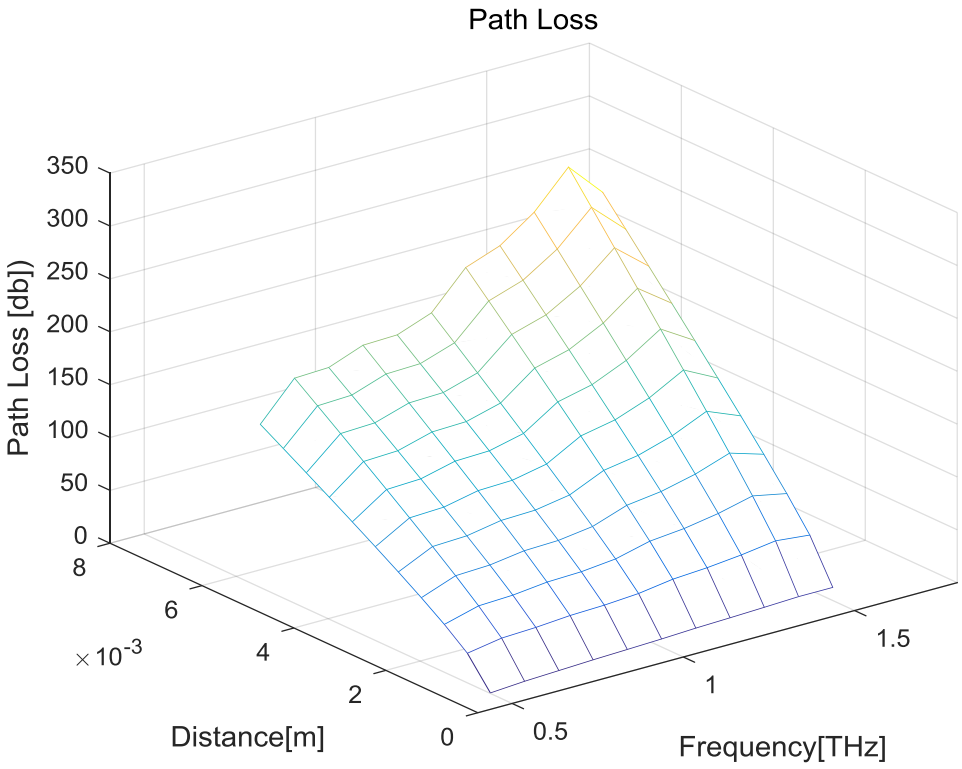

Figure 2-4 Path loss as the function of frequency and distance (10% of water vapour)

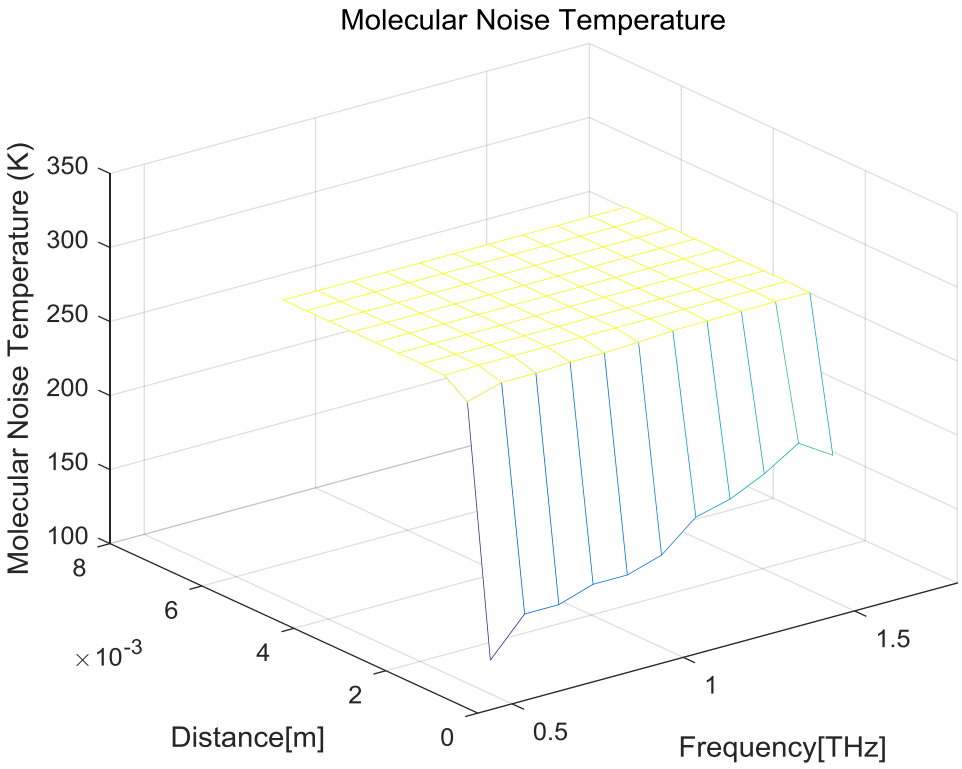

Figure 2-5 Molecular noise temperature as functions of frequency and distance (10% of water vapour)

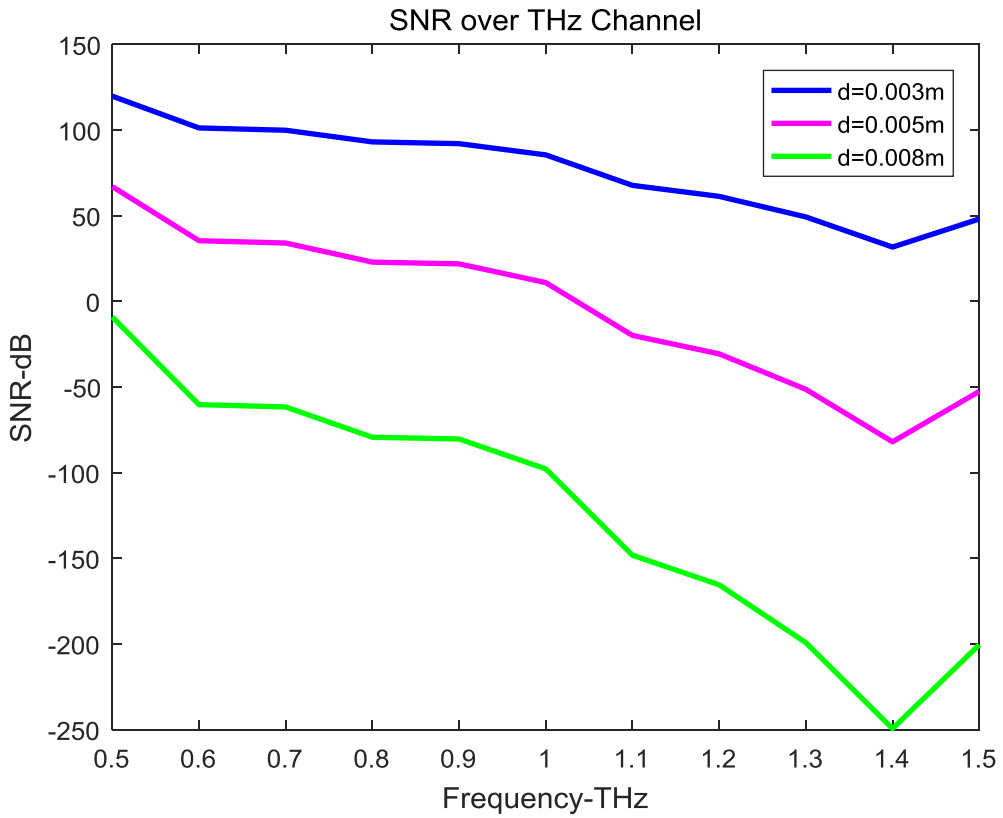

Figure 2-6 SNR as the function of frequency for different transmission distances.

With respect to the capacity, Figure 2-8 illustrates that when the transmission distance is very short. i.e. under 1 mm, this does not change significantly but when distance exceeds 1 mm it decreases more and more sharply. Hence, it is possible to estimate the suitable transmission distance for communication in THz band. In addition, within a suitable distance, the capacity is sufficient.

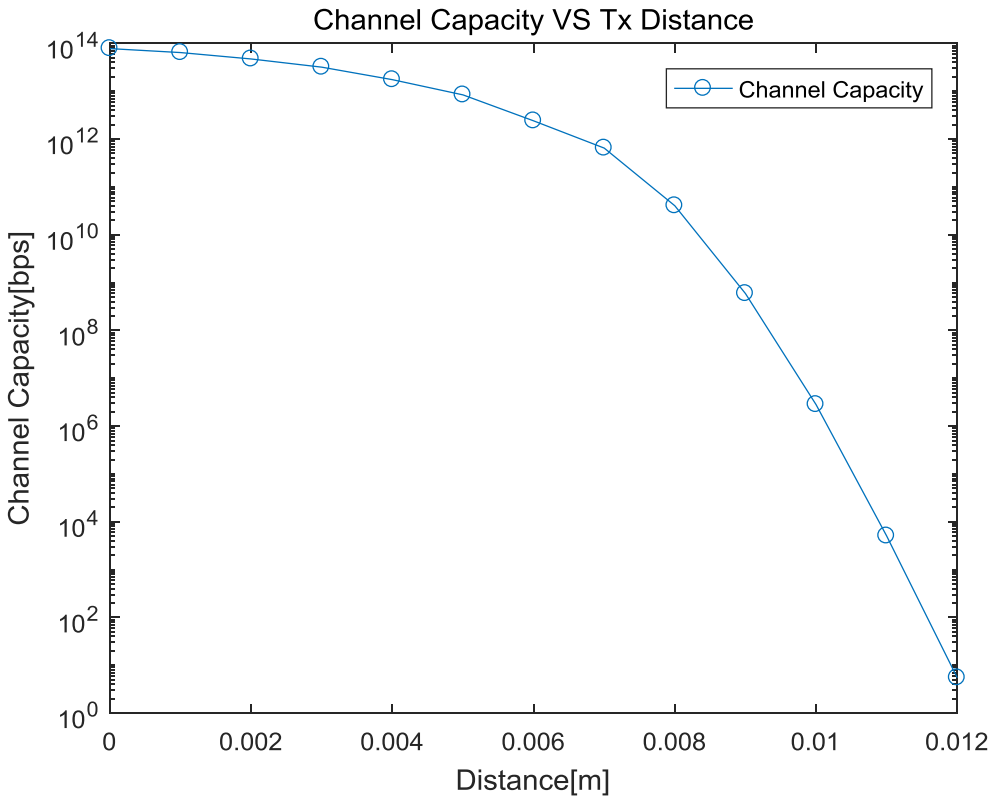

Figure 2-7 Channel Capacity at 1.5THz as a function of distance.

2.5 Conclusions

In this chapter, the channel model for nanoscale communication in the THz band has been presented. Related research on the channel modelling of the THz band has been reviewed. A recent and appropriate propagation model for EM communication in the THz band in terms of the total path loss and noise has been introduced. The path loss trends to grow with the increase of frequency and transmission distance. However, the molecular absorption coefficients vary sharply in some frequencies which results in the reduction of the total path loss at such frequencies. For molecular noise temperature, the trend is the same as it is for the SNR. The channel capacity has also been calculated by dividing the channel into sub-bands as the capacity of the channel

is frequency selective. It is seen that for transmission distances of a few mm, the theoretical channel capacity can be very high.

Chapter 3

Relay-Assisted Nanoscale Communication in the Terahertz Band

The THz channel model for nanosensor networks has been studied in Chapter 2. In this chapter, the bit error rate (BER) performance of a relaying transmission scheme for wireless nanosensor networks in the Terahertz (THz) Band is investigated. Nanosensor networks comprising several graphene-based devices deployed at the nanoscale are considered. Both amplify-and-forward (AF) and decode-and-forward (DF) relaying modes are studied. The channel model described in Chapter 2 is utilised which takes into account both spreading loss and molecular absorption loss. Given the high path loss and level of noise from significant random fluctuations through the THz channel, relay assisted schemes offer advantages in terms of significant performance improvements. To quantify the likely benefits, the predicted bit error rate (BER) of the proposed scheme is derived. Then a simulation of the proposed relay schemes based on the THz channel model utilizing a Monte-Carlo method is presented. The results obtained show that a performance improvement of 2.2 dB for AF and of 5 dB for DF is achievable at a target bit error rate (BER) of 10^{-5}.

3.1 Introduction and related work

In this chapter, the performance of graphene-based EM nanosensor networks is considered. One of the advantages of graphene-based devices is that they enable operation in the frequency range of 0.1THz-10.0 THz (the target THz band) at the

nanoscale [27]. However, the most important characteristic of the THz channel is the high path loss and noise due to the molecular absorption of EM waves [64]. Moreover, the resulting noise is frequency selective, which makes the channel depart significantly from the ideal flat band and greatly decreases transmission performance and subsequently the transmission distance. These are the main bottlenecks that limit the application of THz communications at the nanoscale.

In traditional EM communications, relaying channels have been widely investigated as a way to achieve significant data transmission performance improvements since the 1960s [123]–[126]. The classical three-terminal relay channel model was originally developed by van der Meulen [124]. Then Cover and El Gamal worked on the information theoretic characteristics of the discrete memoryless and AWGN channels and determined the capacity for the three-terminal relay channels [125]. In [125], an assumption has been made that all the three nodes operated in the same frequency band. With the rapid developments of recent decades, various extension works have been proposed in case of multiple relays [127]–[130]. In [128], a multiple access channel is considered, where multiple sources transmit signals to one destination via a single relay. Some studies have been published for the application of relaying protocols in nanonetworks using molecular communications [131]–[133]. However, for nanonetworks based on the THz band, it is still a lack of work in relation to cooperative communication and relay channels. In [134], Pierobon et al. have proposed a routing framework for nanonetworks based on THz communications. A forwarding scheme for nanonetworks in the THz band was investigated in [135]. Both works were focused on analysing the system throughput but not the relaying channels. Recently, Akyildiz and Jornet introduced the concept of Ultra-massive Multiple Input

and Multiple Output (UM MIMO) communication in the THz band [74], which envisions THz multi-hop communications in the future. To date, there is still no clear research on how to configure a THz relaying network. This chapter investigates for the first time a possible configuration for a nanoscale THz relaying scheme. The proposed relay-assisted transmission scheme in the THz band thus seems a promising approach to overcome the channel limitations resulting in significant transmission performance improvements.

The remainder of this chapter is organized as follows. Section 3.2 presents the THz channel model that the relaying schemes operate on. Section 3.3 demonstrates the two proposed relaying configurations in detail. The numerical results are given in section 3.4, where the simulation set up is illustrated, and the BER performances are presented. The last section concludes the chapter.

3.2 THz Propagation Channel Model

In contrast to the traditional EM relaying channels, the THz relaying channel is highly frequency-selective due to the impact of molecular absorption. A propagation model for THz communication among nanosensors is essential. In Chapter 2, channel models for THz communication have been briefly investigated. In this Chapter, THz relaying schemes are developed based on the channel model presented in Chapter 2. Moreover, considering the energy dissipation and transceiver complexity for nanoscale communication systems, differential binary phase shift keying (DBPSK) modulation is used as the channel access scheme due to its low energy consumption and non-coherent demodulation process [136], [137].

3.3 System Model

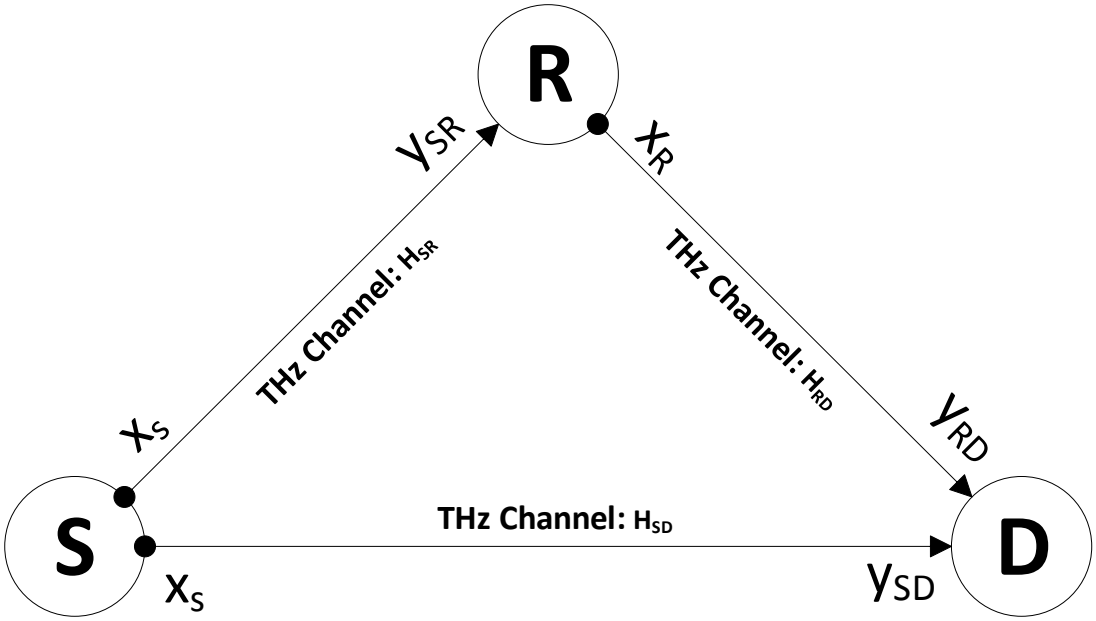

Figure 3-1 System model of single relay assisted data transmission in the THz band at the nanoscale.

In this section, with the consideration of the unique properties of the THz channel, a brief demonstration of THz relaying protocols is presented. The relay model for nanoscale communications in the THz band under consideration is a classical three-terminal relay system with one source, one fixed relay, and one destination. As shown in Figure 3-1, ***S*** is the source node which transmits information both to the destination node ***D*** directly and to the relay node ***R*** via a link, where the relay assists the information transmission via the ***S*** to ***R*** and ***R*** to ***D*** links over the THz band. It is assumed that all these three nodes operate in the same THz band and the lengths of each link are the same. i.e. $d_0 = 1mm$. The system models based on Amplify and Forward (AF) and Decode and Forward (DF) relaying protocols are introduced in the following paragraphs.

3.3.1 AF Relaying Protocol

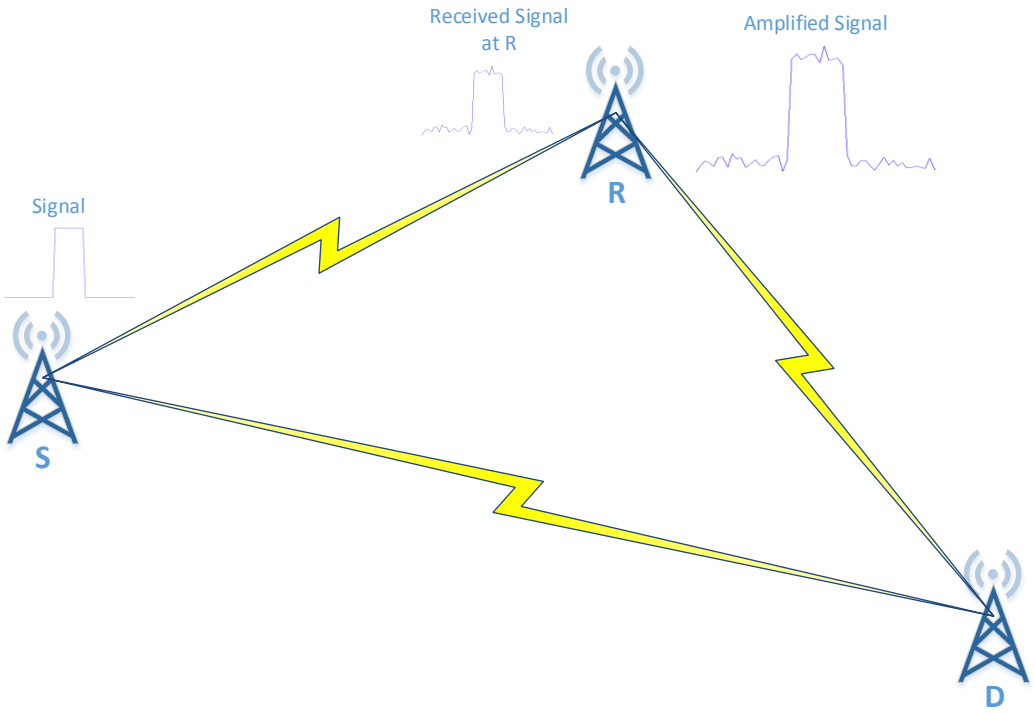

Figure 3-2 The configuration of a three-terminal Amplify-and-Forward relaying protocol.

In a AF relaying scheme as shown in Figure 3-2, the relay node amplifies the received signal from the source and just transmits it to the destination without conducting any coding and decoding process.

Here, the transmission process can be divided into two steps. First, the source node broadcasts its signal x_S to the destination and the relay node simultaneously in the first step. Therefore, the received signal at the relay node is given by [126] :

$$y_{S,R} = \frac{\sqrt{P}g_{S,R}}{\sqrt{L_{S,R}}} x_S + n_{S,R} \tag{3.1}$$

While the received signal at the destination node is:

$$y_{S,\mathrm{D}} = \frac{\sqrt{P} g_{S,\mathrm{D}}}{\sqrt{L_{S,D}}} x_S + n_{S,\mathrm{D}} \tag{3.2}$$

where P is the transmitted power from the source; as studies in [138] have shown that molecule absorbed energy can be re-radiated as EM wave at the same frequency, it is assumed that the signal wave is radiated by the water vapour distributed in the channel and following Rayleigh distribution, $g_{S,R}$, $g_{S,D}$ and $g_{R,D}$ in the following represent the corresponding channel coefficients of the two paths and are complex normally distributed ~ $\mathcal{CN}(0,1)$; $L_{S,R}$, $L_{S,D}$ and $L_{R,D}$ in the follwing are the path loss in the corresponding link (given in (2.1)); $n_{S,R}$, $n_{S,D}$ and $n_{R,D}$ are the respective noise terms within the source to relay and source to destination paths. The molecular absorption noise is considered as the main noise factor within the THz propagation channel. According to [135], [139], the power spectral density of the absorption noise for a fix distance d_0 is given by:

$$N(f) = k_B T_0 \left(1 - e^{-k(f) d_0}\right) \tag{3.3}$$

where k_B refers to the Boltzmann constant. As communications among different nodes are operated in the same frequency band, it is assumed that the absorption noise within the three channels ***S*** to ***R***, ***R*** to ***D*** and ***S*** to ***D*** may be represented by independent instances of the same distribution.

Interference occurs when symbols arrive at the destination from different nanosensors concurrently and overlap. According to [121], the overall interference can be modelled as a Gaussian distribution, which gives,

$$\mathcal{N}_I\left(\mu_I = E[I]; \sigma_I^2 = N_I\right) \tag{3.4}$$

where

$$E[I] = \sum_{u=2}^{U} \frac{A^u}{\zeta} \tag{3.5}$$

$$N_I = \sum_{u=2}^{U} \left(\frac{\left(A^u\right)^2 + N}{\zeta} \right) p(x_1) + 2 \sum_{u=2<v}^{U} \left(\frac{p(x_1)}{\zeta} \right)^2 A^u A^v - \left(\sum_{u=2}^{U} \frac{A^u}{\zeta} p(x_1) \right)^2 \tag{3.6}$$

where U is the number of nanosensors, A^u is the amplitude of signal transmitted from u to the destination, N refers to the channel noise power from the nanosensors to the destination. $p(x_1)$ refers to the probability of sending a pulse and ζ is the ratio of the symbol duration to the pulse duration; for the DBPSK and BPSK modulation schemes in this chapter it is set to 1. Therefore, the total noise and interference is

$$N_0 = N + N_I \tag{3.7}$$

The total noise and interference of the three links have the same noise power density, i.e. $N_{S,D} = N_{S,R} = N_{R,D} = N_0$.

During the next step, the received signal at the relay (i.e. $y_{S,R}$) is amplified with gain β, in order to comply with the relay power constraint, the amplifying gain should satisfy [126]:

$$\beta \leq \sqrt{\frac{P}{\frac{P}{L_{S,R}} \left| g_{S,R} \right|^2 + N_0}} \tag{3.8}$$

In this thesis, β is chosen to be *equal* to the right hand side of (3.8).

As may be seen from (3.8)**,** the amplification gain depends on the THz channel gain from source to relay, the source power and the noise power. Therefore, the received signal at the relay is now amplified to be:

$$y_{AF} = \beta y_{S,R} \tag{3.9}$$

which has the equal power with the transmitted signal from source, i.e. P.

As a result, the received signal from the relay at the destination is:

$$\begin{aligned} y_{R,D}^{AF} &= \frac{\sqrt{P}}{\sqrt{L_{R,D}}} g_{R,D} y_{AF} + n_{R,D} \\ &= \frac{\sqrt{P}}{\sqrt{L_{R,D}}} g_{R,D} \beta y_{S,R} + n_{R,D} \\ &= \frac{\sqrt{P}}{\sqrt{L_{R,D}}} g_{R,D} \sqrt{\frac{P}{\frac{P}{L_{S,R}}\left|g_{S,R}\right|^2 + N_0}} y_{S,R} + n_{R,D} \\ &= \frac{\sqrt{P}}{\sqrt{L_{R,D}}} g_{R,D} \sqrt{\frac{P}{\frac{P_s}{L_{S,R}}\left|g_{S,R}\right|^2 + N_0}} \frac{\sqrt{P} g_{S,R}}{\sqrt{L_{S,R}}} x_S + n'_{R,D} \\ &= \sqrt{\frac{P}{\frac{P}{L_{S,R}}\left|g_{S,R}\right|^2 + N_0}} \frac{P}{\sqrt{L_{R,D}}\sqrt{L_{S,R}}} g_{R,D} g_{S,R} x_S + n'_{R,D} \end{aligned} \tag{3.10}$$

where the equivalent noise $n'_{R,D}$ is given as,

$$n'_{R,D} = \sqrt{\frac{P}{\frac{P}{L_{S,R}}\left|g_{S,R}\right|^2 + N_0}} \frac{\sqrt{P} g_{R,D}}{\sqrt{L_{R,D}}} n_{S,R} + n_{R,D} \tag{3.11}$$

Assume that the power of the transmitted signal from relay is equal to . As $n_{S,R}$ and $n_{R,D}$ are independent, the variance of $n'_{R,D}$ is therefore,

$$N'_0 = \left(\frac{P}{\frac{P}{L_{S,R}}\left|g_{S,R}\right|^2 + N_0} \frac{P\left|g_{R,D}\right|^2}{L_{R,D}} + 1 \right) N_0 \tag{3.12}$$

The signal from the source $y_{S,D}$ is then combined with the signal from the relay $y_{R,D}$ at destination, to obtain,

$$y = \alpha_1^{AF} y_{S,D} + \alpha_2^{AF} y_{R,D}^{AF} \tag{3.13}$$

where α_1^{AF} and α_2^{AF} are the parameters the maximal ratio combining (MRC) method is used to combine the two received signals so as to achieve a maximized signal-to-interference-noise ratio (SINR) at the destination.

As was mentioned previously, it is assumed that the absorption noise within the three channels follows the same distribution, therefore, the two signals at the destination are affected equally by the channel noise n with a power spectral density of N. In this case, the combined signal at the destination can also be expressed as:

$$y = \sum_{i=1}^{2} \alpha_i e^{-j\phi_i} y_i \tag{3.14}$$

where $y_i = g_i e^{j\phi_i} x_i + n$, ϕ_i represents the phase shift of the signal and α_i represents the MRC coefficients.

The MRC output SINR of (3.12) is given by:

$$\gamma = \frac{\left(\sum_{i=1}^{2} \alpha_i g_i \right)^2}{N_0 \sum_{i=1}^{2} \alpha_i^2} \tag{3.15}$$

This can be maximized by using the Cauchy-Schwartz inequality,

$$\left(\sum_{i=1}^{2} \alpha_i g_i \right)^2 \leq \left(\sum_{i=1}^{2} \alpha_i^2 \right) \left(\sum_{i=1}^{2} g_i^2 \right) \tag{3.16}$$

the maximal SINR in (3.13) can be obtained when the equality of (3.14) is achieved by making

$$\alpha_i = \frac{g_i}{\sqrt{N_0}} \tag{3.17}$$

By Substituting (3.2) and (3.10) into (3.12), one obtains:

$$y = \alpha_1^{AF}\left(\frac{\sqrt{P}}{\sqrt{L_{S,D}}} g_{S,\mathrm{D}} x_S + n_{S,\mathrm{D}}\right) + \alpha_2^{AF}\left(\sqrt{\frac{P}{\frac{P}{L_{S,R}}\left|g_{S,R}\right|^2 + N_0}} \frac{P}{\sqrt{L_{S,R}L_{R,D}}} g_{R,D} g_{S,R} x_S + n'_{R,D}\right) \tag{3.18}$$

To achieve the maximal SINR, the optimal values of the parameters in (3.11) are designed in a similar way to [140] as:

$$\alpha_1^{AF} = \frac{\frac{\sqrt{P}}{\sqrt{L_{S,D}}} g_{S,D}^*}{N_0} \tag{3.19}$$

and

$$\alpha_2^{AF} = \frac{\beta \frac{P}{\sqrt{L_{S,R}L_{R,D}}} g_{S,R}^* g_{R,D}^*}{\left(\beta^2 \frac{\left|g_{R,D}\right|^2}{L_{R,D}} + 1\right) N_0} \tag{3.20}$$

where g^* represents the complex conjugate of g; this is designed to make the two received signals equal.

The corresponding MRC output SINR at the destination for the system is given by [141] :

$$\gamma = \gamma_{S,D} + \gamma_{S,R,D} \tag{3.21}$$

For the AF model, the SINR expressions for the two paths are:

$$\gamma_{S,D} = \frac{\left| \alpha_1^{AF} \frac{\sqrt{P}}{\sqrt{L_{S,D}}} g_{S,D} \right|^2}{\left| \alpha_1^{AF} \right|^2 N_0} = \frac{P \left| g_{S,D} \right|^2}{L_{S,D} N_0} \tag{3.22}$$

and

$$\begin{aligned}
\gamma_{S,R,D} &= \frac{\left| \alpha_2^{AF} \beta \frac{P}{\sqrt{L_{S,R} L_{R,D}}} g_{S,R} g_{R,D} \right|^2}{\left| \alpha_2^{AF} \right|^2 \left(\beta^2 \frac{P \left| g_{R,D} \right|^2}{L_{R,D}} + 1 \right) N_0} \\
&= \frac{\left| \sqrt{\frac{P}{\frac{P}{L_{S,R}} \left| g_{S,R} \right|^2 + N_0}} \frac{P}{\sqrt{L_{S,R} L_{R,D}}} g_{S,R} g_{R,D} \right|^2}{\left(\frac{P}{\frac{P}{L_{S,R}} \left| g_{S,R} \right|^2 + N_0} \frac{P \left| g_{R,D} \right|^2}{L_{R,D}} + 1 \right) N_0} \\
&= \frac{1}{N_{S,D}} \frac{\frac{P P^2 \left| g_{S,R} \right|^2 \left| g_{R,D} \right|^2}{P L \left| g_{S,R} \right|^2 + L^2 N_0}}{\frac{P^2 \left| g_{R,D} \right|^2}{P \left| g_{S,R} \right|^2 + L N_0} + 1} \\
&= \frac{1}{L N_0} \frac{P^3 \left| g_{S,R} \right|^2 \left| g_{R,D} \right|^2}{P^2 \left| g_{R,D} \right|^2 + P \left| g_{S,R} \right|^2 + L N_0}
\end{aligned} \tag{3.23}$$

It should be noted that since the distance and frequency of all the three paths are assumed to be the same, the path loss of each path is therefore equal, i.e. $L_{S,D} = L_{S,R} = L_{R,D} = L$.

3.3.2 DF Relaying

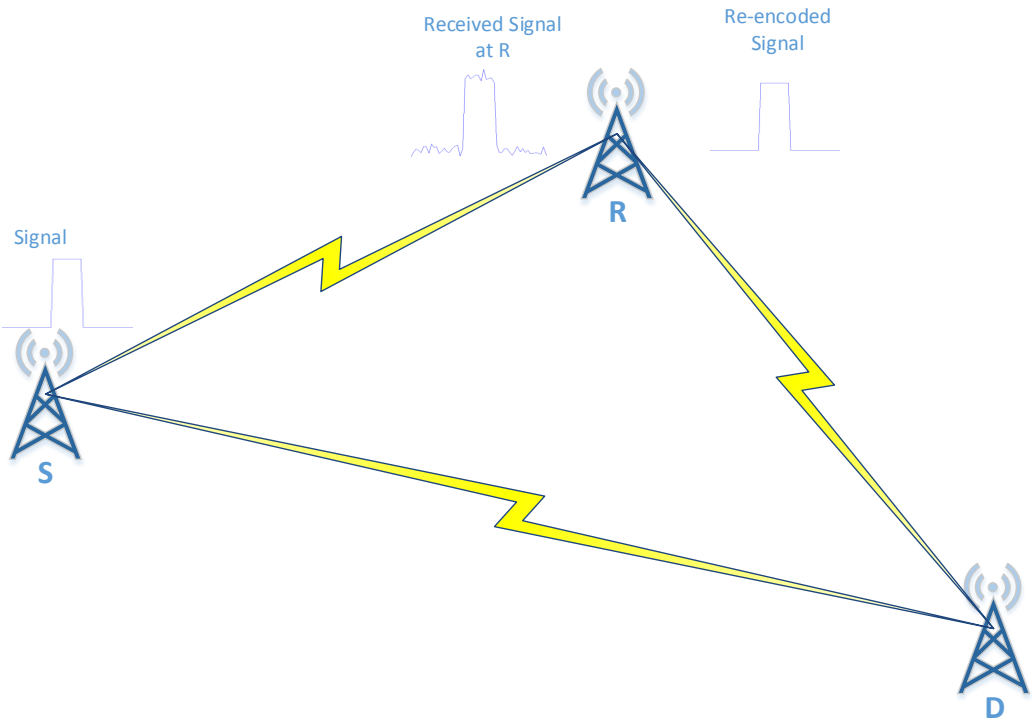

Figure 3-3 The configuration of a three-terminal Decode-and-Forward relaying protocol.

The DF scheme is shown in Figure 3-3, in this case, the relay decodes (demodulates) the received signal from the source node and then forwards the encoded (modulated) signal to the destination. The received signal at the destination after DF relaying is therefore [142]:

$$y_{R,D}^{DF} = \frac{\sqrt{P} g_{R,D}}{\sqrt{L_{R,D}}} y_{DF} + n_{R,D} \tag{3.24}$$

This signal is then combined with the direct signal from the source node at the destination which gives:

$$y = \alpha_1^{DF} y_{S,D} + \alpha_2^{DF} y_{R,D}^{DF} \tag{3.25}$$

α_1^{DF} and α_2^{DF} are the relevant MRC optimal parameters given as:

$$\alpha_1^{DF} = \frac{\sqrt{P} g_{S,D}^*}{\sqrt{L_{S,D}} N_0} \tag{3.26}$$

and

$$\alpha_2^{DF} = \frac{\sqrt{P} g_{R,D}^*}{\sqrt{L_{R,D}} N_0} \tag{3.27}$$

Recalling equation (3.23), in the DF model, the SNR for the two paths can be calculated as:

$$\begin{aligned} \gamma_{S,D}^{DF} &= \frac{\left| \alpha_1^{DF} \frac{\sqrt{P}}{\sqrt{L_{S,D}}} g_{S,D} \right|^2}{\left| \alpha_1^{DF} \right|^2 N_0} \\ &= \frac{P \left| g_{S,D} \right|^2}{L_{S,D} N_0} \\ &= \frac{P}{L N_0} \left| g_{S,D} \right|^2 \end{aligned} \tag{3.28}$$

and

$$\begin{aligned} \gamma_{S,R,D}^{DF} &= \frac{\left| \alpha_2^{DF} \frac{\sqrt{P}}{\sqrt{L_{R,D}}} g_{R,D} \right|^2}{\left| \alpha_2^{DF} \right|^2 N_0} \\ &= \frac{P \left| g_{R,D} \right|^2}{L_{R,D} N_0} \\ &= \frac{P}{L N_0} \left| g_{R,D} \right|^2 \end{aligned} \tag{3.29}$$

3.4 Numerical results

In this section, the simulation results of the system introduced above are presented. It is assumed that the destination knows the channel state information (CSI). The simulation is based on MATLAB and the simulation process is shown in Figure 3-4 and Figure 3-5. The simulations were firstly conducted using DBPSK modulation to access the single AF and DF THz channel. Then BPSK modulation was utilised and the results compared with those for the DBPSK scheme. The channel gain was based on the THz channel model. For a target minimum error probability of 10^{-5}, Monte-Carlo simulations were implemented. For simplicity, no channel codes were used to encode the raw data in either relaying case meaning that the decoding process was therefore simply demodulation.

Figure 3-6 shows the simulated bit error rate (BER) performance of the two relay schemes compared with direct transmission without a relay. The figure plots the BER of the AF and DF relay protocols as a function of Eb/N_0 and it can clearly be seen that both types of relay assisted transmission to improve the BER performance significantly. Moreover, DF has much better performance than AF in line with expectations based on established cooperative communication principles. The AF relay amplifies not only the signal itself but also the channel noise. The relaying gain at 10^{-5} is approximately 2.2 dB for AF and 5 dB for DF. The extra 2.8 dB represents the benefit for the complexity of DF compared to AF. The simulated results are compared with the theoretical results as well both in Figure 3-6 for DBPSK and Figure 3-7 for BPSK. The theoretical values come from the normal 2-way AWGN channel with Rayleigh fading. Sine each sub-band of the THz channel is considered as local

flat, the simulated results match the theoretical results well. When BPSK modulation is applied, the results shown in Figure 3-7 and Figure 3-8 indicate that BPSK provides better BER performance than DBPSK. However, as mentioned previously, DBPSK is set as the channel access scheme to reduce the complexity and energy consumption.

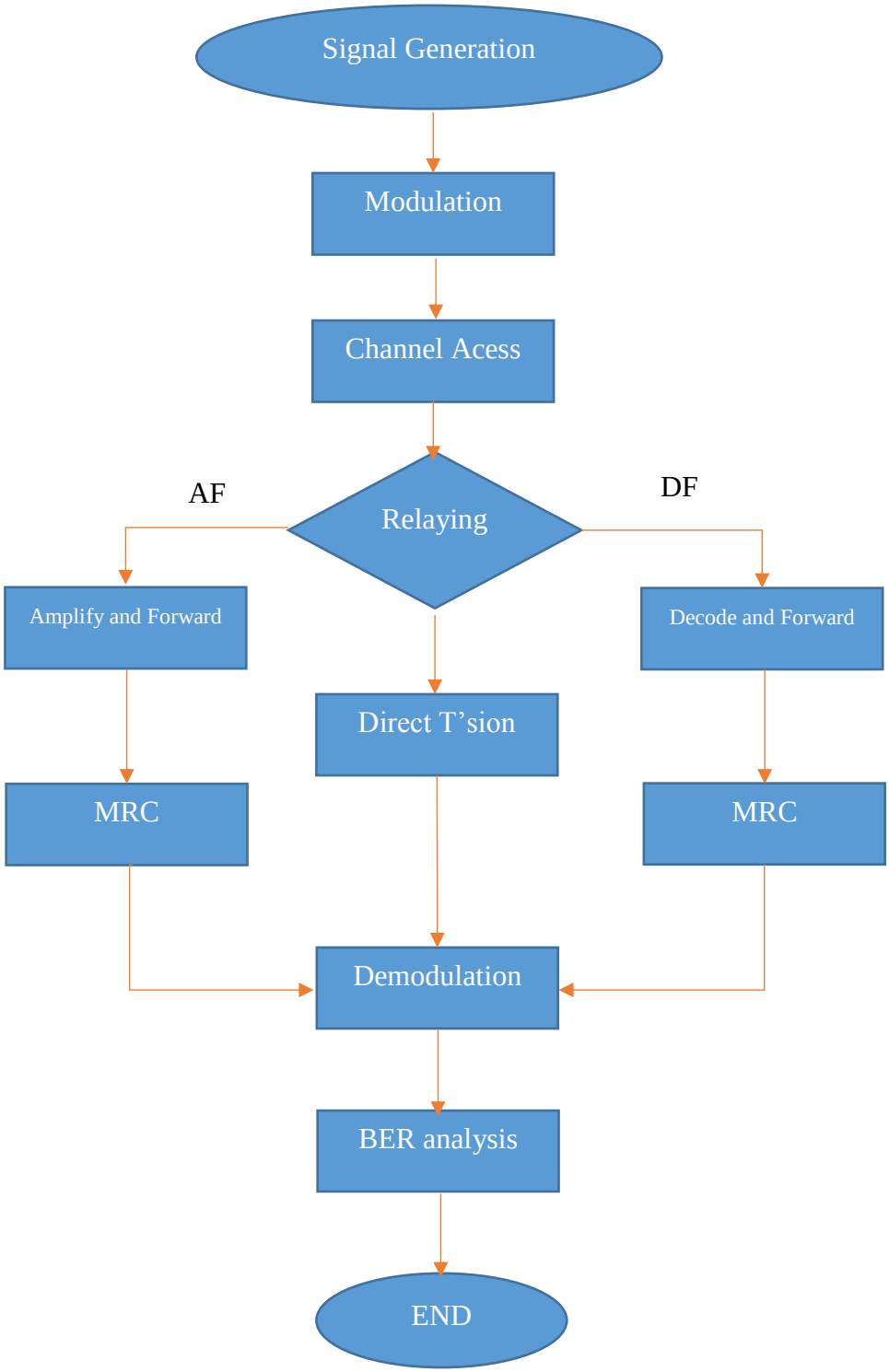

Figure 3-4 Simulation process diagram.

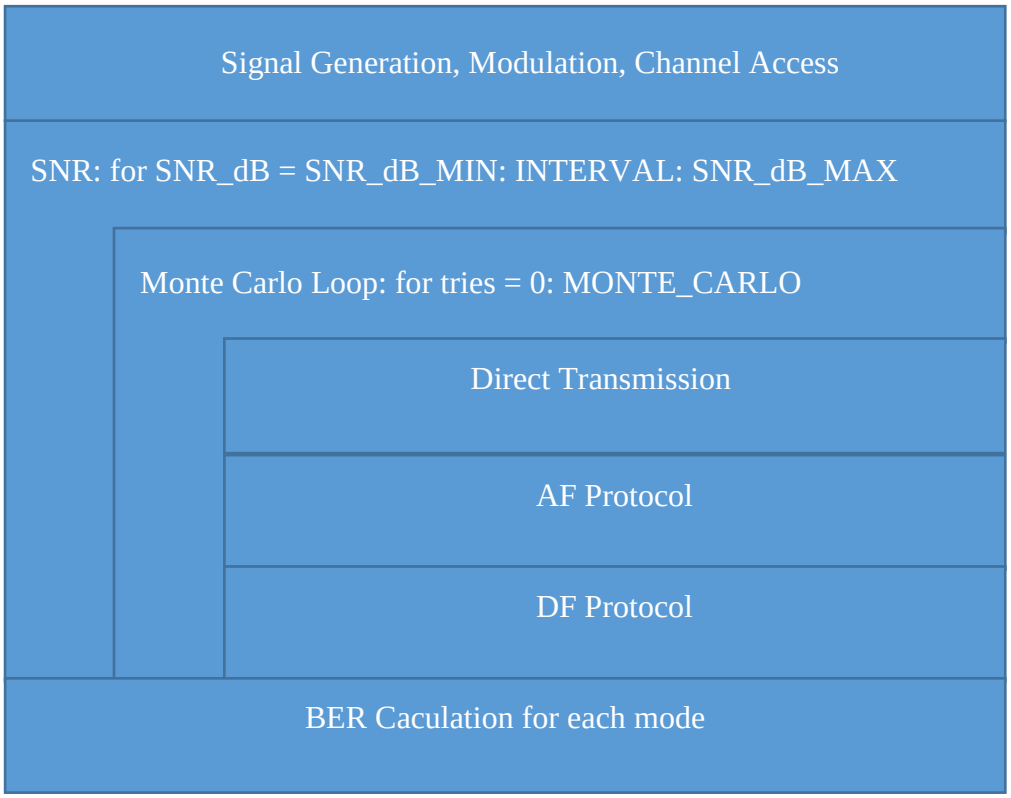

Figure 3-5 Simulation process diagram.

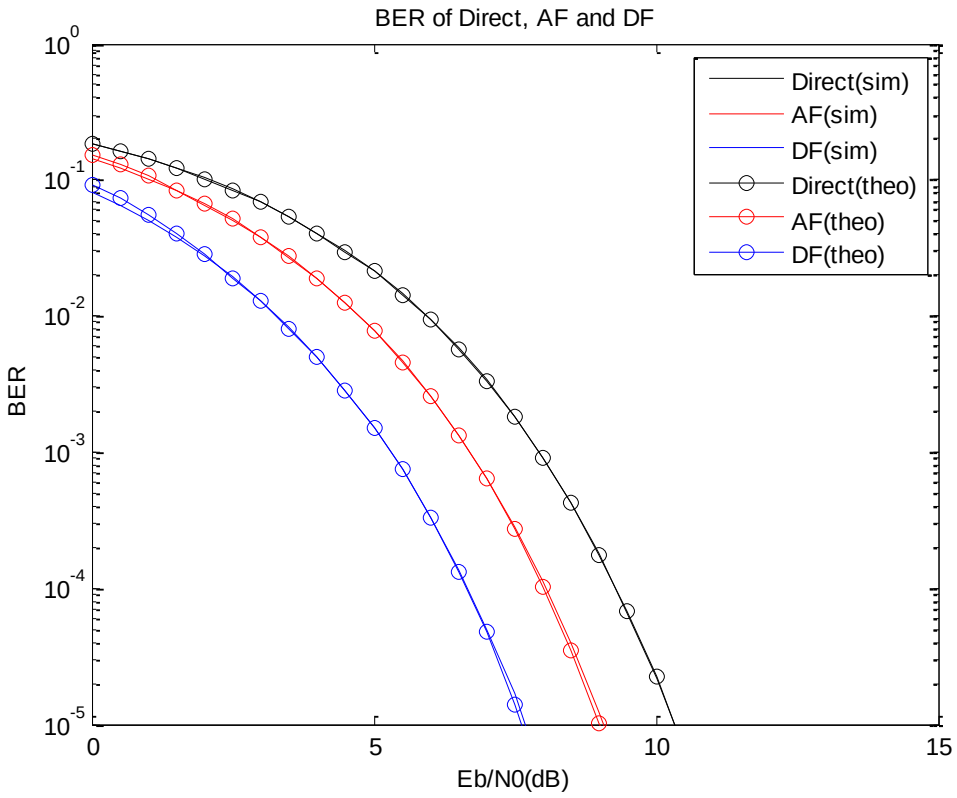

Figure 3-6 BER against Eb/No simulation and theoretical results of AF, DF and direct data transmission over the THz band using DBPSK.

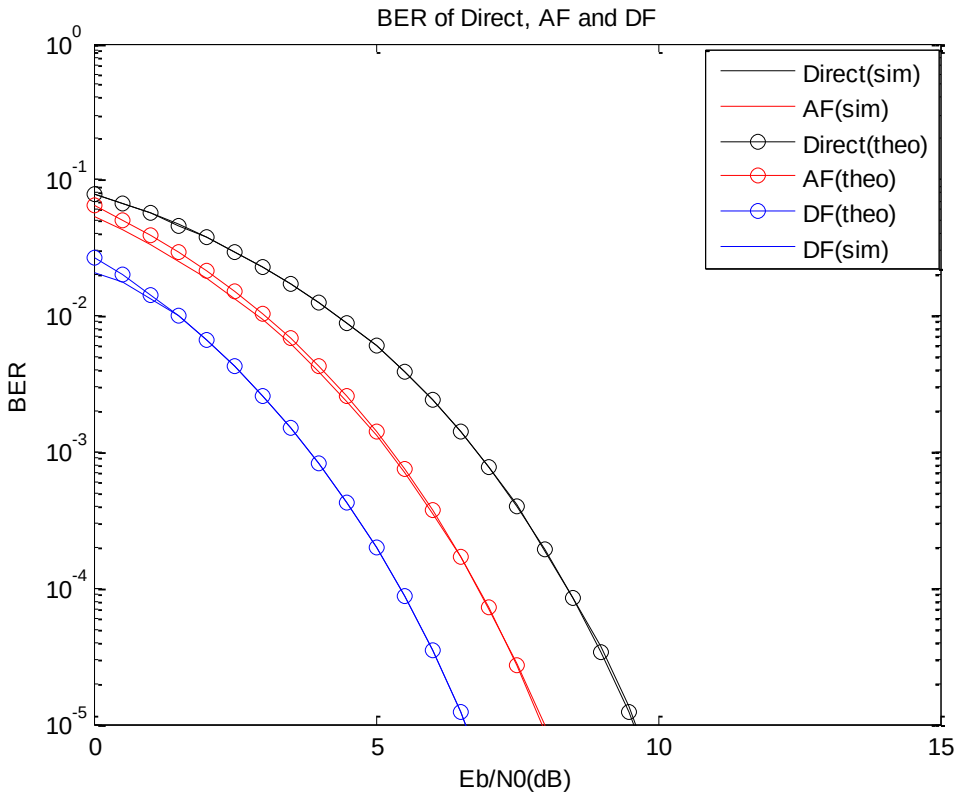

Figure 3-7 BER against Eb/No simulation and theoretical results of AF, DF and direct data transmission over the THz band using BPSK.

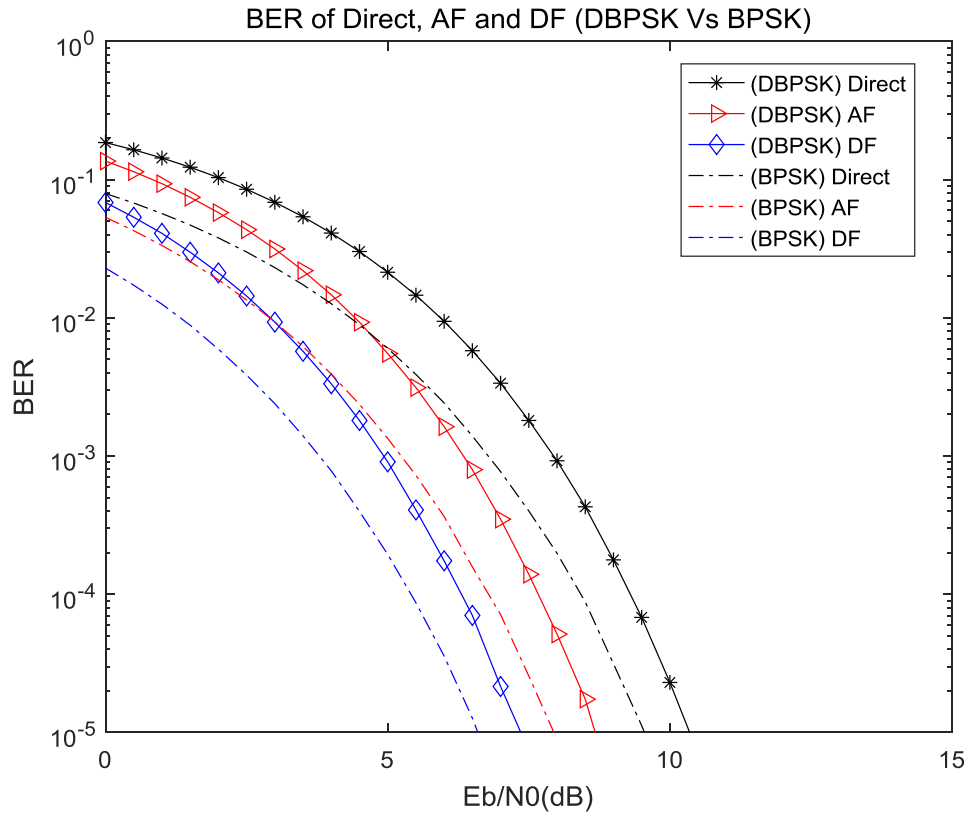

Figure 3-8 Comparison of BER against Eb/No simulation results of AF, DF and direct data transmission over the THz band using DBPSK and BPSK.

3.5 Conclusions

In this chapter, a single relay assisted communication scheme in the THz band for nanoscale networks has been introduced. Both AF and DF relays are studied in the THz channel employing DBPSK modulation to reduce the complexity and lower the power dissipation in the system. The simulation results have shown that relay-assisted transmission provides a significant improvement over the original direct transmission. The application of the DF scheme provides better performance than that of AF because the latter not only amplifies the signal but also the noise in the channel. Given the

energy and transceiver limitations for nanoscale operation, channel coding has not been considered in this first investigation. Furthermore, due to the complexity of the system at the nanoscale, only the single relay scheme is analysed in this chapter.

Chapter 4

Energy Harvesting for Body-Centric Nanonetworks in the THz Band Based on Nano-Rectennas

In Chapter 3, the relaying communication channel of Nanonetworks in the THz band was studied; in this chapter, an energy harvesting scheme in Nanonetworks is proposed for purpose of healthcare applications, i.e. Body-Centric Nanonetworks. One of the main challenges in the network is caused by the very limited power that can be stored in nano batteries in comparison with the power required to drive the device to communicate. Recently, novel rectifying antennas (rectennas) based on carbon nanotubes (CNTs), metal and Graphene have been proposed [143]–[145]. At the same time, research on simultaneous wireless information and power transfer (SWIPT) schemes has progressed apace [146]–[149]. Body-Centric nano-networks can overcome their energy bottleneck using these mechanisms. In this chapter, a nano-rectenna energy harvesting model is developed which provides a promising solution to the power supply for Body-Centric Nanonetworks. The energy harvesting is realized by a nano-antenna and an ultra-high-speed rectifying diode combined as a nano-rectenna. This device can be used to power nanosensors using part of the terahertz (THz) information signal without any other external system energy source. The broadband properties of nano-rectennas enable them to generate direct current (DC) electricity from inputs with THz to optical frequencies. The output power

generated by the nano-rectenna is calculated and compared with the power required for nanosensors to communicate in the THz band. The calculation and analysis suggest that the nano-rectenna can be a viable approach to provide power for nanosensors in Body-Centric Nanonetworks.

4.1 Motivations and Related Work

Healthcare and bioengineering is one of the most promising applications of Nanonetworks. In the domain of healthcare and bioengineering applications, the purpose is to develop a therapeutic nano-device network which is capable of working either on or inside the human body so as to support immune system monitoring, health monitoring, drug delivering systems and bio-hybrid implants [59]. A Wireless Body-Centric Nanonetwork consists of various nano-sized sensors with the purpose of healthcare application. As mentioned in the previous chapters, there are two main approaches for wireless communications at the nanoscale i.e. molecular and electromagnetic (EM) communications [9]. EM-based communication commonly operates in the terahertz (THz) band (0.1-10 THz) and is believed to be a promising technique for supporting data exchange in nano-sensor networks for healthcare application or Body-Centric Nanonetworks. As been demonstrated previously, given the limited size of implantable and on-body nanosensors, the frequency radiated by their antennas would be in the optical range, resulting in a very large channel attenuation that might render wireless communication at the nanoscale unfeasible. To overcome this limitation, Graphene-based antennas have been developed, which have dimensions of just a few μm but are able to resonate in the THz band at frequencies up to two orders of magnitude lower than metallic antennas of the same size [64].

4.1.1 Body-Centric Nanonetworks

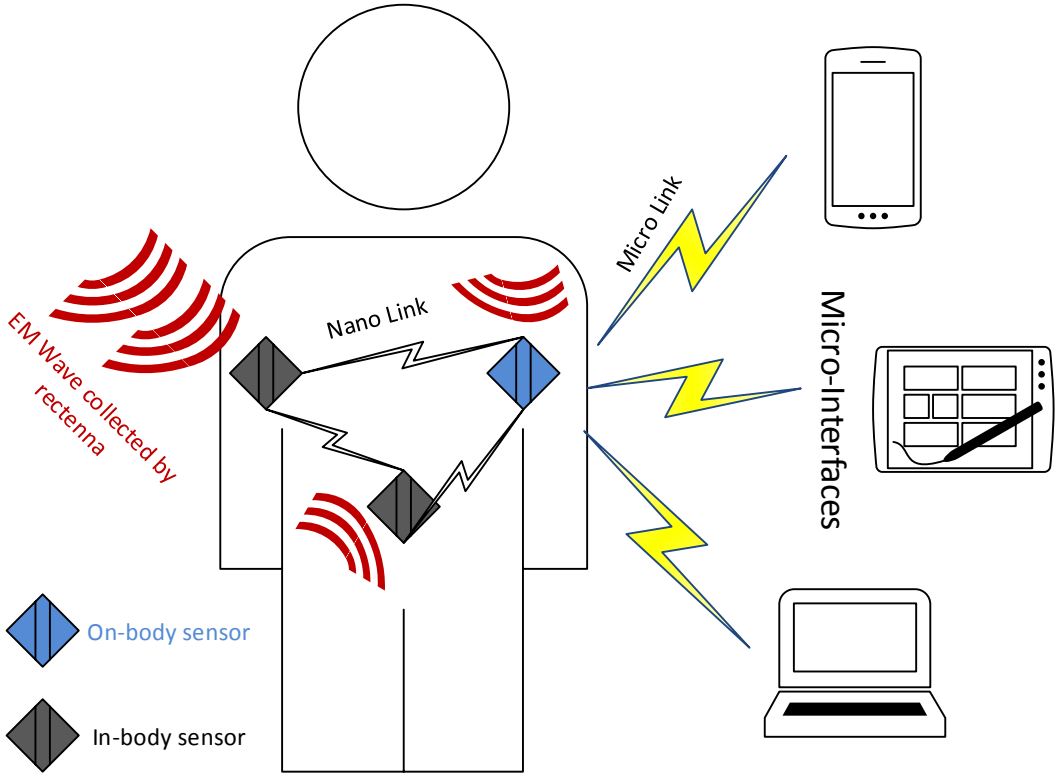

Figure 4-1 Architecture for Wireless Body-Centric Nanonetworks. Different nanosensors, distributed around and inside the body, can be used to gather and exchange data. The sensors are equipped with nano-rectennas for harvesting energy and nano-antennas for processing information. A wireless interface among micro devices and nanosensors is used to collect these data for healthcare centre.

A Body-Centric Nanonetwork shown in Figure 4-1 describes the communication among nano-sensors either distributed on the body, inside the body or on the body. In the Body-Centric Nanonetwork, nanosensors communicate with each other inside the body and a body worn interface is equipped to collect these data. The micro-interface then transmits the data to a healthcare provider. The nanosensors communicate in the THz band but the THz signal carries not only information but also energy [146].

Therefore, a nano rectenna integrated within nanosensors can harvest energy from the THz signal.

Body-area and Body-Centric networks have been widely studied in recent years [150], across a broad range of frequencies. Great achievements have been made in the research of body area networks based on microwave frequencies. Such networks built from traditional sensors are capable of monitoring all types of human data from outside the body. However, there are many extremely important parameters inside the body need to be measured and monitored [151]. The requirement of reducing the size of medical sensors and devices has attracted more and more research interest and made nanoscale technology an emerging and promising research area [152], [153]. Graphene and CNT-based nanoscale sensors operating at THz frequencies are capable of working inside the human body which opens the door to developing Body-Centric Nanonetworks in the THz band [154]. On account of the very short wavelength of THz waves and molecular resonances, THz radiation can be used to detect biomaterial tissues and liquids contents variations. Therefore, the properties of THz communication open up opportunities for developing diagnostic, detection and treatment tools for some skin disease by using the propagation of THz waves [155]. For example, implantable nanomedical devices, wearable medical sensors, and medical information exchange terminals. For the purpose of Body-Centric Nanonetworks, communication and information exchange among implantable nanosensors is the most significant aspect as it enables the control and monitoring of the molecular release or flow, biochemical compounds and other important functions inside the human body. Information collected from the body area can be then sent via a micro-interface to a healthcare centre.

4.1.2 Piezoelectric Nanogenerator

One of the major challenges in Body-Centric Nanonetworks is caused by the very limited power storage of a nano battery. Traditional harvesting mechanisms such as solar cells can convert light wave into direct current (DC) signals, however, at the nanoscale, due to the size limitation, the efficiency of solar cells is extremely low and they cannot therefore meet the necessary energy demand. Moreover, sunlight is not available for implanted nano-sensors and some other parts of the body.

Recently, a range of new energy harvesting methods for powering nanodevices has been proposed [43], [45], [48], [143], [156]–[160]. For instance, in [43], a piezoelectric based nanoscale energy harvesting system was experimentally demonstrated. While Jornet and Akyildiz [46], [161], have proposed an energy harvesting system for Nanonetworks based on a piezoelectric nano-generator. Recently, an ultrasound-driven piezoelectric nano-generator has also been proposed for powering in-body nano-sensors [47]. In [162], an energy harvesting protocol is designed for application in Body Area Nanonetworks. All of the subsequent developments followed from [42], where the seminal mechanism was developed based on the piezoelectric effect of ZnO (Zinc Oxide) nanowires. Two significant properties of ZnO make it an ideal candidate for self-powering nanosystems [42]. First, the existence of polar surfaces creates widespread unique nanostructures. Second, the short of centre symmetry leads to a piezoelectric effect, which is capable of converting mechanical stress and strain into electrical energy. For example, an electric current can be produced at the nanowire edges when bending or compressing them. Otherwise, an electric current is produced in the other direction when releasing the nanowires.

Therefore, by applying external energy, vibrations can be created to drive the compress-release cycles[43].

In [163], the power density of a ZnO nanowire-based nanogenerator is reported to be around 83 $\mathrm{nWcm^{-3}}$. The ZnO nanogenerator is applied to charge a supercapacitor in nanonetworks [46], where the size of the nanogenerator is 1000 μm^2, and the energy density of the supercapacitor is close to 1 $k\mathrm{W\ cm^{-3}}$ [164]. The ZnO nanowires of the nanogenerator are driven by an air system (vibration frequency = 50 Hz [46]), human heart beat (vibration frequency = 1Hz [46]) and ultrasonic waves (vibration frequency = 50 Hz [47]).

4.1.3 Nano rectenna Systems

However, a piezoelectric energy harvesting system is limited to some parts of the body because the power source of this technique is mechanical stress or vibration. For device implanted in the body, the energy harvesting system requires an outside power source such as ultrasound. In contrast, wireless power transfer mechanisms based on rectifying-antennas (rectennas) offer another promising technique for powering nanodevices in the Nanonetwork [143]–[145], [157]. Unlike traditional photovoltaic energy harvesters which rely entirely on sunlight, rectennas can operate at THz and microwave frequencies which enable them to work during the night. Moreover, traditional solar cells employ the quantum properties of light and are therefore limited by thermodynamic efficiency, only those photons with energy higher than the band gap of the semiconductor material can be absorbed. In contrast, rectennas operate in a completely different way which receives the radiation in wave form. Since EM waves carry not only information but also energy [146], nano-rectennas can therefore share the same signal that is used for transporting information

within Nanonetworks. As a result, simultaneous wireless information and power transfer (SWIPT) becomes a pivotal technique for powering Nanonetworks and is a promising solution to energy bottlenecks [146], [147], [149]. Research on SWIPT has been widespread in traditional EM wireless communications [147], [149], [165], but there are still no existing studies in the area of THz band communications at the nanoscale. In this chapter, the focus is on the design of nano-rectennas which the key elements of SWIPT systems in the THz band will be. A major advantage of the technique is that the proposed nano-rectennas are able to convert an EM signal into a DC (direct current) signal without any external system power source. Moreover, the achievable energy conversion efficiency for a rectenna in principle is very high. For example, efficiencies of around 85% have been reported in [166].

In this chapter, a novel energy harvesting method for nanosensors based on a nano-rectenna is proposed for Nanonetworks in a healthcare application. The available energy that a nano-rectenna can harvest at a nano-sensor is calculated and the potential output power is computed. For both a CNT rectenna array and an Au/CuO/Cu rectenna array, analytical expressions for time taken to charge a supercapacitor is presented and this is compared to the performance of the existing system (piezoelectric with ultrasound). The results show that a 25 element Au/CuO/Cu rectenna array provides the best performance and is able to meet the energy requirement in a Body-Centric Nanonetwork. The findings show that the proposed system has a great advantage over the existing system.

The rest of the chapter is organized as: Section 4.2 illustrates the fundament layout of a rectenna. Section 4.3 introduces the energy harvesting system with different nano rectennas. The following Section demonstrates the power output of

energy harvesting system and the corresponding performance. Numerical results for comparison among different systems are also presented in this section. Finally, Section 4.5 concludes the key findings and the future work of the chapter.

4.2 State of Art of Rectennas

4.2.1 Review of Rectennas

In 1964, the world's first rectenna was made by William Brown supported by the US Air Force [167]. The rectenna converted microwave to electricity that successfully powered a micro-helicopter. By using a fast-switching Schottky barrier diode with an optimized matching configuration between antenna and diode, the efficiency of the 2.45 GHz rectenna was successfully increased to 92% by Brown's later work [168]. Motivated by Brown, rectenna devices operating at RF/microwave frequencies have been extensively investigated [166], [169]–[171]. The great achievements for such rectennas have inspired increasing research interest and the extension to THz and much higher frequencies. Attempts to manufacture rectennas in the THz band have been started over several decades [172]–[174]. For example in [174], a high-efficiency device for converting solar power to DC electricity was proposed which consists of a dipole antenna array and an insulating sheet. In 1996, Lin et al. experimentally illustrated a sub-nanostructure device that absorbs and rectifies waves at optical frequency, where a parallel dipole antenna array was fabricated on a p-type silicon substrate [175]. More recently, most investigations have focused on characterizing metallic nano particles in the optical band [176]–[179]. The observed surface plasmon oscillations are not only useful for visible and infrared structures but also helpful for THz antennas [180]. In [181], Kotter et al. have successfully manufactured

nanoantennas on a flexible substrate, which can be applied to form a nano-rectenna. To complete the device a sufficiently fast enough rectifier is needed for the THz signals. Making the use of tunnelling effect is the only way to achieve rectification in THz frequencies [144]. Semiconductor-based diodes or rectifiers are therefore not available for THz rectennas as they are limited by their physical properties. The operating frequencies of traditional p-n junction diodes are limited due to the transit time of charge carriers. A type of Schottky diode that works in the THz frequency range has been presented in [182]. It is reported in [183] that Schottky diodes are fast enough for frequencies lower than 25 THz, with very good anti-noise performance for frequencies under 5 THz. At higher speeds, metal-insulator-metal (MIM) diodes using the concept of tunnelling through insulators are the most suitable devices [184]. The integration of a nano MIM diode with a nano antenna will therefore form a nano rectenna.

In [15]–[19], [24] and [25], different kinds of nano-rectennas have been experimentally demonstrated. A unipolar nano-diode based on an asymmetric nanochannel has been reported in [158]. The diode is a self-switching device (SSD) and operates at frequencies of up to 1.5 THz; in the paper, the nano-diode is coupled with a THz bowtie antenna to form a rectenna paradigm. Zhu et al. proposed a rectenna with a high-performance Graphene geometric diode integrated with a Graphene bowtie antenna in [16], and a metallic bowtie antenna in [21]. Later in [159], Dragoman et al. introduced a Graphene-based THz receiver, where two diodes made from Graphene are fabricated with a dipole, and a bowtie THz antenna, respectively. The rectennas operating at frequencies of up to 10 THz obtained nearly constant responsivity over the entire band with a peak (0.42 AW^{-1}) at 5 THz. Then in [144]

and [156], a bowtie dipole gold nano-antenna coupled with a metal-insulator-metal (MIM) diode has been fabricated and measured. The rectenna, which operates around 28.3 THz and higher frequencies, can harvest energy from the THz signal or from waste energy in the ambient environment. The device comprised an insulating copper oxide layer (CuO) sandwiched between gold (Au) and copper (Cu) to make the Au/CuO/Cu MIM structure and had a responsivity at zero bias of 5 AW^{-1}. In [48], a Graphene rectenna operating in the 0.4-1.1 THz band has been proposed where the antenna and rectifier are fabricated in an integrated manner. As a result of this construction, the impedance mismatch between the antenna and the diode is eliminated. It is reported that the measured conversion efficiency of the Graphene rectenna is as good as an RF rectenna, being 58.43% at 0.9 THz. A CNT based rectenna has been proposed in [143] which consisted of millions of CNTs operating as nano-antennas with their tips fabricated from Insulator-Metal (IM) to behave as diodes. The CNT rectenna showed great potential for wireless EM powering Body-Centric nanodevice applications.

4.2.2 Operation Principle of Rectennas

A typical rectenna, shown schematically in Figure 4-2, is a combination of an antenna and a rectifying device, usually a diode. The antenna collects the power from the ambient EM waves and generates an AC voltage, the diode then rectifies the AC to DC current.

For the purpose of energy harvesting in Nanonetworks, the EM waves are received by a nano-antenna and then coupled to a high-speed rectifier to complete the rectenna configuration. Therefore, the core components of a nano-rectenna are a high-speed rectifier (diode) and a nanoscale antenna, which can be used for harvesting

energy from THz and higher frequencies. As nano-sized antennas operate in the THz band, their associated rectifying diodes need a fast response so that they can react appropriately to the incoming THz signal and deliver a DC signal. The nanoantenna collects high frequency freely propagating EM which it converts into AC current that passes to the ultrafast diode, which then converts this current to DC.

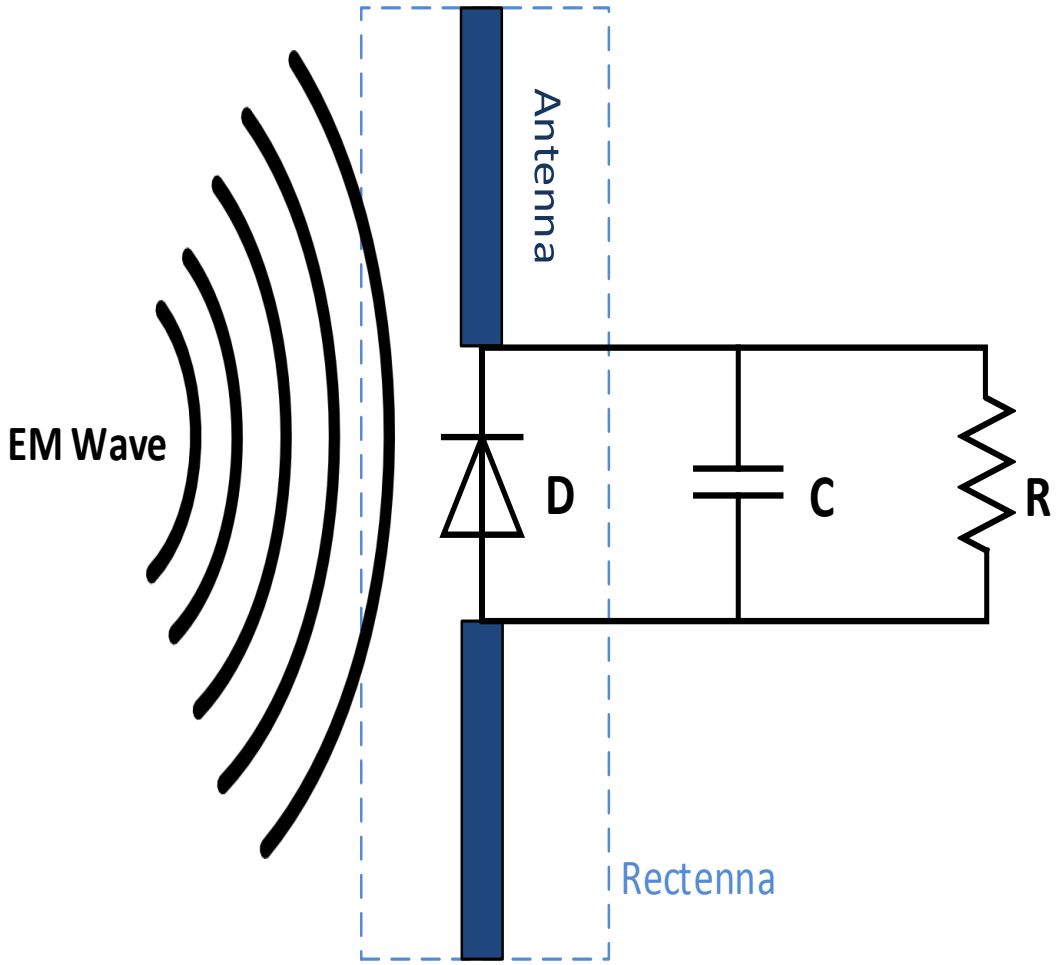

Figure 4-2 The schematic diagram of a rectenna. A dipole antenna and a diode coupled to a rectenna [185].

4.2.3 Ultrafast Diodes for THz rectennas

It is essential to find the fast-enough diodes that work at THz and higher frequencies. As aforementioned, two kinds of ultrafast diodes have been reported recently, i.e. MIM diodes and geometric diodes. Figure 4-3 shows the energy band diagram of a typical MIM diode without bias [186]. For a MIM diode, the charge carriers tunnel from one metal with a higher barrier to the other lower barrier metal through the insulator (an oxide with the thickness of some nanometres) [187]. For the Au/CUO/Cu

MIM diode, the two metals are gold and copper, with a work function of 5.1 eV and 4.7 eV respectively. Moreover, for the CNT rectenna, the tips act as MWNT-I-M diodes[188], shown in Figure 4-6. In order to achieve higher power transfer efficiency, impedance matching between the MIM diode and the antenna should be met using circuit analysis. Zhu et al. claim that low barrier height i.e. less than 0.5 eV can lower down the impedance of a MIM diode to be around 100 Ω [189].

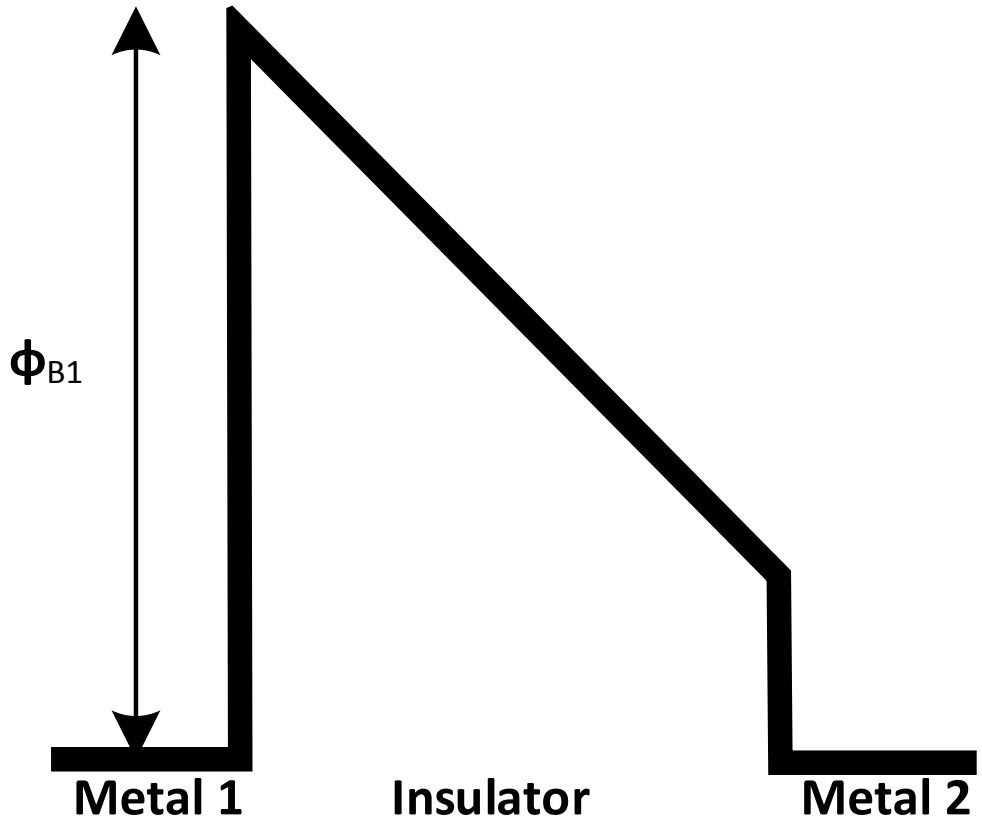

Figure 4-3 Band diagram of a MIM diode. The barrier height of Metal 1 is larger than Metal 2[186].

For a geometric diode shown in Figure 4-4, as a result of the funnelling effect, the movement of charge carriers is easier from the forward direction (left to right) than the movement from the opposite direction [145].This physical shape asymmetry

causes an asymmetric charge carrier movement probability between forward and backward directions which creates diode behaviours in such devices. The neck region is the critical region of a geometric diode. For charger carriers moving forward, they are more likely to channel through the neck region or be reflected off the diagonal boundaries crossing the neck, other than the opposite moving charge carriers which are highly likely impeded by the flat boundaries. In contrast to parallel-plate structural diodes (e.g. MIM diodes), geometric diodes have a planar structure which results in much smaller capacitance. Moreover, since geometric diodes are fabricated from continuous conductive materials such as graphene, their resistances are also quite low, which is a benefit to match the impedance of antennas.

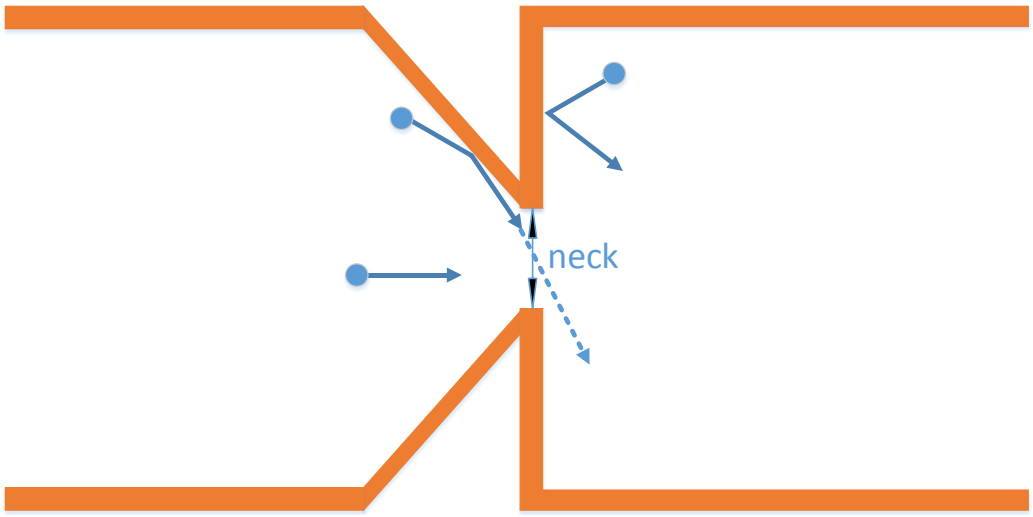

Figure 4-4 A inverse arrowhead geometric diode [145].

4.3 Nanosensor Energy Harvesting

In this section, a Body-Centric Nanonetwork energy harvesting system using CNT nano-rectenna and a nano-rectenna with an Au/CuO/Cu MIM diode is studied. As stated above, since traditional energy harvesting schemes are not available for Body-Centric Nanonetworks, a rectenna-based scheme is promising. If the rectenna is treated as a nano-generator as shown in Figure 4-5, it consists of a nano-rectenna e.g. a nanotube rectenna and an ultra-nanocapacitor. The rectenna is represented by its series resistance R_G and output voltage. The antenna receives an EM wave and produces a voltage V_G, which is rectified by the diode to supply a DC charging current to a ultra-nanocapacitor C_{cap} .

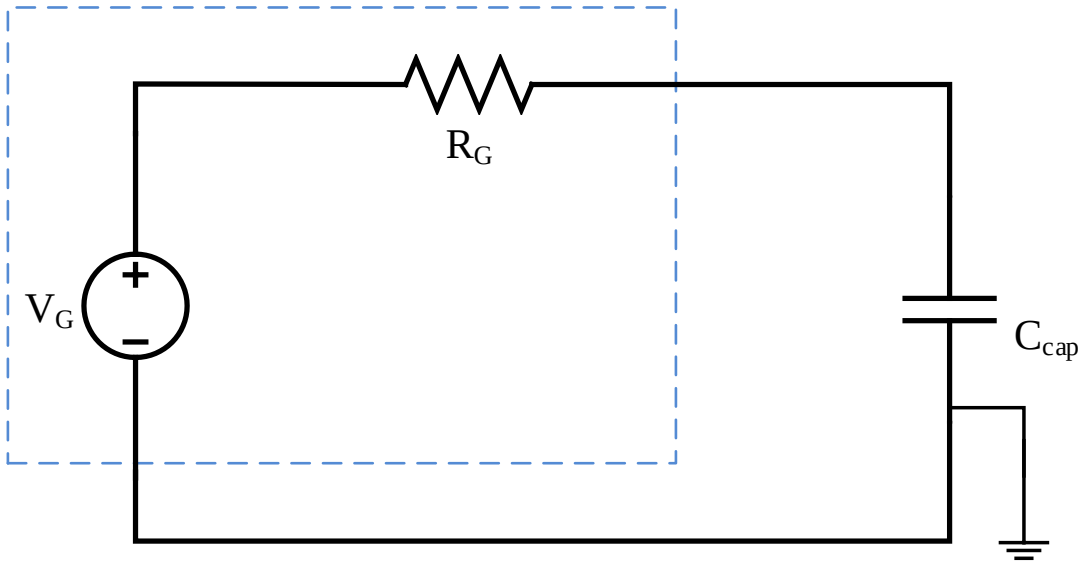

Figure 4-5 An equivalent circuit by treating the rectenna as a voltage source.

For example in [143], the CNT rectenna device is shown in Figure 4-6, and the CNTs behave as antennas with their small tip areas act as rectifying diodes. When the CNTs absorb EM radiation, a DC current will be generated after rectification by the tip area. This converted current is used to charge a capacitor [143]. The conversion

process continues using the THz signal within the system and ambient free EM so the energy source of such a nano-rectenna generator needs no other specific external power source.

In [144], [145], [156], [157], bowtie dipole nano-rectennas have been proposed, and have the form shown in Figure 4-7; they are fabricated in gold with lengths of approximately 5-6 μm with two 2-3 μm triangular sections. The antenna thickness is 100 nm, and the nano diodes, made from Graphene [145], [157] or MIM [144], are located in the middle of the bowtie antenna gap area, producing the rectenna action. A series of these rectennas can be connected to form a nano-rectenna array as shown in Figure 4-7. The bowtie dipole antenna receives EM radiation and converts the signal to AC current flow to the nano diode. The diode then rectifies the AC electricity to DC electricity. When connected to an ultra-nanocapacitor as shown in Figure 4-2, the rectified DC electricity can be harvested and used by nanosensors.

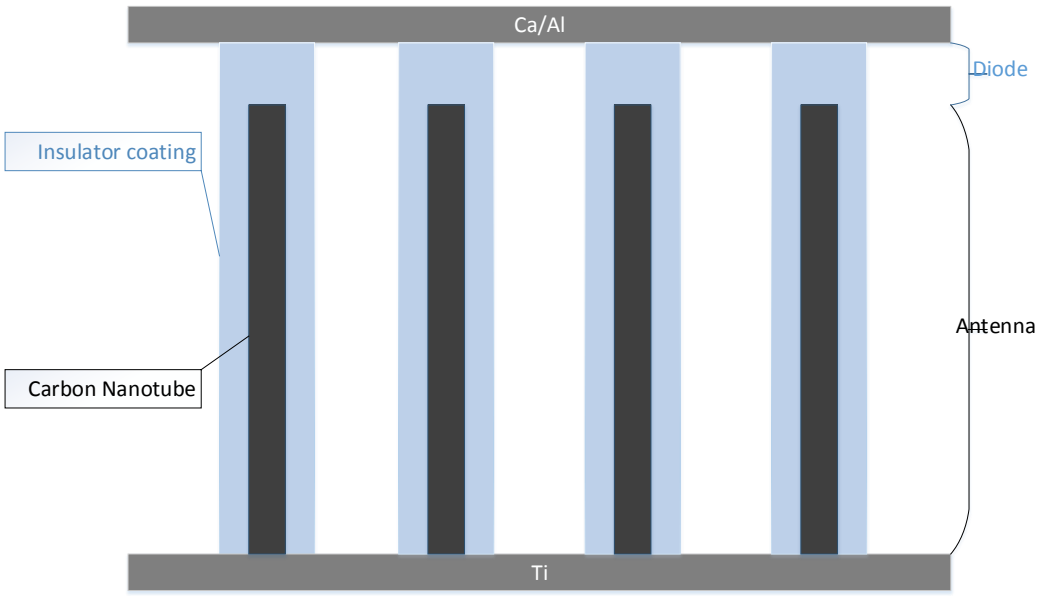

Figure 4-6 Schematic diagram of the CNT rectenna. Insulator-coated CNTs are vertically aligned at a density of 10^{10} cm^{-2} on a coated metal (Ti) substrate, and with

their tips capped with Ca/Al. The CNTs behave as antennas which collect EM waves to the tip areas (which act as diodes), where the waves are converted to DC

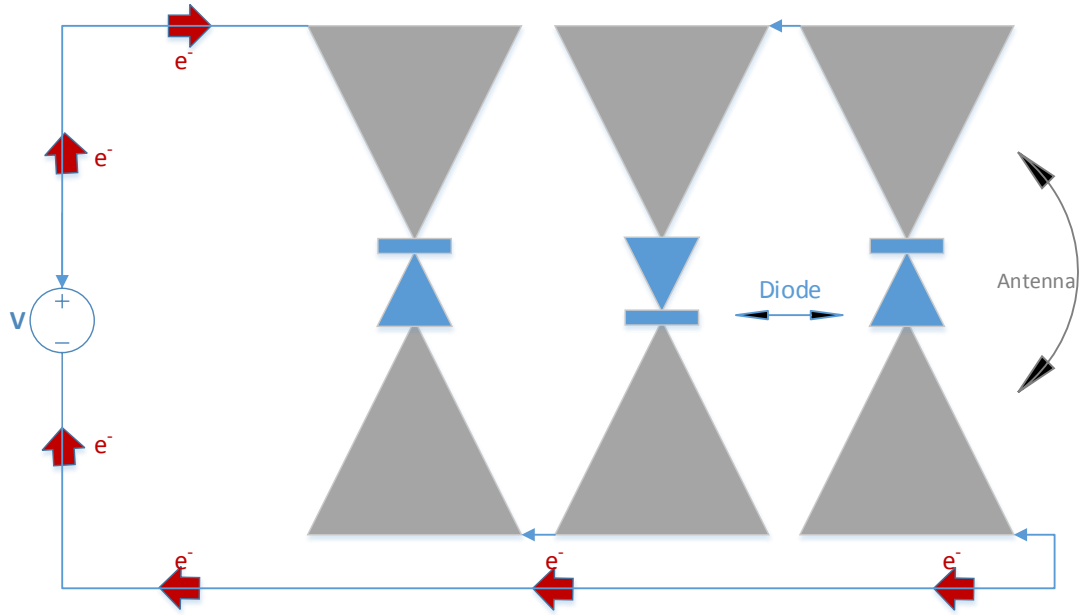

Figure 4-7 Schematic diagram of bowtie nano-rectenna array.

For the THz frequency range, the nano-rectenna can be analysed using the classical formulas for macroscale devices [190]. The performance of a nano-rectenna is mainly determined by three characteristics, the first and the most important one is responsivity which is defined as the direct current generated by the induced EM radiation power over the rectenna. It represents the amount of DC current that can be induced for a given input AC EM wave power and can be calculated as [191]:

$$\xi = \frac{1}{2}\frac{I''(V_{bias})}{I'(V_{bias})} \tag{4.1}$$

which is the ratio of the second to the first derivative of the current. For the purpose of energy harvesting, the bias voltage will be set to zero.

The diode resistance is the second important characteristic which determines the performance of the rectenna. Therefore, resistance matching between the antenna and the diode is important. For instance, in [144], the reported rectenna has an antenna resistance of 100 Ω and a diode resistance of 500 Ω which results in a relatively good match.

Thirdly, the diode's cut-off frequency is another important characteristic. The rectenna EM wave absorption efficiency is limited by this cut-off frequency, all frequencies lower than this frequency can be harvested. Moreover, for a nanoantenna, the required frequency is in the THz range. The cut-off frequency of a rectenna can be calculated as:

$$f_c = \frac{1}{2\pi R_{rec} C_D} \tag{4.2}$$

where R_{rec} is the rectenna's equivalent resistance and C_D is the capacitance of the diode (determined from the standard expression in terms of the device permittivity and physical dimensions).

The DC current generated by the rectenna can be calculated from:

$$I = [I(V_{bias}) + \frac{1}{2}\frac{\xi}{R_d} V_{ac}^2] \tag{4.3}$$

where V_{ac} is the input AC voltage and R_d is the rectifier differential resistance.

Otherwise, the current generated by the rectenna can also be calculated based on the input power from:

$$I = P_{in} A_{eff} \eta_a \xi \eta_c \tag{4.4}$$

where P_{in} is the input EM wave power, A_{eff} is the effective area of the antenna, $\eta_a \eta_a$ is the absorption efficiency of the antenna and η_c is the rectenna coupling efficiency given by:

$$\eta_C = 4\frac{\dfrac{R_a R_d}{\left(R_a + R_d\right)^2}}{1+\left(2\pi f \dfrac{R_a R_d}{R_a + R_d} C_D\right)^2} \tag{4.5}$$

where f is the frequency of the radiation received by the antenna and R_a is the resistance of the antenna (Figure 4-8).

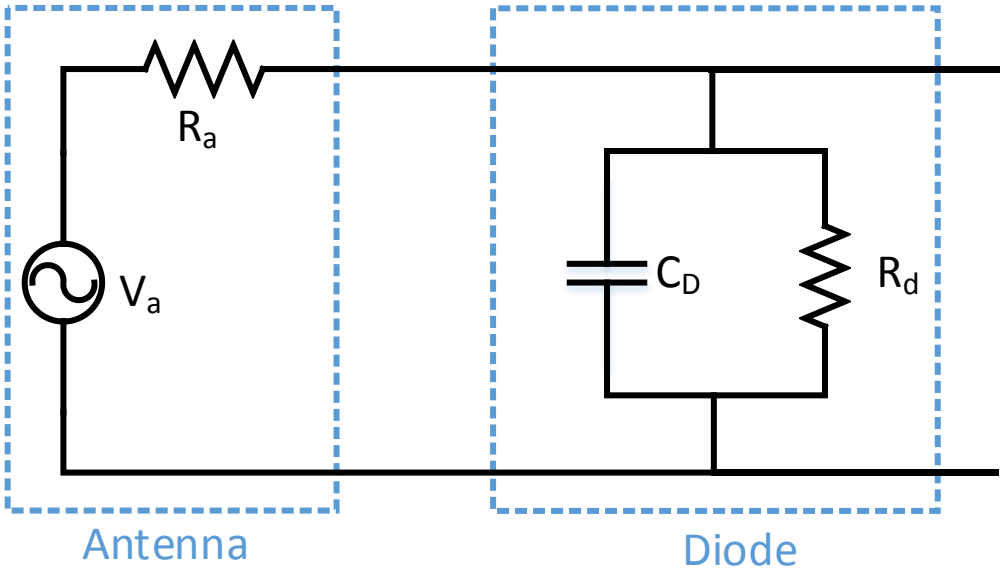

Figure 4-8 Small-signal circuit diagram of a rectenna [190].

The DC voltage generated from the rectenna is given by:

$$V_D = -\frac{1}{2}\xi V_{opt}^2 \tag{4.6}$$

Therefore, the output power of the rectenna can be calculated from the formula below:

$$P_{out} = -\frac{\xi^2 V_{opt}^4}{16 R_d} \tag{4.7}$$

where V_{opt} is the AC output voltage of the antenna.

4.4 Performance Analysis and Comparisons

In this section, the performance of different rectenna devices is analysed. The output powers of the proposed schemes are calculated, and the results are compared with the existing schemes.

According to the results reported in [143], the output voltage generated by the CNT rectenna is of the order of tens of millivolts. For instance, the output power using a 1064 nm input EM wave can be calculated based on the results obtained from [143] , which are V_{opt} = 68 mV, ξ = 0.4 A W^{-1}, and R_d = 80 Ω, permitting calculation of the output power of the rectenna from (4.7) as 2.67 nW. In accordance with [59], [121], a femtosecond pulse based channel access scheme will be applied to the Nanonetwork, shown in Figure 4-5, those digits "1" are transmitted using 100 fs (i.e. T_p=100fs) long pulse while digits "0" are transmitted as silence. For example, in Figure 4-9 the sequence "110100" is transmitted. According to [121], the required peak pulse power is reported to be 1 to 10 μW (i.e. 10^{-18} J of energy). As the separation time among adjacent bits (symbol duration) is 1000 times the pulse duration (T_s=100ps), the average power will be brought back to the nW level [47]. Thus, the output power of the CNT rectenna is able to satisfy the power requirement of the system. As stated above, the rectenna in [144], has a responsivity of 5 A W^{-1} and zero bias resistance of 500 Ω. The contact area of the diode is 0.0045 μm^2, with a 7 nm thickness and the relative dielectric constant of CuO is 18.1. Using these values gives the diode's capacitance as approximately 10^{-16} F. The rectenna coupling efficiency can, therefore, be calculated from (4-3) to be 17.4% operating with a 28.3 THz EM input. As reported in [192], the effective area of the antenna is 37.5 μm^2 and the absorption efficiency is 37%. When a power density of 49 $mW \cdot mm^{-2}$ forms the input to the rectenna,

according to (4.4), the output DC current is 0.47μA and hence the calculated power output of this single nano-rectenna is 0.11 nW.

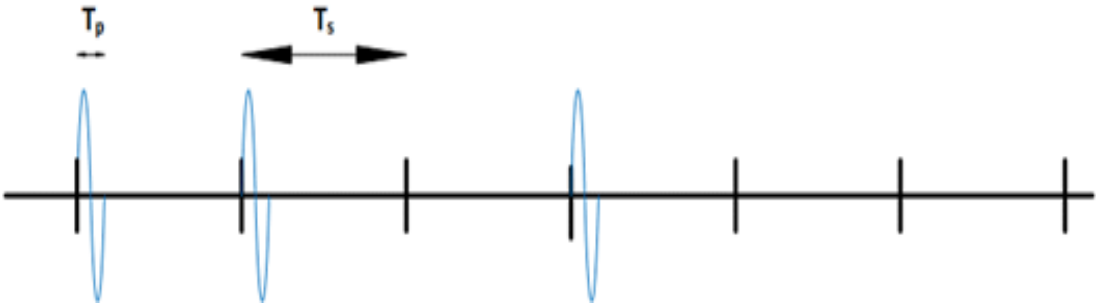

Figure 4-9 Transmitting the sequence "110100" with pulse duration of 100 fs and symbol duration of 100 ps.

According to the previous results computed for a CNT rectenna, it can generate a power output of nearly 3 nW with a CNT 5000 μm^2 containing about 10^8 nanotube rectennas. The single bowtie rectenna is 10.6 μm long with a 50° bow angle and the size is reported to be around 37.5 μm^2. However, the target size of the implantable nanosensors is expected to be 10 to 1000 μm^2, hence, the CNT rectenna is better for use in powering on body devices whilst the bowtie rectenna can be used for implantable nanodevices. As the power output of a single bowtie rectenna is 0.11 nW, an array of these rectennas can be used to obtain the required power and size. More elements connected in series can increase the production of current and power, Figure 4-10 illustrates the energy production ability for different number of array elements. It is assumed that the rectenna array consists of 25 elements, which are all perfectly coupled to give a maximum output power of 2.75 nW. As is shown in Figure 4-3, the rectenna is treated as a generator with an ideal power source V_G and a resistance R_G. The charging voltage to the ultra-capacitor is

$$V_c = V(1 - e^{-t/RC_{cap}}) \tag{4.8}$$

The energy that stored in the ultra-nanocapacitor is then calculated as:

$$E = \frac{1}{2} C_{cap} V_c^2 \tag{4.9}$$

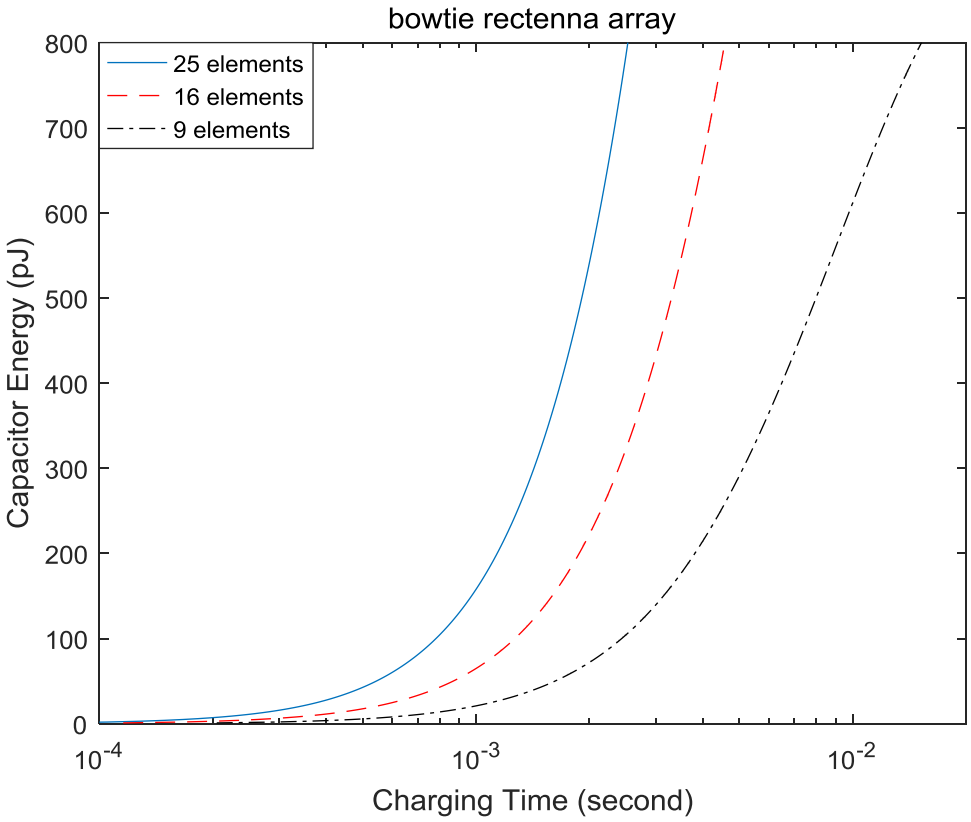

Figure 4-10 Energy production ability compassion among different number of array elements for bowtie rectenna

In [46], a 9 nF ultra-nanocapacitor (with the areal capacitance of $0.9\,\mathrm{mF}\cdot\mathrm{cm}^{-2}$ and a size of $1000\,\mu\mathrm{m}^2$) was used and the resulting maximum capacity from (4.9) was about 800 pJ. The harvesting system based on the piezoelectric technique takes 50 seconds to charge a 9 nF nanocapacitor for 50Hz external vibrations (i.e. ultrasound) and some 42 minutes using 1 Hz external vibrations [46], [47], [161]. For a CNT rectenna device, the maximum output voltage reported is 68 mV and for a 25-

element bowtie rectenna array it is 170 mV. Therefore, according to (4.9), a bowtie rectenna array delivers more charge than the CNT rectenna. As is shown in Figure 4-10, when both these rectenna devices are used to charge the same ultra-nanocapacitor (9 nF) it is apparent that the CNT rectenna takes more time (over 6 minutes) because of its very high junction resistance. While for the bowtie rectenna, the resistance is comparably very small thus it just takes about 6 ms to supply more energy for the capacitor. In [193], a novel 3D structure ultra-capacitor has been demonstrated, which supports an areal capacitance over 100 $\mathrm{mF \cdot cm^{-2}}$, for instance, a 350 μm^2 sized capacitor was used to compare the charging time for different energy harvesting devices i.e. a CNT rectenna, a 25-element bowtie array rectenna and a piezoelectric nano-generator. According to the results shown in Figures 4-10, 4-11 and 4-12, it takes 30 minutes to charge the capacitor reaching 800 pJ energy for a CNT rectenna, and 2.2 seconds, 86 seconds, 71.7 minutes for a 25-element bowtie array rectenna, a piezoelectric nano-generator with 50 Hz and 1 Hz external vibration, respectively. Therefore, the smallest sized 25-element bowtie rectenna is the most efficient and moreover, this rectenna does not need any external system energy source while producing DC directly from EM signals of broadband frequencies as well as the CNT rectenna. While a piezoelectric generator requires external system driving power (ultrasound) which is a big drawback in contrast to nano-rectennas. However, the piezoelectric nano-generator supply the highest output voltage i.e. 0.42 V, which enables the application of more requirements for nanosensors. Furthermore, in contrast to an RF rectenna, where its antenna and rectifier work independently, the two components of both CNT rectenna and bowtie rectenna are fabricated compactly which can reduce the propagation loss and achieve a good conversion efficiency [143],

[144]. Table 4-1 shows the general properties of different schemes. Note that the total size of a piezoelectric nano-generator is comprised of an area of 1000 μm^2 nanowires, 1000 μm^2 ultra-capacitor and space for wiring.

Table 4-1: General properties of different nanoscale energy harvesting schemes

Schemes	Size	Output voltage	Energy Source
Piezo(50Hz) [46],[47]	>2000 μm^2	0.42 V	Air-conditioning system or Ultrasonic Wave (system external)
Piezo(1Hz) [46]	>2000 μm^2	0.42V	Human Heart Beat (system external)
CNT Array [143]	~5000 μm^2	68mV	THz to optical
Bowtie Array (25 elements) This work	~1000 μm^2	170mV	~28THz

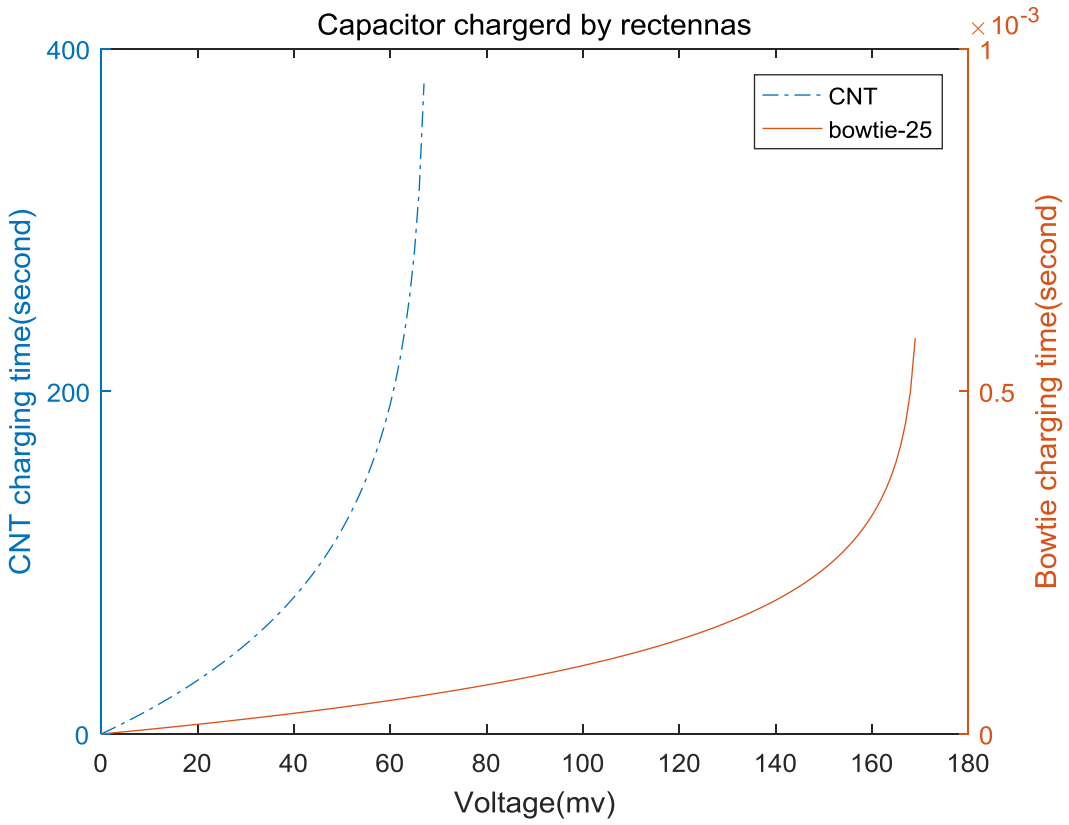

Figure 4-11 Time taken for CNT rectenna and 25 elements bowtie rectenna array charging the ultra-nano-capacitor, the bowtie rectenna array produce a higher voltage output.

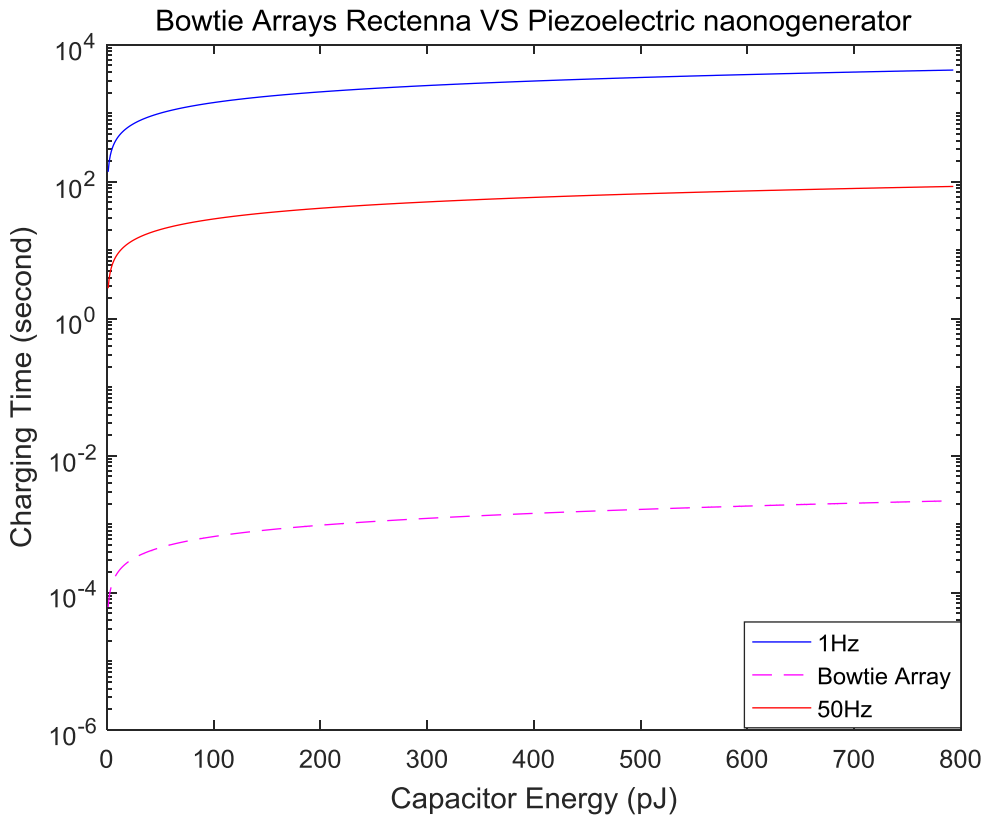

Figure 4-12 Time taken for 25 elements bowtie rectenna array and Piezoelectric nano-generators charging the ultra-nano-capacitor.

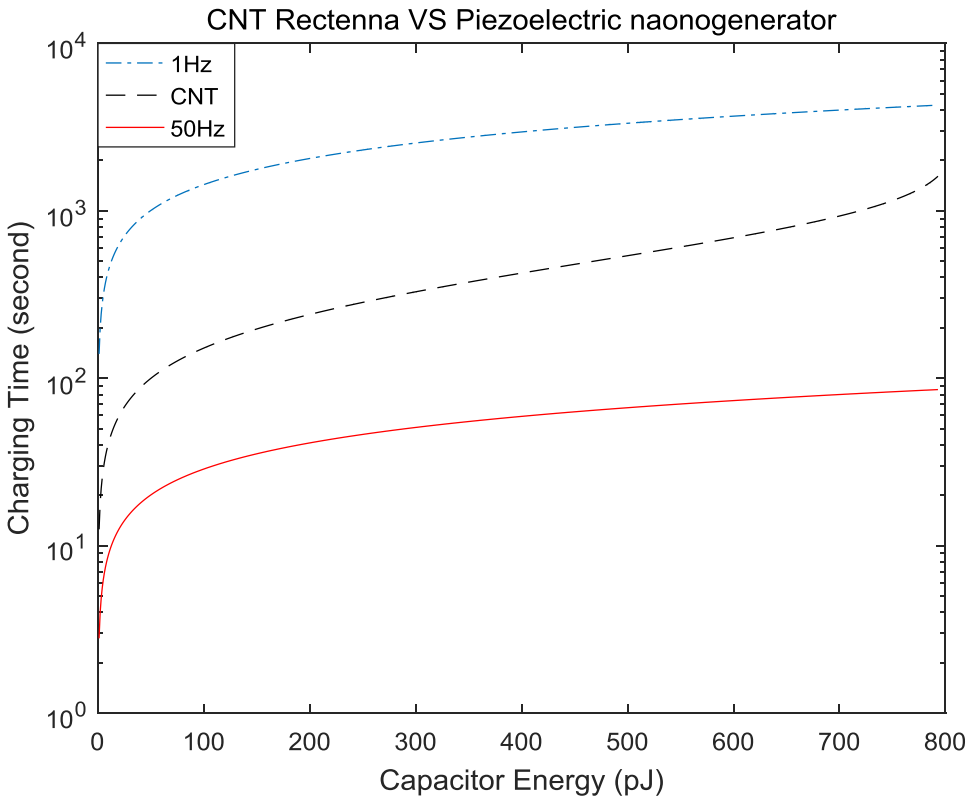

Figure 4-13 Time taken for CNT rectenna and Piezoelectric nano-generators charging the ultra-nano-capacitor.

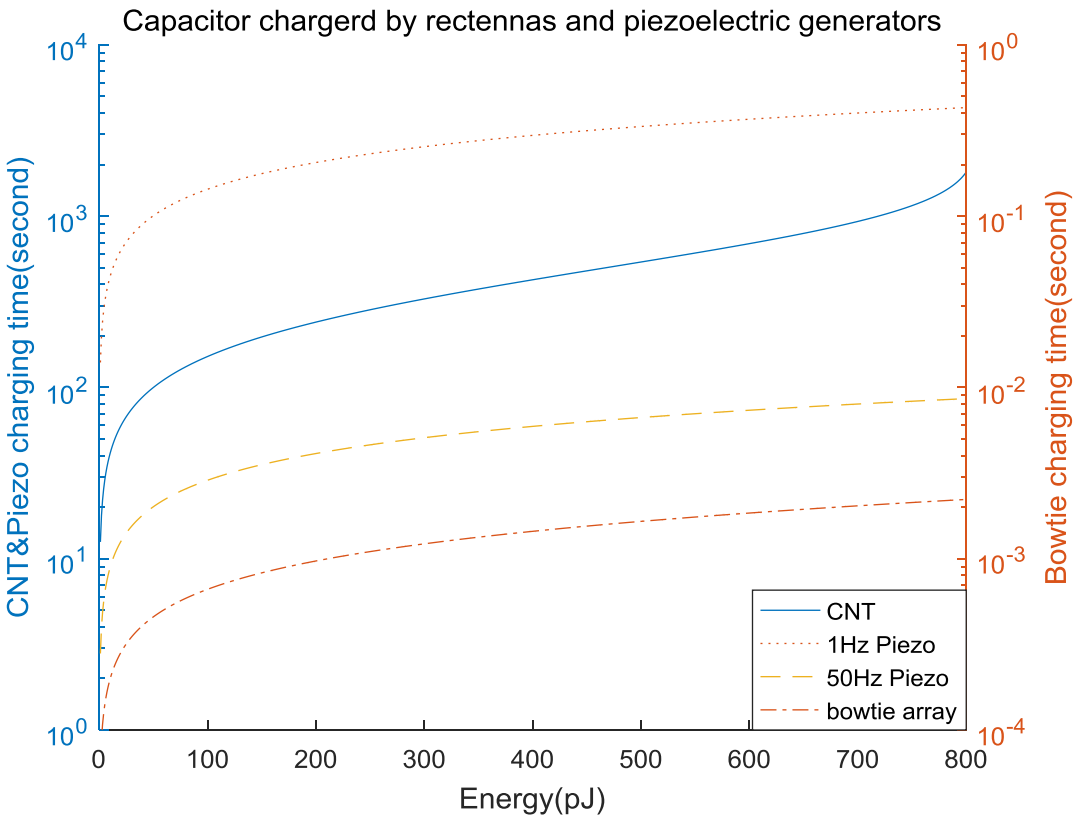

Figure 4-14 Time taken for CNT rectenna and 25 elements bowtie rectenna array and Piezoelectric nano-generators charging the ultra-nano-capacitor, the bowtie rectenna array is the most efficient while Piezoelectric nano-generator supply the highest output voltage.

4.5 Conclusions

In this chapter, an energy harvesting system based on nano-rectennas for wireless Body-Centric Nanonetworks has been proposed. This is developed based on nanoscale rectennas which act as generators in the system. Along with the continuing advancement of the SWIPT technique, the pioneering CNT array rectenna and the bowtie array nano-rectenna open the door for the wireless powering of nanosensors.

Since a nano-rectenna is able to power nanosensors without any external system source and its broadband property enables rectenna to be a very efficient and promising way to power implanted and body area nanodevices. An analysis of the new energy harvesting mechanism and its application in nanosensor network has been presented. The CNT array rectenna can successfully supply the power required by wireless Body-Centric nanonetworks at around 27.5 nW. Moreover, the bowtie array rectenna is of a much smaller size but provides similar power. There has also been a comparison of the two nano-rectennas with a piezoelectric nano-generator. Although nano-rectennas cannot provide as high a voltage when compared to a piezoelectric nano-generator, a bowtie nano-rectenna array is much more efficient while producing DC directly from the THz signal within the system and ambient EM signal without any other system external power source.

Chapter 5

Simultaneous Wireless Information and Power Transfer for AF Relaying Nanonetworks in the Terahertz Band

As mentioned in the previous chapters, a nanonetwork is comprised of nanoscale sensors and communicating devices facilitating communication at the nanoscale, which is a promising technology for application in health applications such as intra-body health monitoring and drug delivery. However, the performance of communication within a nanonetwork is substantially limited by the energy loss as the Electromagnetic (EM) wave propagates along the channel. Energy harvesting for nanosensor networks can provide a way to overcome the energy bottleneck without considering the lifetime of batteries. Moreover, relaying protocols for nanoscale communications have been proposed in Chapter 3 to improve the communication performance and extend the transmission distances among nanosensors within nanonetworks. The combination of energy harvesting and a relaying protocol provides an emerging solution to not only overcome the aforementioned energy issues but also enhance the system performance. Therefore, in this chapter, simultaneous wireless information and power transfer Nanonetworks in the Terahertz (THz) Band are proposed. An amplify and forward (AF) relaying nanonetwork in this band is investigated, where the relay harvests energy from the received THz signal and consumes this energy to forward the information to the destination. Performance based

on both time-switching and power-splitting protocols is analysed. The numerical results show the optimal power-splitting ratio and time switching ratio that achieve the maximum throughput at the destination as well as the impact of transmission distance on system performance. It is seen that the Power-Splitting protocol gives greater throughput than that of the Time-switching protocol.

5.1 Introduction and related works

In Chapter 3, relay channels in the THz band have been studied. It was seen that a relaying protocol is a promising way to improve the communication performance and to extend transmission distances [194]. Nevertheless, the performance of THz communication within the IoNT is also limited by the energy loss and the storage capacity of nano batteries [46], [161]. In Chapter 4, energy harvesting systems that are applicable to nanonetworks in the THz band have been investigated. Harvesting energy from the ambient environment provides a promising approach to enhance the lifetime and performance of energy constrained THz communication nanonetworks [8]. Traditional energy harvesting mechanisms such as solar energy are not available in nanonetworks as the efficiency of solar cells is quite low given the size limitations [161]. Therefore, novel energy harvesting mechanisms need to be developed. Recently, energy harvesting schemes for nanonetworks have been proposed [44], [46], [161], [195]. Limited by the size of powering units within nanonetworks, these works are mostly based on nanowires which satisfy the size limitation when providing the required energy. Alternatively, harvesting energy from ambient EM waves has become more and more attractive over the last decade [196]. Furthermore, energy harvesting using THz electronics (i.e. rectennas) has been widely studied and forms a

promising solution to powering nanonetworks. In the THz band, some new nano-rectennas have been proposed and manufactured [144], [188] opening the door of energy harvesting based on EM in nanonetworks.

Moreover, since EM signals carry not only information but also energy this inspires a way to collect energy and accomplish information processing from ambient EM signals simultaneously [146], [147], [149], [197]. In tradition EM communications, the simultaneous wireless information and power transfer system (SWIPT) has been investigated with the idea of transmitting power and information simultaneously being first proposed by Varshney [146] who also proposed a capacity-energy tradeoff function to analyze the fundamental performance of SWIPT. In [147], as an extended work of [146], SWIPT via a frequency selective channel with AWGN was analyzed, where a significant trade-off between information transfer and power transfer through power allocation was found. Most of the current research in SWIPT has focused on point-to-point (P2P) systems [198]. In [198], a SWIPT system with single-input-single-output (SISO) setup over the flat-fading channel was investigated. While Liu et al. considered single-input-multiple-output (SIMO) systems for SWIPT [199], and [200]–[202] studied the multiple-input-multiple-output (MIMO) systems. In [201], a three node MIMO broadcasting SWIPT system was introduced, it consists of two receivers for energy harvesting and information decoding, respectively. In [202], the authors studied the same MIMO broadcasting system for SWIPT with the consideration of imperfect CSI. In [203], the authors investigated the performance limits of a MIMO AF relaying system with an energy harvesting receiver. Orthogonal space-time block codes were applied in the information transmission process and joint optimal source and relay precoders were derived to accomplish trade-offs between the

information throughput and the energy harvesting capacity. A multi-user information and power transfer system was studied in [204]. In the study, to ensure sufficient energy arrives at the decoder, the standard constrained multiple access channel was considered. It was found that the energy harvesting abilities of the second hop determine the design of the transmission strategy in the first hop for the multi-hop channel with a single energy harvesting relay. Wireless information and energy transfer has also been applied to systems using orthogonal frequency division multiplexing (OFDM) techniques [205]. In [206], the impact of radio frequency (RF) energy harvesting on cognitive radio (CR) networks has been investigated. A new CR network architecture has been proposed where the secondary transmitters harvest energy from the RF signal that is transmitted by primary transmitters. Ishibashi et al. studied the outage probability of energy harvesting cooperative communications [207], where they assumed sufficient energy storage in the relay. A three-node AF relay with energy harvesting constraints network was studied in [208], where the outage performance of the network was investigated. Then in [209], a DF relay network with SWIPT was investigated and the power allocation strategy and the system outage probability were studied. Those great achievements made in traditional communications motivate the development of transmitting power and information simultaneously in the THz band. This provides an exciting approach to overcoming the above obstacle of energy constrained nanoscale communication networks.

To date, there has been no research in wireless energy harvesting and information transfer for nanonetworks in the THz band. Motivated by this, in this chapter, an AF relaying simultaneous wireless Information and power transfer for such networks is developed. The scenario is that an AF relay harvests EM energy from the

received THz signal transmitted by a source node, then it consumes this energy to amplify and forward the signal to the destination node [210]. In the chapter, both time-switching and power-splitting protocols are adopted [165], in the former, the received signal at the relay will be firstly used for energy harvesting for some time, and then used for information transmission in the remaining time. In the latter, the signal will be divided into two portions, one for energy harvesting and the other one for information processing. The word ‘simultaneously’ in SWIPT implies that the system completes the two tasks of ‘receiving energy’ and ‘receiving information’ within a unit time over a single noisy channel. For the time switching protocol, the unit time is divided into two parts, one of which is used for receiving energy and the other for receiving information. The key point of the use of the term ‘simultaneous’ here is that the same channel and the same signal can be used in part for transporting energy and in part for transmitting information. The objective of the study here is to find the optimal time switching fraction and power splitting ratio that achieve the maximal throughput at the destination. In the chapter, both the instantaneous and time-delayed throughput are investigated.

The rest of the chapter is comprised of four sections. In Section 2, the propagation model in the THz band is presented. The following section，Section 3, investigates the time switching and power splitting AF relaying protocols in detail. Section 4 shows the numerical results and the analysis of the obtained results. Lastly, Section 5 concludes the chapter.

5.2 Channel Model

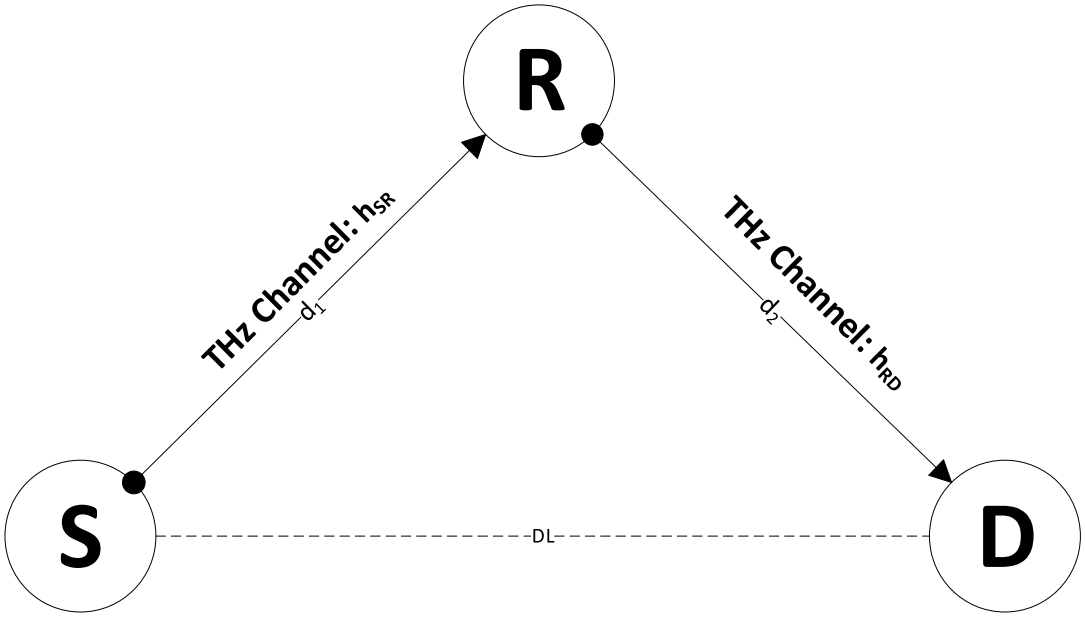

Figure 5-1 Illustration of the three-terminal Amplify-and-Forward relaying channels in the THz band.

In this chapter, the system is developed based on the THz channel model presented in Chapter 2. Recalling Equation (2.7), the channel response $H(f,d)$ is rewritten to be $H_c(f,d)$.

By applying the inverse Fourier transformation to the channel frequency response $H_c(f,d)$, the impulse response can be obtained as [121]:

$$h_c(t,d) = \mathfrak{F}^{-1}\left\{H(f,d)\right\} \tag{5.1}$$

For the system, the impulse repose is given as [121]:

$$h = h_a^{Tx} * h_c * h_a^{Rx} \tag{5.2}$$

where h_a^{Tx} and h_a^{Rx} are the impulse responses of transmission and reception antennas, respectively.

In the THz band at the nanoscale, the major noise power at the receiver is contributed by molecular absorption noise, given by [64]:

$$N_{abs}(f,d) = k_B T_0 \left(1 - e^{-k(f)d}\right) \tag{5.3}$$

It is assumed that the source to relay link and the relay to destination link contain noise sources which are independent of each other. As water vapor in the air makes the major contribution to the total absorption [64], the system is in this chapter assumed operate in air with a 0.1% water vapor content.

5.3 System Model

In this section, a relay-assisted wireless link in the THz band with information and power transfer simultaneously is studied. As illustrated in Figure 5-1, a three-node AF relaying system is studied, where the source node (**S**) transmits information to the destination node (**D**) with the assistance of the relay (**R**). As the direct link between **S** and **D** could be out of the THz signal coverage and there might be obstacles between the **S** and **D**, it is assumed that the direct link does not exist. It is also assumed that all the nodes are equipped with a single antenna and are half-duplex. Moreover, the relay is assumed to be energy constrained where it consumes the harvested energy from the source signal to forward the received information to the destination. Both time switching and power switching schemes (shown in Figure 5- 2) are considered and the total communication time is assumed to be T. Following the previous research [211], [212], for the purpose of simplicity, it is assumed that the destination knows the THz channel state information perfectly in line with previous works in this field; it can estimate the THz channel concurrently with the information transmission. The power

required for signal processing is assumed to be negligible in comparison with the power used for signal transmission [210], [213]. Differential binary phase shift keying (DBPSK) is applied as the channel access scheme due to its low energy consumption and non-coherent demodulation process (reduced system complexity) [136], [137].

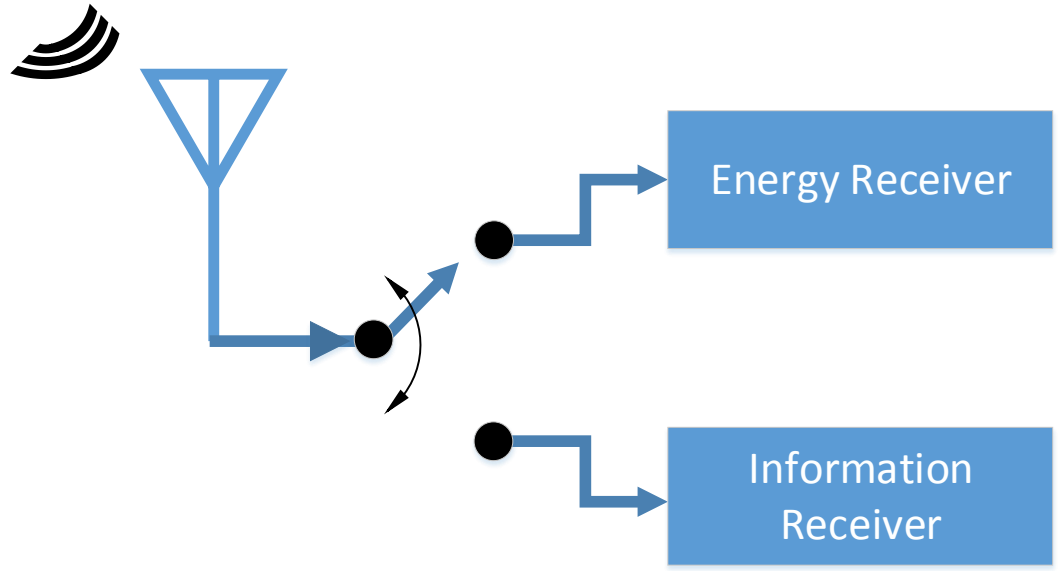

(a) Time-Switching

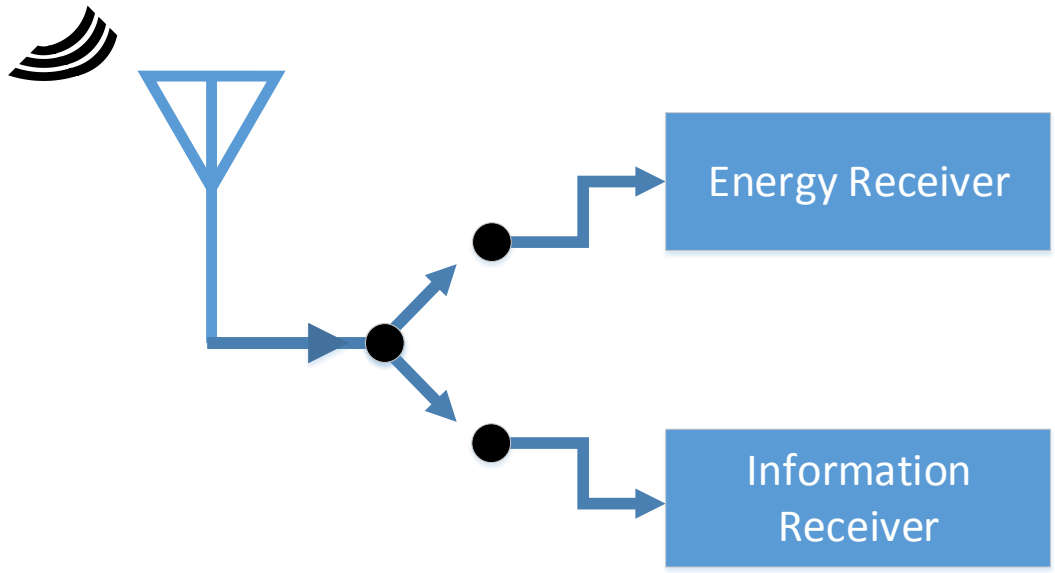

(b) Power-Splitting

Figure 5-2 System Models of (a) Time-Switching Protocol, and (b) Power-Splitting Protocol.

5.3.1 Time Switching

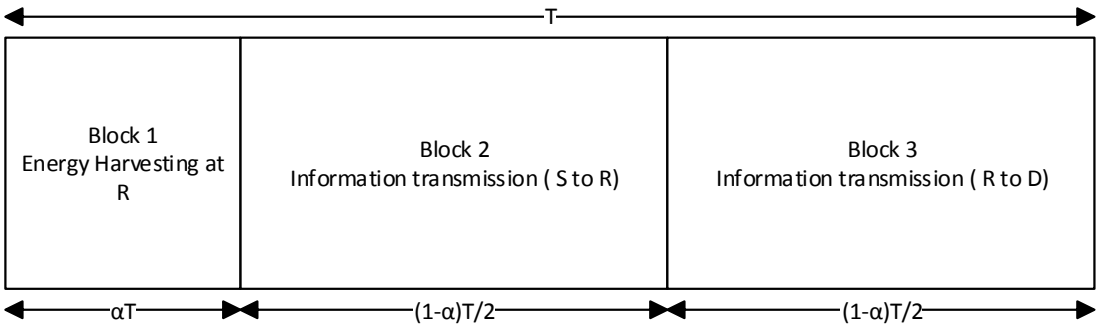

Figure 5-3 Illustration of the process and key parameters of the Time-Switching protocol

In the time switching protocol shown in Figure 5-3, a fraction αT of the total communication time T source to destination is used for **R** to harvest energy from **S**. The remaining time is used for information transfer, which is divided in half, $(1-\alpha)T/2$ for information transmission from **S** to **R** and $(1-\alpha)T/2$ for information transmission from **R** to **D**. Therefore, the received signal at **R** (during Block 1 and Block 2) is given by [126]:

$$y_R = \sqrt{P_s} h_{S,R} x_s + n_R \tag{5.4}$$

where P_s is the transmitted power from **S**, h is the THz channel gain in (5.2), hence $h_{\mathrm{S,R}}$ represents the channel gain of the source to relay link, x_s is the normalized transmitted signal of the source; n_R refers to the overall noise at the relay. Note that the overall noise introduced by the relay's receiver is comprised of the channel noise, the system electronic noise and the antenna noise. According to [64] and [214], the second two noise sources are ultralow for nanomaterials, therefore for graphene-based nanonetworks in the THz band, this study only considers the noise contributed by the THz channel, i.e. n_R is the overall molecular absorption noise given in (5.3). The noise introduced by the **R** at **D** is considered to be the same.

The harvested energy at the relay from the source can be obtained using (5.4),

$$E_h = \eta P_s \left| h_{S,R} \right|^2 \alpha T \tag{5.5}$$

where $0 < \eta < 1$ is the THz wave to energy conversion efficiency factor.

During the next step, the received signal (Block 2) at the relay y_R is amplified and forwarded to the destination, and this process consumes the harvested energy from the source (Block 1), i.e. E_h, therefore the received signal at the destination is expressed as:

$$y_D = \sqrt{P_r} h_{R,D} \beta y_R + n_D \tag{5.6}$$

where $h_{R,D}$ is the THz channel gain of the relay to destination link, n_D represents the overall noise at the destination, P_r is the transmission power of the relay, which can be obtained as:

$$P_r = \frac{E_h}{(1-\alpha)\frac{T}{2}} = \frac{2\alpha}{1-\alpha} \eta P_s \left| h_{S,R} \right|^2 \tag{5.7}$$

β is the amplification gain of the relay, which is taken to be [126]:

$$\beta = \sqrt{\frac{1}{P_s \left| h_{S,R} \right|^2 + N_{0R}}} \tag{5.8}$$

Here, substituting (5.8) into (5.6), gives,

$$\begin{aligned} y_D &= h_{R,D} \sqrt{P_r} \sqrt{\frac{1}{P_s \left| h_{S,R} \right|^2 + N_{0R}}} y_R + n_D \\ &= \frac{\sqrt{P_r} h_{R,D}}{\sqrt{P_s \left| h_{S,R} \right|^2 + N_{0R}}} y_R + n_D \end{aligned} \tag{5.9}$$

Substituting (5.4) into (5.9), the received signal is:

$$
\begin{aligned}
y_D &= \frac{\sqrt{P_r}h_{R,D}}{\sqrt{P_s\left|h_{S,R}\right|^2+N_{0R}}}\left(\sqrt{P_s}h_{S,R}x_s+n_R\right)+n_D \\
&= \frac{\sqrt{P_rP_s}h_{S,R}h_{R,D}x_s}{\sqrt{P_s\left|h_{S,R}\right|^2+N_{0R}}}+\frac{\sqrt{P_r}h_{R,D}n_R}{\sqrt{P_s\left|h_{S,R}\right|^2+N_{0R}}}+n_D
\end{aligned}
\tag{5.10}
$$

Then, substituting (5.5) into (5.10), it gives,

$$
y_D = \underbrace{\frac{\sqrt{2\alpha\eta\left|h_{S,R}\right|^2}P_sh_{S,R}h_{R,D}x_s}{\sqrt{(1-\alpha)}\sqrt{P_s\left|h_{S,R}\right|^2+N_{0R}}}}_{signal}+\underbrace{\frac{\sqrt{2\alpha\eta\left|h_{S,R}\right|^2P_s}h_{R,D}n_R}{\sqrt{(1-\alpha)}\sqrt{P_s\left|h_{S,R}\right|^2+N_{0R}}}+n_D}_{noise} \tag{5.11}
$$

Therefore, the instantaneous Signal to noise ratio (SNR) at the destination for the entire THz band is given by:

$$
\begin{aligned}
\gamma &= \frac{\mathbb{E}\left\{\left|signal\ \ part\ in\ (5.11)\right|^2\right\}}{\mathbb{E}\left\{\left|noise\ \ part\ in\ (5.11)\right|^2\right\}} \\
&= \frac{\dfrac{2\alpha\eta P_s^2\left|h_{S,R}\right|^4\left|h_{R,D}\right|^2}{(1-\alpha)P_s\left|h_{S,R}\right|^2+N_{0R}}}{\dfrac{2\alpha\eta P_s\left|h_{S,R}\right|^2\left|h_{R,D}\right|^2N_{0R}}{(1-\alpha)P_s\left|h_{S,R}\right|^2+N_{0R}}+N_{0D}} \\
&= \frac{2\alpha\eta P_s^2\left|h_{S,R}\right|^4\left|h_{R,D}\right|^2}{2\alpha\eta P_s\left|h_{S,R}\right|^2\left|h_{R,D}\right|^2N_{0R}+(1-\alpha)P_s\left|h_{S,R}\right|^2N_{0D}+N_{0R}N_{0D}} \\
&= \frac{\dfrac{P_s\left|h_{S,R}\right|^2}{N_{0R}}\eta\dfrac{2\alpha}{1-\alpha}\dfrac{P_s\left|h_{S,R}\right|^2\left|h_{R,D}\right|^2}{N_{0D}}}{\eta\dfrac{2\alpha}{1-\alpha}\dfrac{P_s\left|h_{S,R}\right|^2\left|h_{R,D}\right|^2}{N_{0D}}+\dfrac{P_s\left|h_{S,R}\right|^2}{N_{0R}}+1\big/(1-\alpha)} \\
&= \frac{\gamma_{S,R}\gamma_{R,D}}{\gamma_{R,D}+\gamma_{S,R}+1\big/(1-\alpha)}
\end{aligned}
\tag{5.12}
$$

where $\mathbb{E}\{\cdot\}$ refers to the expectation operator. N_{0R} and N_{0D} are the noise powers at the receivers of the relay and the destination respectively.

5.3.1.1 Throughput Analysis

The following section analyses the instantaneous throughout and the delay-limited throughput performance of the AF relaying nanonetworks with THz energy harvesting and the optimal time switching factor and power splitting ratio are investigated.

According to the THz channel model given in the previous chapter, the band is frequency-selective and the molecular absorption noise is non-white. Thus, the entire THz band is divided into a number of narrow enough sub-bands with centre frequency f_i ($i = 1,2,3 \ldots M$) and $\Delta f = f_{i+1} - f_i$ is the corresponding sub-bandwidth. Therefore, these sub-bands behave as frequency non-selective and the noise can be considered as white [64]. The SNR for each sub-band at the destination is obtained by rewriting (5.12) as:

$$\begin{aligned}\gamma(f_i) &= \frac{2\alpha\eta P_{s(i)}^2 \left|h_{S,R}(f_i)\right|^4 \left|h_{R,D}(f_i)\right|^2}{2\alpha\eta P_{s(i)} \left|h_{S,R}(f_i)\right|^2 \left|h_{R,D}(f_i)\right|^2 \sigma_R^2 + (1-\alpha) P_{s(i)} \left|h_{S,R}(f_i)\right|^2 \sigma_D^2 + \sigma_R^2 \sigma_D^2} \\ &= \frac{\dfrac{P_{s(i)} \left|h_{S,R}(f_i)\right|^2}{\sigma_R^2} \dfrac{2\alpha\eta}{(1-\alpha)} \dfrac{P_{s(i)} \left|h_{S,R}(f_i)\right|^2 \left|h_{R,D}(f_i)\right|^2}{\sigma_D^2}}{\dfrac{2\alpha\eta}{(1-\alpha)} \dfrac{P_{s(i)} \left|h_{S,R}(f_i)\right|^2 \left|h_{R,D}(f_i)\right|^2}{\sigma_D^2} + \dfrac{P_{s(i)} \left|h_{S,R}(f_i)\right|^2}{\sigma_R^2} + \dfrac{1}{(1-\alpha)}} \\ &= \frac{\gamma_{S,R}(f_i)\gamma_{R,D}(f_i)}{\gamma_{R,D}(f_i) + \gamma_{S,R}(f_i) + 1/(1-\alpha)}\end{aligned} \tag{5.13}$$

where $P_{s(i)}$ is the transmitted power at the source within the i_{th} sub-band , for the entire band it gives $\sum_i^I P_{s(i)} = P_s$, $h_{S,R}(f_i)$ and $h_{R,D}(f_i)$ are the i_{th} sub-channel gain within the source to relay link and the relay to destination link, respectively which can be

calculated from (5.2) using the centre frequency f_i and a fixed distance d, σ_R^2 and σ_D^2 are the variance of the overall additive white Gaussian noise (AWGN) in the i_{th} sub-band at the relay and the destination respectively. In addition, $h(f_i)$ is dominated by f_i and d .

Based on (5.13), the resulting instantaneous throughput at the destination can be obtained by summing the throughput of each sub-band [17]:

$$\Re_I = \frac{(1-\alpha)}{2} \times \sum_i^M \log_2\left(1+\gamma(f_i)\right) \tag{5.14}$$

From (5.14), the optimal α when achieving the maximum instantaneous throughput can be obtained.

The outage probability is the probability of SNR going below a fixed threshold γ_{th} or a fixed transmission rate $R_{th} = \log_2(1+\gamma_{th})$, which is expressed as:

$$p_{out} = \mathfrak{pr}\left\{\gamma \le \gamma_{th}\right\} \tag{5.15}$$

For nanonetworks in the THz band, the entire band is divided into many sub-bands, so that each sub-band is flat. The outage probability is, therefore, the product of the outage probability of each sub-band. Recalling (5.12), (5.15) can be rewritten for the entire THz band as [213],

$$\begin{aligned} p_{out} &= \frac{1}{M}\sum_i^M \mathfrak{pr}\left\{\gamma(f_i) \le \gamma_{th}\right\} \\ &= \frac{1}{M}\sum_i^M \mathfrak{pr}\left\{\frac{\gamma_{S,R}(f_i)\gamma_{R,D}(f_i)}{\gamma_{R,D}(f_i)+\gamma_{S,R}(f_i)+1/(1-\alpha)} \le \gamma_{th}\right\} \end{aligned} \tag{5.16}$$

Therefore, the throughput of delay-limited transmission within the nanonetwork is given as [165], [215]:

$$\Re_{DL} = (1-p_{out}) R_{th} \frac{(1-\alpha)T/2}{T} = \frac{R_{th}(1-\alpha)(1-p_{out})}{2} \tag{5.17}$$

5.3.2 Power Splitting

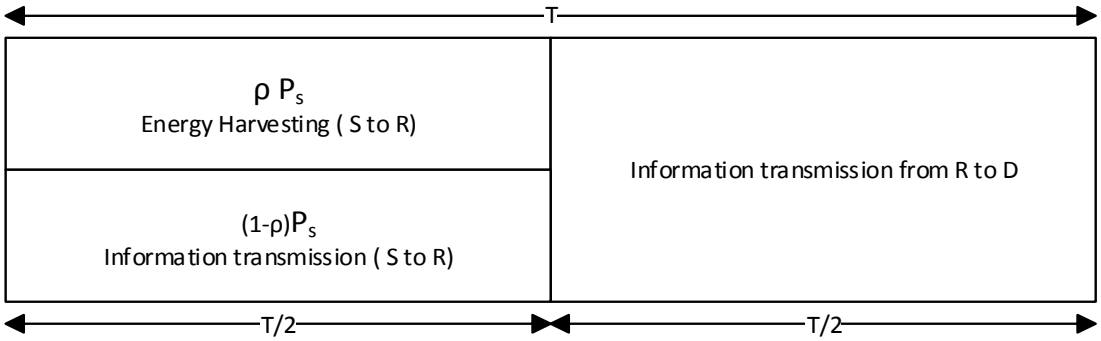

Figure 5-4 Illustration of the process and key parameters of the Power-Splitting protocol

The process of the power-splitting model is illustrated in Figure 5-4, the first half of the block time is used for energy harvesting and information transmission from source to relay, while during the other half of the time, information transmission is conducted from relay to destination. The parameter $\rho, (0 < \rho < 1)$ is the power fraction factor of the signal, i.e. ρP_S is allocated for energy harvesting and the left part $(1-\rho)P_S$ is used for information transmission. As the time-switching model, it is assumed that all the harvested energy at the relay is used for information transmission from the relay to the destination. The objective of this study is to find the optimal ρ that achieves the maximum throughout at destination.

The power of the received signal at **R** is split into two portions, i.e. one portion of the signal $\sqrt{\rho} y_R$ is transmitted for energy harvesting, and hence the harvested energy at the relay is expressed as:

$$E_h = \eta \rho P_s \left| h_{S,R} \right|^2 \left(\frac{T}{2} \right) \tag{5.18}$$

The other portion of the signal $\sqrt{1-\rho}y_R$ is sent to the information receiver for information transmission, the received signal at the relay is therefore given by:

$$y_R = \sqrt{(1-\rho)P_s}h_{S,R}x_s + n_R \tag{5.19}$$

where the parameters are those defined in (5.4). As in time switching, the channel noise dominates and so here only the noise contributed by the THz channel alone, i.e. n_R, is considered. The relay amplification factor for the power-splitting model is given by [126]:

$$\beta = \sqrt{\frac{1}{(1-\rho)P_s\left|h_{S,R}\right|^2 + N_{0R}}} \tag{5.20}$$

Here, the noise at the receivers (of **R** and **D**) n_R and n_D is modelled as independent AWGN sources with variances N_{0R} and N_{0D}, respectively. By substituting (5.20) into (5.6), the received signal at the destination for the power-splitting model is given as:

$$\begin{aligned} y_D &= h_{R,D}\sqrt{P_r}\left(\sqrt{(1-\rho)P_s}h_{S,R}x_s + n_R\right)y_R + n_D \\ &= \frac{\sqrt{P_r}h_{R,D}}{\sqrt{(1-\rho)P_s\left|h_{S,R}\right|^2 + N_{0R}}}y_R + n_D \end{aligned} \tag{5.21}$$

Then substituting (5.20) into (5.21), y_D is now,

$$\begin{aligned} y_D &= \frac{\sqrt{P_r}h_{R,D}}{\sqrt{(1-\rho)P_s\left|h_{S,R}\right|^2 + N_{0R}}}\left(\sqrt{(1-\rho)P_s}h_{S,R}x_s + n_R\right) + n_D \\ &= \frac{\sqrt{(1-\rho)P_rP_s}h_{S,R}h_{R,D}x_s}{\sqrt{(1-\rho)P_s\left|h_{S,R}\right|^2 + N_{0R}}} + \frac{\sqrt{P_r}h_{R,D}n_R}{\sqrt{(1-\rho)P_s\left|h_{S,R}\right|^2 + N_{0R}}} + n_D \end{aligned} \tag{5.22}$$

The transmitted power of the relay for power-splitting protocol is given as,

$$P_r = {E_h}/{(T/2)} = \eta\rho P_s \left|h_{S,R}\right|^2 \tag{5.23}$$

Now, using (5.18) and substituting (5.23) into (5.22),

$$y_D = \underbrace{\frac{\sqrt{\rho(1-\rho)\eta\left|h_{S,R}\right|^2}P_s h_{S,R}h_{R,D}}{\sqrt{P_s\left|h_{S,R}\right|^2(1-\rho)+N_{0R}}}x_s}_{signal} + \underbrace{\frac{\sqrt{\rho\eta\left|h_{S,R}\right|^2 P_s}h_{R,D}n_R}{\sqrt{P_s\left|h_{S,R}\right|^2(1-\rho)+N_{0R}}}+n_D}_{noise} \tag{5.24}$$

The SNR of the system is therefore obtained using (5.24) as,

$$\begin{aligned}
\gamma &= \frac{\mathbb{E}\left\{\left|signal\ \ part\ in\ (5.24)\right|^2\right\}}{\mathbb{E}\left\{\left|noise\ \ part\ in\ (5.24)\right|^2\right\}} \\
&= \frac{\eta(1-\rho)\rho P_s^2\left|h_{S,R}\right|^4\left|h_{R,D}\right|^2}{\eta\rho P_s\left|h_{S,R}\right|^2\left|h_{R,D}\right|^2 N_{0R}+(1-\rho)P_s\left|h_{S,R}\right|^2 N_{0D}+N_{0R}N_{0D}} \\
&= \frac{(1-\rho)\dfrac{P_s\left|h_{S,R}\right|^2}{N_{0R}}\rho\eta\dfrac{P_s\left|h_{S,R}\right|^2\left|h_{R,D}\right|^2}{N_{0D}}}{\rho\eta\dfrac{P_s\left|h_{S,R}\right|^2\left|h_{R,D}\right|^2}{N_{0D}}+(1-\rho)\dfrac{P_s\left|h_{S,R}\right|^2}{N_{0R}}+1} \\
&= \frac{\gamma_{S,R}\gamma_{R,D}}{\gamma_{R,D}+\gamma_{S,R}+1}
\end{aligned} \tag{5.25}$$

For nanonetworks in the THz band, the entire channel is divided into a number of sufficiently narrow sub-bands in the say was as for the time-switching protocol. The SNR for power splitting protocol in each sub-band is expressed via:

$$\gamma(f_i)=\frac{(1-\rho)\rho\eta P_{s(i)}^2\left|h_{S,R}(f_i)\right|^4\left|h_{R,D}(f_i)\right|^2}{\eta\rho P_{s(i)}\left|h_{S,R}(f_i)\right|^2\left|h_{R,D}(f_i)\right|^2\sigma_R^2+(1-\rho)P_{s(i)}\left|h_{S,R}(f_i)\right|^2\sigma_D^2+\sigma_R^2\sigma_D^2}$$
$$=\frac{(1-\rho)\dfrac{P_{s(i)}\left|h_{S,R}(f_i)\right|^2}{\sigma_R^2}\rho\eta\dfrac{P_{s(i)}\left|h_{S,R}(f_i)\right|^2\left|h_{R,D}(f_i)\right|^2}{\sigma_D^2}}{\rho\eta\dfrac{P_{s(i)}\left|h_{S,R}(f_i)\right|^2\left|h_{R,D}(f_i)\right|^2}{\sigma_D^2}+(1-\rho)\dfrac{P_{s(i)}\left|h_{S,R}(f_i)\right|^2}{\sigma_R^2}+1}$$
$$=\frac{\gamma_{S,R}(f_i)\gamma_{R,D}(f_i)}{\gamma_{R,D}(f_i)+\gamma_{S,R}(f_i)+1}$$

(5.26)

σ_R^2 and σ_D^2 are the variances of the overall AWGN in the i_{th} sub-band at the relay and the destination, respectively.

5.3.2.1 Throughput Analysis

The following part is to determine the throughput at the destination of the power-splitting protocol, given the SNR at the destination in (5.26), using (5.13), the outage probability for power splitting protocol can be obtained as:

$$\begin{aligned}p_{out}&=\frac{1}{M}\sum_i^M \mathfrak{pr}\left\{\gamma(f_i)\le\gamma_{th}\right\}\\&=\frac{1}{M}\sum_i^M \mathfrak{pr}\left\{\frac{\gamma_{S,R}(f_i)\gamma_{R,D}(f_i)}{\gamma_{R,D}(f_i)+\gamma_{S,R}(f_i)+1}\le\gamma_{th}\right\}\end{aligned}\qquad(5.27)$$

Also, the power splitting throughput at the destination is:

$$\Re_I=\frac{1}{2}\sum_i^M\log_2\left(1+\gamma(f_i)\right)\qquad(5.28)$$

Given the fixed transmission rate, the delay-limited throughput at the destination is:

$$\Re_{DL}=(1-p_{out})R_{th}\frac{T/2}{T}=\frac{R_{th}(1-p_{out})}{2}\qquad(5.29)$$

5.4 Comparison of results and discussion

In this section, numerical results will be presented to validate the analysis expressed previously. For the purpose of simplicity, the frequency band used for calculation ranges from 0.5 to 1.5 THz and Δf is fixed at 0.01 THz. The distances of S to R and R to D are set to be 10 mm. The threshold transmission rate is set as $R_{th} = \log_2\left(1+\gamma_{th}\right) = 5 \text{ bps Hz}^{-1}$ the threshold SNR is, therefore $\gamma_{th} = 2^{R_{th}} - 1 = 31$. The energy harvesting efficiency is set as $\eta = 0.5$ and the THz signal power is set to be 1dBm.

For the purpose of simplicity, it is assumed that the distances **S** to **R** and **R** to **D** are the same and are both represented by d. Firstly, the effect of α and ρ at a fixed distance i.e. d=10mm is analysed as is shown in Figure 5-5 and Figure 5-6. As shown in Figure 5-5, for the time-switching protocol, the delay-limited throughput at the destination rises with α until it approaches the optimal value and the throughout reaches its maximum and then the throughput decreases more gently along with the increase of α. According to the result obtained, the optimal value of α for this system is around 0.35. The reasons are, on one hand when α is smaller than its optimal value, this implies that less energy is harvested at the relay, the SNR at the relay to destination link is getting worse which dominates the overall SNR at the destination (refer to (5.12)). On the other hand, when α is larger than its optimal value, there is less information transmitted and more time is spent on energy harvesting and more signal is wasted. As a result, the throughput at the destination getting smaller as the factor $(1-\alpha)/2$ in (5.12) getting smaller; the trend for instantaneous throughput of the system is similar.

For the power splitting protocol, as is shown in Figure 5-6, the delay-limited throughput at the destination grows gently with increasing ρ from zero to the optimal value (0.8 in this system); it then decreases quickly from the peak with further increases in ρ. The explanation for this trend are similar those for the time switching protocol; when ρ is smaller than its optimal value, the relay harvests less energy from the received signal. Consequently, the transmission power from relay gets smaller and therefore the SNR at the relay to destination link gets worse which dominates the overall SNR at the destination (given by (5.12)) resulting in the increase of outage probability as per (5.24). Furthermore, when ρ is larger than its optimal value, the relay harvests more than enough energy from the received signal with the increase of ρ, which result in reduced information transmission from S to R, i.e. the more power used for energy harvesting the more signal that gets wasted. The smaller and smaller strength information signal is then amplified and forwarded by the relay via the noisy R to D link to the destination, the SNR at the destination becomes smaller and the outage probability gets larger. The trend for the instantaneous throughput of the system is similar.

Recalling (5.1), it can be seen that the THz channel gains will be affected by the transmission distance of the signal. Figure 5-7 and Figure 5-8 show the impact of distances on the system throughput at the destination. When the **S** to **R** and **R** to **D** distances increase from 0.1 mm to 1 mm, the effect on throughout at the destination is clear in the figures. As one might expect, for longer the distances the throughput is smaller. Moreover, for transmission distances smaller than a few millimetres, the power of the signal is much higher than the noise power at the receivers of **R** and **D** which provides a much high achievable throughput at the destination. For larger

transmission distances, the power of the received signals and the power of molecular absorption noise both decrease but the signal power decreases more drastically (with the noise power effectively being able to be treated as constant). According to the results shown in Figure 5-7 and Figure 5-8, it can be seen that suitable transmission distances for nanonetwork in the THz band fall in the range of a few millimetres. Moreover, based on all the results, the power-splitting protocol can provide more throughput than that of the time-switching protocol. However, the power-splitting protocol brings more complexities of components which are a challenge for nanoscale communications systems.

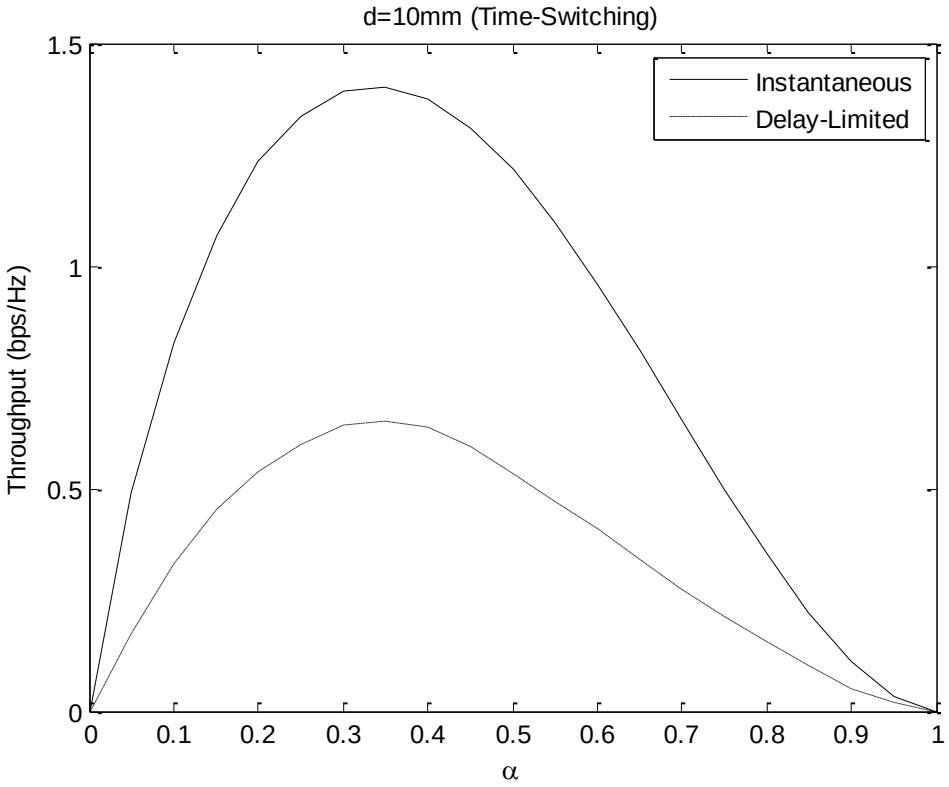

Figure 5-5 Instantaneous and delay-limited throughput at the destination for time-switching protocol with the distance of 10 mm.

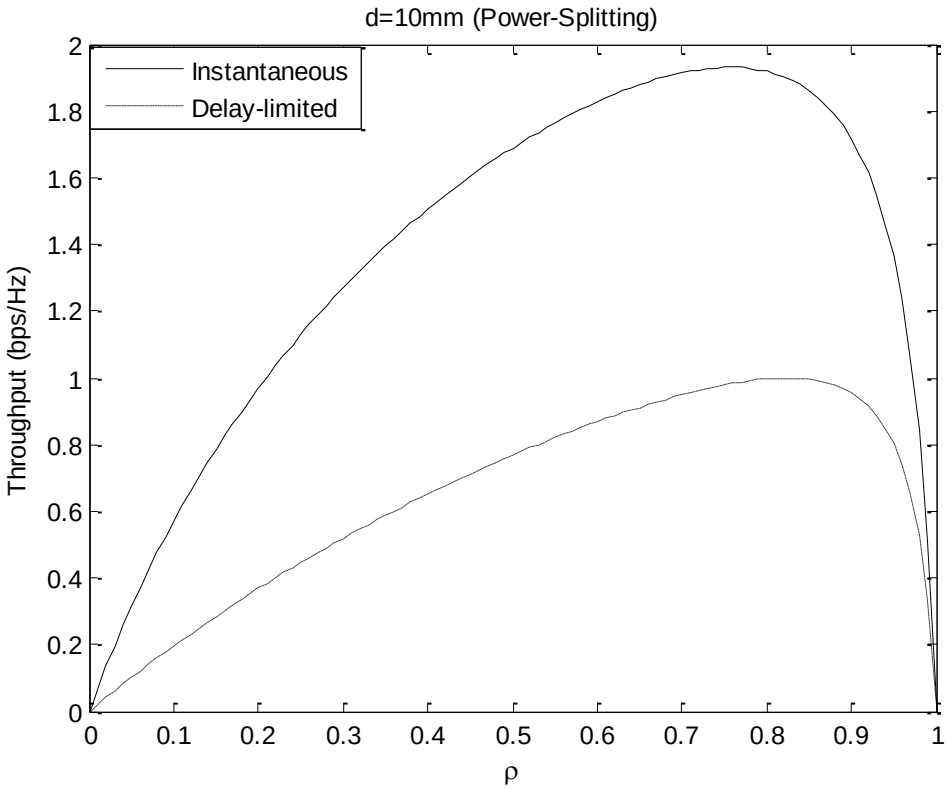

Figure 5-6 Instantaneous and delay-limited throughput at the destination for power-splitting protocol with the distance of 10 mm

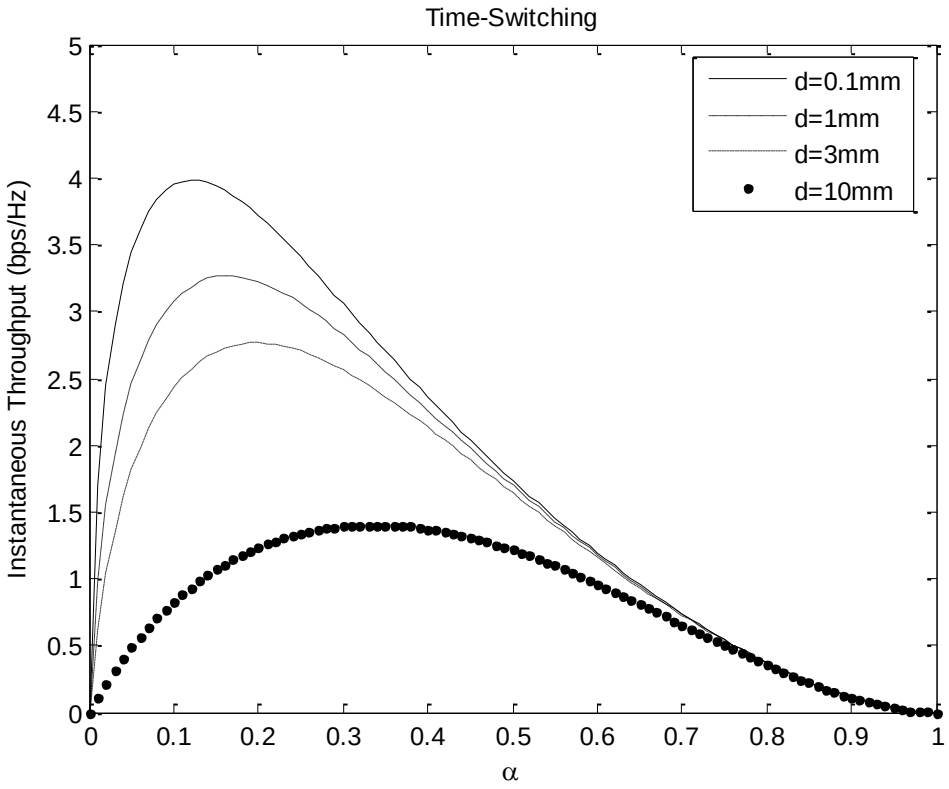

Figure 5-7 The impact of transmission distances on throughout at the destination for time-switching protocol.

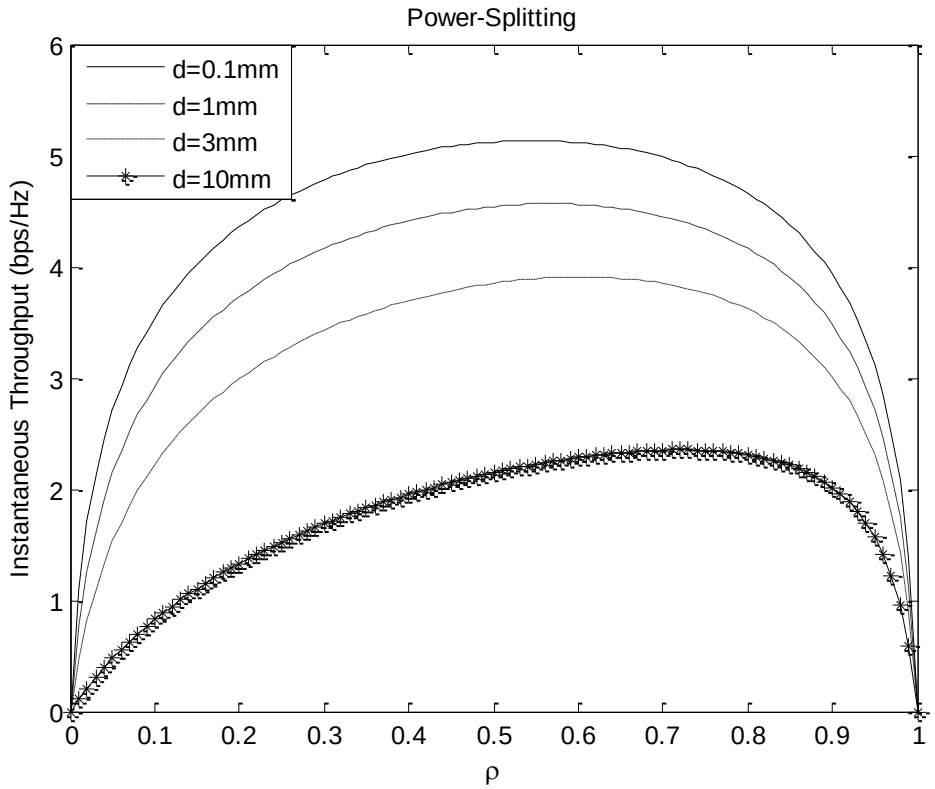

Figure 5-8 the impact of transmission distances on throughout at the destination for the power-splitting protocol.

5.5 Conclusions

In this chapter, simultaneous wireless information and power transfer for AF relaying nanonetworks in the THz band has been investigated. The AF harvests energy from the received signal and consumes this to amplify and forward the information to the destination. Both time switching and power splitting protocols have been studied. The entire THz band was divided into a number of narrow sub-bands for analysis. In order to determine the optimal time switching factor as well as the optimal power splitting ratio, the instantaneous throughout and the delay-limited throughput at the destination were derived to evaluate the performance of the variety of time factors and power ratios. The results have shown the optimal factors and power ratios for different

transmission distances numerically. For time switching, the optimum time factor is approximately 0.35, whereas for power splitting the corresponding power ratio is 0.8. In the chapter, it was assumed that the source to relay and relay to destination distance is equal.

Chapter 6
Rate-Energy Trade-off Analysis of SWIPT System in the THz Band

6.1 Introduction

In this chapter, a new protocol for SWIPT in the THz band is proposed. With the consideration of the unique peculiarities of the THz band. The new protocol makes the use of the selective frequency over the channel by splitting the entire band into two parts, one for information transfer and the other for energy harvesting. The new protocol is different from either the time switching, or the power splitting schemes described in chapter 5 which is called the channel splitting protocol and can be considered as new power splitting scheme. In the proposed scheme, the entire THz is divided into a number of narrow enough sub bands. These sub bands are then split into two groups, one group with the best some sub channels are used for information transfer the other group with the worst sub bands are used for energy harvesting. Different power resource allocation methods are adopted such as water filling, equal power and adaptive resource allocation. The objective of the study is to analyse the trade-off between information transfer and energy transfer over the THz channel and to find best power allocation method, the optimal splitting fraction and the grouping scheme of all the sub bands.

The rest of the chapter is organized as: Section 6.2 illustrate the novel power splitting schemes, the water filling power allocation, equal power allocation, and

adaptive power allocation methods in detail. In Section 6.3, numerical results and analysis are given. Section 6.4 concludes the chapter.

6.2 System Model

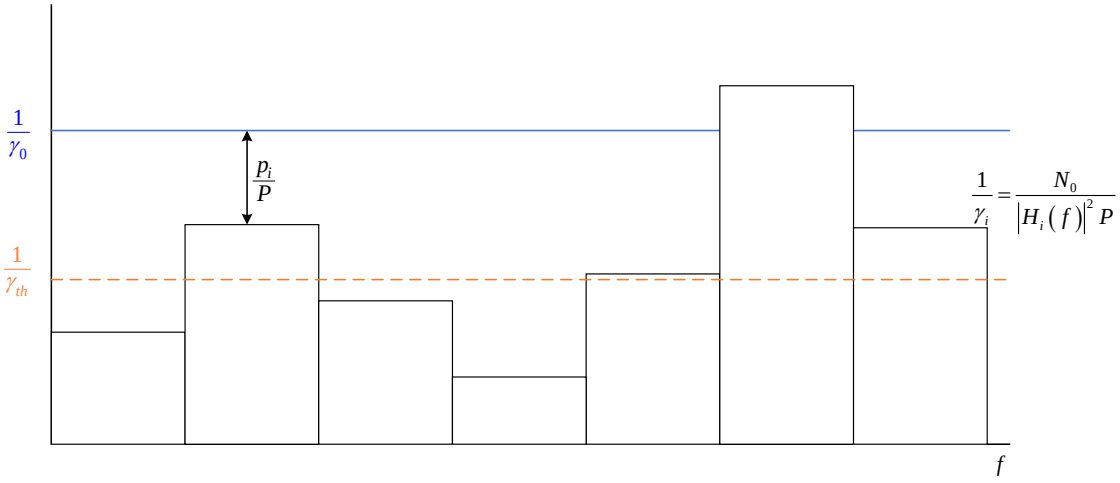

Figure 6-1 Water-filling power allocation scheme

As is described in Chapter 5, the entire THz band is divided into a number of narrow enough sub bands. For information transfer, the objective is to maximize the information rate over the entire channel with a total transmit power constraint. For the frequency selective channel, using water-filling principle can maximize the channel capacity by allocating more power to those sub bands with better SNR [216]. However, the water filling scheme will also bring more system complexity as the transmitter requires CSI feedback. Another power allocation scheme allocates power to each sub band equally, which is more feasible for THz systems. In this chapter, both water filling and equal power schemes are analysed for power allocation in the SWIPT system.

For the water filling power allocation scheme illustrated in Figure 6-1, the channel capacity over the entire channel is calculated as,

$$C = \max_{p_i} \Delta f \sum_{i=1}^{M} \log_2 \left(1 + \frac{\left| H_i(f) \right|^2 p_i}{N_0} \right) \tag{6.1}$$

where Δf is the bandwidth of each sub band, p_i is the transmit power allocated to i^{th} sub channel, $i = 1, 2, 3...M$, the total transmit power at the transmitter is constrained by

$$\sum_{i=1}^{M} p_i \le P \tag{6.2}$$

The problem is then to find the power set $\{p_i\}$ that maximize the channel capacity subject to the total power constraint. The problem can be solved by using Lagrange multipliers [217],

$$\mathcal{L}(\gamma_0, \{p_i\}) = \sum_{i=1}^{M} \log_2 \left(1 + \frac{\left| H_i(f) \right|^2 p_i}{N_0} \right) + \gamma_0 \left(\sum_{i=1}^{M} p_i - P \right) \tag{6.3}$$

Let $\frac{\partial \mathcal{L}}{\partial P} = 0$ and $\frac{\partial \mathcal{L}}{\partial \gamma_0} = 0$, the optimized power allocation scheme is

$$\frac{p_i}{P} = \begin{cases} \frac{1}{\gamma_0} - \frac{1}{\gamma_i} & \gamma_i \ge \gamma_0 \\ 0 & \gamma_i < \gamma_0 \end{cases} \tag{6.4}$$

where

$$\gamma_i = \frac{\left| H_i(f) \right|^2 P}{N_0} \tag{6.5}$$

For the equal power allocation scheme illustrated in Figure 6-2, the total transmit power is allocated equally to each sub bands, therefore,

$$p_i = \frac{P}{M} \tag{6.6}$$

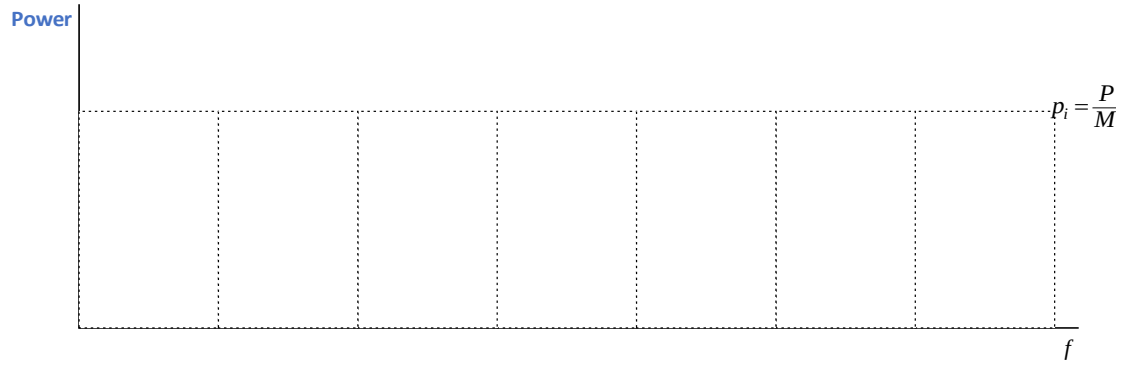

Figure 6-2 Allocating power equally to sub bands

6.2.1 The channel splitting protocol

As is shown in Figure 6-3, in the proposed power splitting protocol, all the sub channels are resorted from the best to the worst. By applying a splitting number Λ, these sub channels are split into two groups, with frequency responses of $\{H_j\}$ and $\{H_k\}$ respectively. Those $\{H_j\}$ channels are selected for information transfer and $\{H_k\}$ channels for energy harvesting. By varying the splitting number, channels allocated for information transfer and energy harvesting are varied. The splitting numbers are discrete which ranges from 0 to M (the total number of the sub channels).

Therefore, the information rate (in bps/Hz) in the SWIPT system is given by [149]:

$$R = \frac{1}{J}\sum_{j=1}^{J}\log_2\left(1+\frac{|H_j|^2 p_j}{N_0}\right) \tag{6.7}$$

where $j = 1,2,3 \ldots J$.

The harvested energy at the receiver is thus,

$$E_h = \varsigma\sum_{k=1}^{K}|H_k|^2 p_k \tag{6.8}$$

where $0<\varsigma<1$ is the energy conversion efficiency factor, $k = 1,2,3 \ldots K$ and $J + K = M$.

Moreover, the transmit power allocated to information transfer and energy harvesting have the following relation,

$$\sum_{j=1}^{J} p_j = P - \sum_{k=1}^{K} p_k = \rho P \tag{6.9}$$

where $0<\rho<1$, same as the power splitting scheme described in Chapter 5.

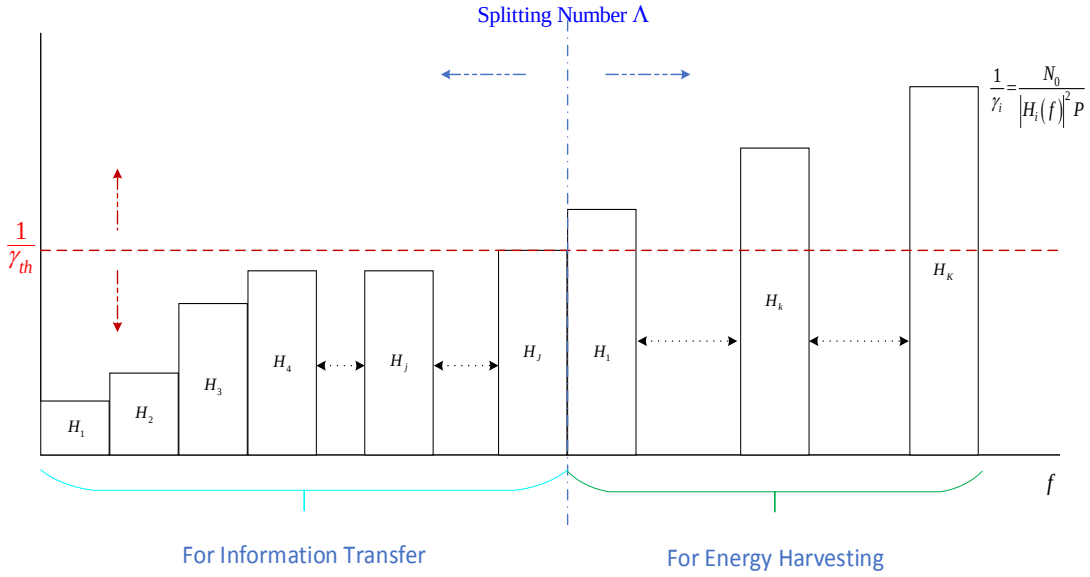

Figure 6-3 The channel splitting scheme

When equal power allocation is applied, the information rate and harvested energy in (6.7) and (6.8) can be rewritten as,

$$R_{EP} = \frac{1}{J}\sum_{j}^{J}\log_2\left(1+\frac{\left|H_j\right|^2\frac{P}{M}}{N_0}\right) \tag{6.10}$$

and

$$E_h^{EP} = \varsigma\sum_{k}^{K}\left|H_k\right|^2\frac{P}{M} \tag{6.11}$$

The upper bund of the on the information rate and harvested energy $\left(R, E_h\right)$ is therefore given as

$$C_{R-E}^{UB}\left(P\right) \triangleq \left\{\left(R, E_h\right): R \le \frac{1}{M}\sum_{i=1}^{M}\log_2\left(1+\frac{\left|H_i\right|^2 p_i}{N_0}\right), E_h \le \sum_{i=1}^{M}\left|H_i\right|^2 p_i\right\} \tag{6.12}$$

In Figure 6-4, the information rate and energy harvesting rate trade-off is illustrated for both the water filling and equal power schemes. It can be seen from the result that the water-filling scheme can maximize the information rate while for energy harvesting, the equal power allocation provides much better performance. This result motivates the study of the performance of new power allocation schemes for the SWIPT systems which is given in the following part.

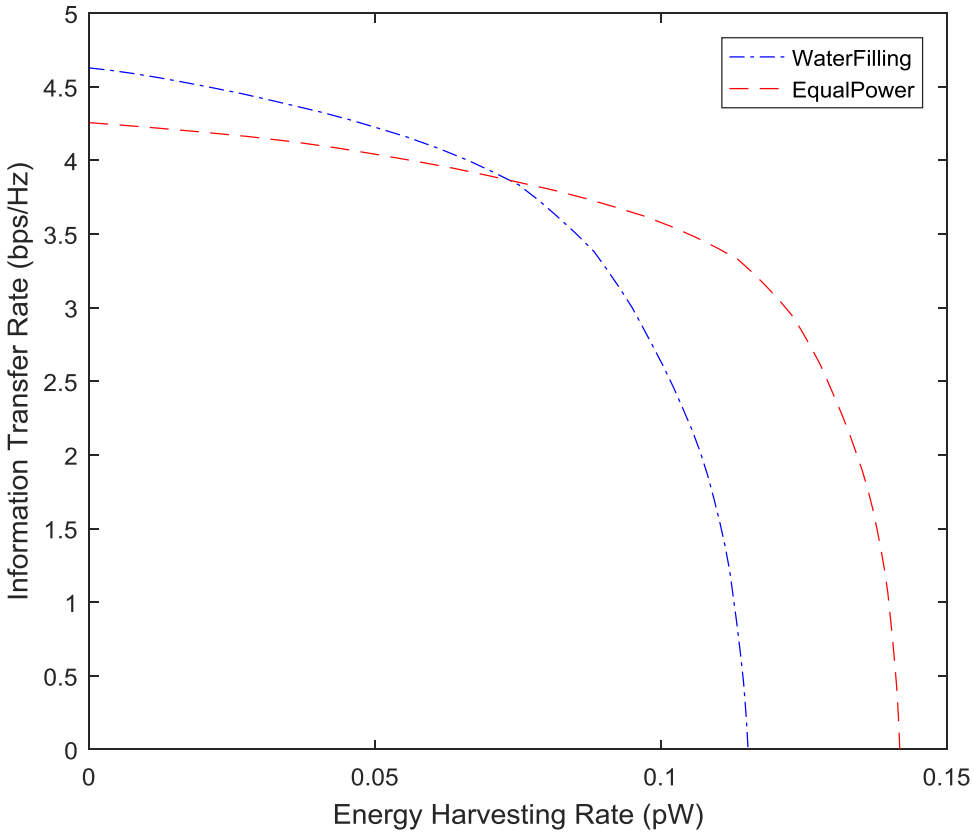

Figure 6-4 Information rate and energy harvesting rate trade off

6.2.2 Adaptive power allocation

In this scheme, the total transmit power is again split into two parts, power allocated to energy harvesting is equally for each subchannel, assume that the harvested energy should meet the minimum energy requirement (the minimum energy required to perform further tasks), therefore,

$$E_h = \sum_{k=1}^{K} \varsigma \left| H_k \right|^2 p_k \geq E_{\min} \tag{6.13}$$

For information transfer, MQAM modulation is used as the channel access scheme, the BER expression of square MQAM as a function of SNR is given as [218]:

$$\mathcal{E}_i(\gamma_i) \approx 0.2\exp\left(\frac{-1.6\gamma_i(p_i/P)}{2^{\kappa_i}-1}\right) \tag{6.14}$$

where the adaptive data rate on the i_{th} subchannel is given as ,

$$\kappa_i(\gamma) = \log_2\left(1-\frac{1.6\gamma_i(p_i/P)}{\ln(5\mathcal{E}_i)}\right) \tag{6.15}$$

Assume that the information transfer should reach a threshold error rate, the average BER is thus [218], [219],

$$\bar{\mathcal{E}} = \frac{\Delta f \cdot \sum_{j=1}^{J} \mathcal{E}_j \cdot \kappa_j}{\Delta f \cdot \sum_{j=1}^{J} \kappa_j} \le \mathcal{E}_0 \tag{6.16}$$

where $\mathcal{E}_0$ is the threshold BER

According to [218], the information rate of the system for discrete sub channels can be expressed as,

$$R = \sum_{j=1}^{J} \kappa_j \tag{6.17}$$

Therefore, the optimization problem can be written as

$$\begin{aligned} &\max_{\{\kappa_j\}} R = \sum_{j=1}^{J} \kappa_j \\ &\text{s.t. } \varsigma \sum_{k=1}^{K} |H_k|^2 p_k \ge E_{\min} \\ &\frac{\Delta f \cdot \sum_{j=1}^{J} \mathcal{E}_j \cdot \kappa_j}{\Delta f \cdot \sum_{j=1}^{J} \kappa_j} \le \mathcal{E}_0 \\ &\sum_{j=1}^{J} p_j + \sum_{k=1}^{K} p_k = \sum_{i=1}^{M} p_i \le P \end{aligned} \tag{6.18}$$

The Lagrangian of (6.18) is therefore[220],

$$\begin{aligned}
&\mathcal{L}\left(\{\kappa_j\},\{p_k\},\mu_1,\mu_2,\mu_3\right)\\
&=\sum_{j=1}^{J}\kappa_j+\mu_1\left(\varsigma\sum_{k=1}^{K}\left|H_k\right|^2 p_k-E_{\min}\right)\\
&+\mu_2\left(\mathcal{E}_0\cdot\Delta f\cdot\sum_{j=1}^{J}\kappa_j-\Delta f\cdot\sum_{j=1}^{J}\mathcal{E}_j\cdot\kappa_j\right)\\
&+\mu_3\left(P-\sum_{j=1}^{J}p_j-\sum_{k=1}^{K}p_k\right)
\end{aligned}\tag{6.19}$$

where μ_1,μ_2 and μ_3 are nonnegative,

By defining

$$\max_{\{\kappa_j\},\{p_k\}}\ \mathcal{L}_j:=\kappa_j+\mu_2\cdot\Delta f\cdot\left(\mathcal{E}_0\kappa_j-\mathcal{E}_j\kappa_j\right)-\mu_3 p_j \tag{6.20}$$

(6.19) can be written as

$$\mathcal{L}=\sum_{j=1}^{J}\mathcal{L}_j+\mu_1\left(\varsigma\sum_{k=1}^{K}\left|H_k\right|^2 p_k-E_{\min}\right)+\mu_3\left(P-\sum_{k=1}^{K}p_k\right) \tag{6.21}$$

To get the optimal solutions, the differentiating of (6.20) to p_j is,

$$\frac{\partial\mathcal{L}_j}{\partial p_j}=-\mu_2\cdot\Delta f\cdot\kappa_j\frac{\partial\mathcal{E}_j}{\partial p_j}-\mu_3 \tag{6.22}$$

where

$$\begin{aligned}
\frac{\partial\mathcal{E}_j}{\partial p_j}&=\frac{\partial\left(0.2\exp\left(\dfrac{-1.6\gamma_j\left(p_j/\rho P\right)}{2^{\kappa_j}-1}\right)\right)}{\partial p_i}\\
&=-\frac{1.6\gamma_j/\rho P}{2^{\kappa_j}-1}\cdot\mathcal{E}_j
\end{aligned}\tag{6.23}$$

According to (6.22) and (6.23), the BER is given as

$$\mathcal{E}_j=\frac{\mu_3\rho P}{\mu_2\cdot\Delta f\cdot\kappa_j}\cdot\frac{2^{\kappa_j}-1}{1.6\gamma_j} \tag{6.24}$$

It can be seen from (6.24) that the BER decrease with the increase of SNR i.e. the channel quality, therefore the optimal power allocation matches the water filling schemes.

The differentiating of (6.20) with respect to κ_j:

$$\frac{\partial \mathcal{L}_j}{\partial k_j} = 1 + \mu_2 \mathcal{E}_0 \cdot \Delta f - \mu_2 \frac{\partial \mathcal{E}_j}{\partial \kappa_j} \cdot \Delta f \cdot \kappa_j - \mu_2 \mathcal{E}_j \cdot \Delta f \tag{6.25}$$

where

$$\frac{\partial \mathcal{E}_j}{\partial \kappa_j} = \mathcal{E}_j \cdot \frac{1.6\gamma_j \dfrac{p_j}{\rho P}}{\left(2^{\kappa_j} - 1\right)^2} \cdot 2^{\kappa_j} \ln(2) \tag{6.26}$$

Therefore, the power allocation that maximize the information rate can is

$$\begin{aligned} p_j &= \max\left\{ \left(\frac{1 + \mu_2 \mathcal{E}_0 \cdot \Delta f}{\mu_2 \mathcal{E}_j \cdot \Delta f} - 1 \right) \cdot \frac{\rho P \left(2^{\kappa_j} - 1\right)^2}{1.1\gamma_j 2^{\kappa_j} \kappa_j}, 0 \right\} \\ &= \max\left\{ \frac{\left(2^{\kappa_j} - 1\right)\left(1 + \mu_2 \mathcal{E}_0 \cdot \Delta f\right)}{\rho \mu_3 2^{\kappa_j} \ln(2)} - \frac{\rho P \left(2^{\kappa_j} - 1\right)^2}{1.1\gamma_j 2^{\kappa_j} \kappa_j}, 0 \right\} \end{aligned} \tag{6.27}$$

and

$$\left\{ \frac{p_j}{P} \right\} = \max\left\{ \frac{\left(2^{\kappa_j} - 1\right)\left(1 + \mu_2 \mathcal{E}_0 \cdot \Delta f\right)}{\rho P \mu_3 2^{\kappa_j} \ln(2)} - \frac{\rho \left(2^{\kappa_j} - 1\right)^2}{1.1\gamma_j 2^{\kappa_j} \kappa_j}, 0 \right\} \tag{6.28}$$

The values of μ_2 and μ_3 are two constants and can be obtained through numerical search, the initial value of μ_2 is chosen as the maximum SNR value, then during every iteration, decrease μ_2 and increase μ_3, the optimal values for both constants can be found.

As aforementioned, the adaptive power allocation is matching the water-filling scheme, which is used in the SWIPT system for those information transfer sub channels. According to the result shown in Figure 6-4, allocating power to those sub channels equally for energy harvesting provides better performance. Therefore, the adaptive power allocation and the equal power scheme are jointly used for the SWIPT system.

6.3 Numerical results

In this section, numerical results will be presented to validate the analysis expressed previously. For the purpose of simplicity, the frequency band used for calculation ranges from 0.1 to 0.6 THz and B is fixed at 0.01 THz. $\varsigma = 0.5$, $\mathcal{E}_0 = 10^{-3}$ and the THz signal power is set to be 1dBm. The distance is fixed for the analysis in this chapter.

As is shown in Figure 6-5, energy harvesting rate is linear (according to 6.13) and information rate is logarithm (refer to 6.15). As the total transmit power is shared, the information rate increase with the increase of power splitting ratio, in contrast to the energy harvesting rate. To meet the minimum energy requirement of the receiver, the value of ρ should be selected within a certain range as well as the position of the channel splitting number shown in Figure 6-3. Note that, the information rate and the energy harvesting rate values are in pair, and they are varying with the change of ρ. The cross point of the two lines indicates the optimal value of ρ, the word 'optimal' here means the good trade-off between the rate and energy has been reached. Sometimes more information are required than energy and verse versa.

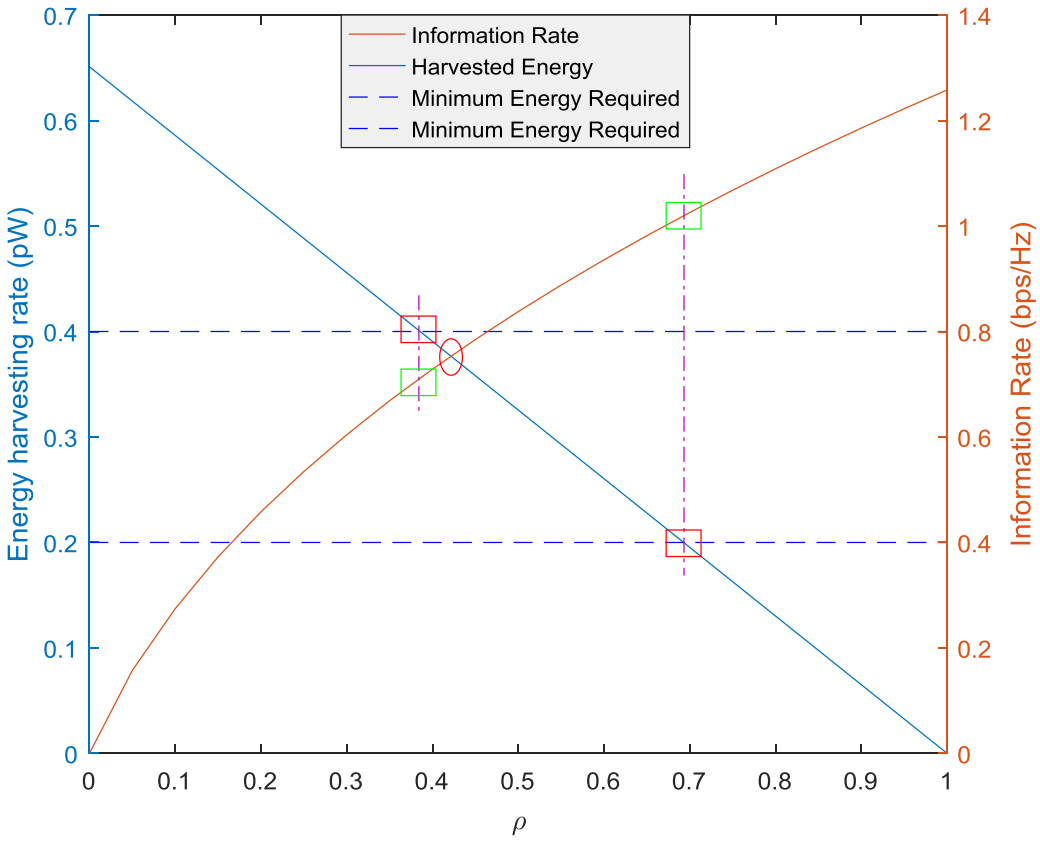

Figure 6-5 Receiver information and energy harvesting rates vs. power splitting ratio.

Figure 6-6 shows the result when the channel splitting number is varied. There are four pairs of data displayed in the figure, including two lines overlapped with the *x*-axis, these are the information rate and energy harvesting rate values when either the all the sub channels are used for energy harvesting or for energy harvesting. The other two pairs of data are displayed in the same colour. The effect of the position of channel splitting number can clearly be seen. Their four crossover points have been circled in red, which are the optimal trade-off points for ρ .

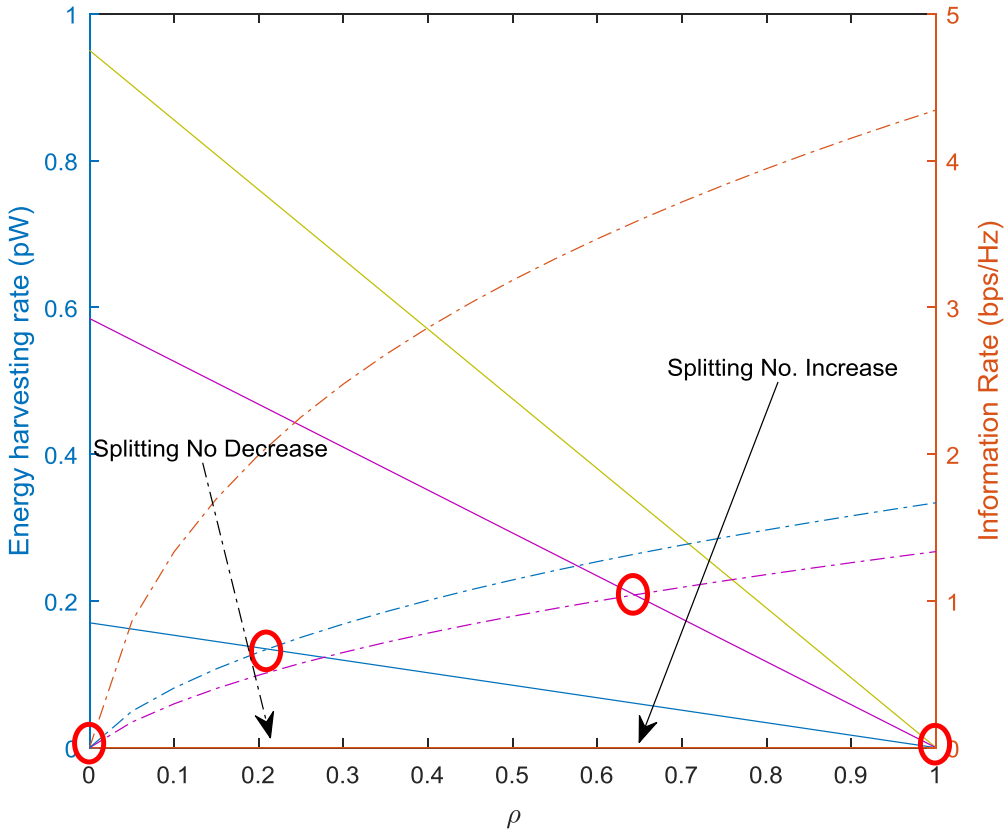

Figure 6-6 Pairs of Rate and Energy data alongside the variation of the channel splitting number.

In Figure 6-7, more pairs of data are plotted along with the change of the splitting number (moving left and right in Figure 6-3). When all the optimal trade-off points are connected (the black line in the figure), the optimal splitting number and power splitting ratio can be obtained. Again, these are the values which enable the best energy and rate trade off. As is shown the figure, the peak point is reached when 24 out of the total 50 sub channels with the best quality are used for information transfer and the optimal power splitting ratio is 0.59.

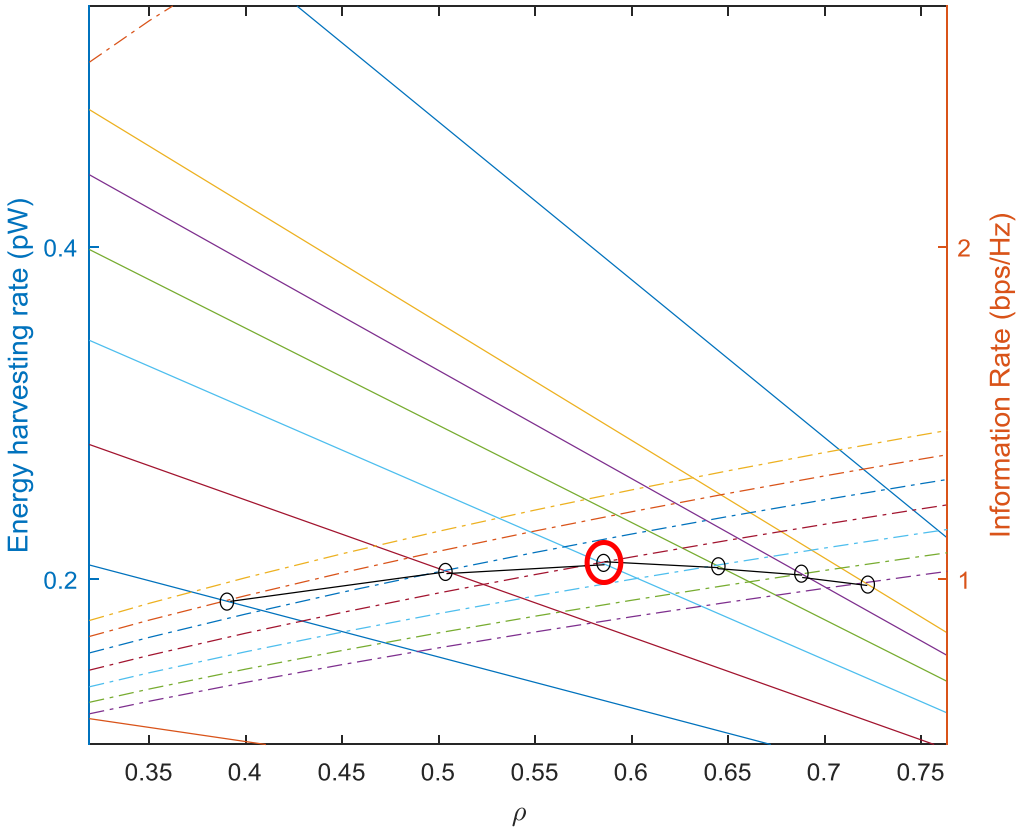

Figure 6-7 The Energy Trade off points are reached.

6.4 Conclusions

In this chapter, Rate-Energy trade-off for SWIPT in the THz band has been analysed. The novel channel splitting protocol has been proposed which captured the peculiarities of the THz channel. Different resource allocation schemes are applied and compared, an optimized power allocation scheme has been developed for the channel splitting SWIPT protocol. It is found that, the water filing power allocation can maximize the system information rate while the equal power allocation method provided better energy harvesting performance. Channel adaptive power allocation and equal power allocation have been jointly used in the optimized THz SWIPT

system, where for the information transfer part, channel adaptive is used and equal power is used for energy harvesting part. The optimal values of channel splitting number and power splitting ratio have been derived which provides the best Rate-Energy trade-off. The optimal channel splitting number is 24 out of 50 and the optimal power splitting ratio is 0.59.

Chapter 7
Conclusions and Future Work

Nanotechnology has introduced a variety of novel devices and thus opened the door to reshape the conventional communication paradigm. Nano-sized sensors are expected to drive the evolution of many areas of information and communication technology. The interconnection among massive numbers of nanosensors in the THz band has enabled the establishment of nanonetworks which can be applied in many fields such as healthcare, military and environmental monitoring. Although there are still many challenges in realizing fully functional nanosensor devices, research towards hardware and investigations concentrated on communications will provide mutual benefits at the initial stage.

In this thesis, the research is focused EM communications among nanosensors in the THz band, which aims to improve the transmission range and performance of the communication. By introducing a three-terminal relaying scheme, a nano-rectenna based energy harvesting mechanism, and a THz-SWIPT system, the objectives of the thesis have been addressed. The contributions of each solution presented in the thesis are summarized as:

Chapter 2 studied the channel model for communications within nanonetworks in the THz band. It reviewed the recent research regarding the channel modelling of the THz band. A very recent and most appropriate channel model for EM communication in the THz band in terms of the total path loss and noise has been presented. It was found that the path loss tended to increase with increasing frequency

and transmission distance. Otherwise, the molecular absorption coefficients varied sharply at some frequencies. As a consequence, the total path loss at such frequencies was substantially reduced. It has also been found that the trend was the same for the molecular noise temperature. In the chapter, the calculation method of the THz channel capacity was introduced, which divided the frequency-selective THz channel into a number of narrow enough and flat sub-bands. It was seen that for transmission distances of a few mm, the theoretical channel capacity can be very high.

In Chapter 3, a fixed three-terminal relaying scheme for communications within nanonetworks in the THz band was introduced for the first time. Two relaying protocols namely AF and DF relays were studied in the THz channel. The system employed DBPSK modulation as the channel access scheme, for the purpose of reducing complexity and lowering power dissipation in the system. According to the simulation results, the proposed relay-assisted transmission provides a significant improvement over the original direct transmission. Moreover, the results illustrated that the DF scheme provides better performance than that of AF because the latter not only amplifies the signal but also the noise in the channel.

An energy harvesting system based on nano-rectennas for wireless Body-Centric Nanonetworks has been described for the first time in Chapter 4. The proposed system was developed based on nanoscale rectennas which acted as generators in the system. Recent research on energy harvesting system for nanonetworks has been reviewed, and two rectenna based schemes were investigated, namely the CNT array rectenna and the bowtie array nano-rectenna. By making use of the significant advantages of nano-rectennas, the proposed energy harvesting system provides a very efficient and promising way to power nanosensors and implanted or body area

nanodevices. A detailed analysis of the nano-rectenna based harvesting mechanisms and their application in nanosensor networks has also been presented. The analysis results shown that the CNT array rectenna can successfully supply the energy required for communication within wireless body-centric nanonetworks, this being approximately 27.5 nW. Moreover, the much smaller sized bowtie array rectenna is able to provide a similar output power. In addition, a comparison between the two proposed nano-rectenna based energy harvesting systems and the piezoelectric based nano-generator system have been given. In general, the study found that nano-rectennas cannot provide as high a voltage when compared to a piezoelectric nano-generator, a bowtie nano-rectenna array is much more efficient while producing DC directly from the THz signal within the system and ambient EM signal without any other system external power source.

In Chapter 5, a pioneer SWIPT system based on AF relaying scheme was proposed for communication within nanonetworks in the THz band. In the system, the relay harvests energy from the received signal and consumes this to amplify and forward the information to the destination. Two protocols have been studied, i.e. time switching and power splitting. Moreover, the entire THz channel was divided into a number of narrow enough flat sub-bands fior analysis. The instantaneous throughput and the delay-limited throughput at the destination were derived to evaluate the performance of the variety of time factors and power ratios in order to determine the optimal time switching factor as well as the optimal power splitting ratio. The numerical results presented in the chapter illustrated the optimal factors and power ratios for different transmission distances. It was found that the optimum time factor

is approximately 0.35 for time switching, whereas the corresponding power ratio is 0.8 for power splitting.

In Chapter 6, a novel SWIPT protocol namely channel splitting was proposed in accordance with the peculiarities of the THz channel. Water-Filling, equal-power and channel adaptive power allocation schemes were analysed and applied to channel splitting SWIPT protocol. Rate-Energy trade-off for SWIPT in the THz band was analysed. According to the result obtained, the water filling power allocation maximized the system information rate while the equal power allocation method provided better energy harvesting performance. The optimal values of channel splitting number and power splitting ratio were derived which provided the best Rate-Energy trade-off. The optimal channel splitting number is 24 out of 50 and the optimal power splitting ratio is 0.59.

7.1 Future work

Despite the vast potential applications and huge benefits that nanonetworks would bring, there is still much lack of knowledge in many aspects of research regarding them. More research is worthy of being conducted in order to overcome the open limitations and fulfill the ultimate vision. The future research direction for this thesis is summarized as follows:

Here, the relaying channel was developed based on the classical three-terminal relaying networks. Due to the complexity of the system at the nanoscale, only the single relay scheme had been is analysed. Since the envisioned nanonetworks are distributed with a large number of nanosensors, multi-relay schemes along with the MIMO techniques should be applied in the future work. A dynamic routing algorithm

should also be investigated for optimizing the transmission routes among nanosensors. In addition, given the energy and transceiver limitations for nanoscale operation, channel coding has not been considered in this first investigation and needs to be considered in the future. Moreover, the study was based on some assumptions for the purpose of simplicity, avoiding the impractical assumptions is necessary to ameliorate the system.

Moreover, for the proposed energy harvesting system in the thesis, MIM based nano-rectennas are developed as two separate parts, the rectifier, and the antenna. For the time being, the characteristics of some nanoscale rectifiers and antennas have been determined experimentally. However, an integrated graphene-based nano-rectenna has not been built. As the conversion efficiency depends on the coupling condition of the two parts, it is essential to develop experimental prototypes of a nano-rectenna as an integrated device.

Furthermore, in Chapter 5, the SWIPT system was designed as a fixed single relay system, in future work, the impact of relay positions should be analyzed. It is assumed that the destination knows the CSI perfectly, which motivates the future work on the impact of imperfect CSI systems. In addition, relays equipped with two antennas are also the subjects of ongoing research, where one of the nanoantennas receives the signal and the other one transmits it. Moreover, multi-relay schemes and full-duplex are also substantial and promising topics for further study.

In Chapter 6, the SWIPT system is a P2P system, in the future work, the system will be applied in a more complex environment. The unavoidable delay caused by CSI feedback requirement for water-filling, channel adaptive and MQAM were neglected,

but will be studied in the future work. Moreover, the system is developed as a single user system which has motivated a further study on a multiuser system.

Bibliography

[1] I. F. Akyildiz, F. Brunetti, and C. Blázquez, "Nanonetworks: A new communication paradigm," *Computer Networks*, vol. 52, no. 12, pp. 2260–2279, 2008.

[2] S. L. Garrett and M. E. Poese, "There's (still) plenty of room at the bottom," *Applied Thermal Engineering*, vol. 61, no. 2, pp. 884–888, 2013.

[3] R. M. Bakker *et al.*, "Enhanced localized fluorescence in plasmonic nanoantennae," in *Applied Physics Letters*, 2008, vol. 92, no. 4, pp. 18–23.

[4] E. Drexler, "Molecular engineering: Assemblers and Future Space Hardware," *American Astronautical Society*. 1986.

[5] C. Hierold, A. Jungen, C. Stampfer, and T. Helbling, "Nano electromechanical sensors based on carbon nanotubes," *Sensors and Actuators, A: Physical*, vol. 136, no. 1, pp. 51–61, 2007.

[6] C. Li, E. T. Thostenson, and T. W. Chou, "Sensors and actuators based on carbon nanotubes and their composites: A review," *Composites Science and Technology*, vol. 68, no. 6, pp. 1227–1249, 2008.

[7] P. Tallury, A. Malhotra, L. M. Byrne, and S. Santra, "Nanobioimaging and sensing of infectious diseases," *Advanced Drug Delivery Reviews*, vol. 62, no. 4–5, pp. 424–437, 2010.

[8] G. Alfano and D. Miorandi, "On information transmission among nanomachines," in *2006 1st International Conference on Nano-Networks and Workshops, Nano-Net*, 2006, pp. 1–5.

[9] I. F. Akyildiz and J. M. Jornet, “Electromagnetic wireless nanosensor networks,” *Nano Communication Networks*, vol. 1, no. 1, pp. 3–19, 2010.

[10] A. A. Tseng, K. Chen, C. D. Chen, and K. J. Ma, “Electron beam lithography in nanoscale fabrication: Recent development,” *IEEE Transactions on Electronics Packaging Manufacturing*, vol. 26, no. 2, pp. 141–149, Apr. 2003.

[11] H. H. Lee, E. Menard, N. G. Tassi, J. A. Rogers, and G. B. Blanchet, “Large area microcontact printing presses for plastic electronics,” *Materials Research Society Symposium Proceedings*, vol. 846, pp. 159–164, 2005.

[12] J. Han, J. Fu, and R. B. Schoch, “Molecular sieving using nanofilters: Past, present and future,” *Lab Chip*, vol. 8, no. 1, pp. 23–33, Dec. 2008.

[13] K. E. Drexler, *Nanosystems: molecular machinery, manufacturing, and computation*. Wiley, 1992.

[14] A. Credi, “Artificial nanomachines based on interlocked molecules,” *Journal of Physics Condensed Matter*, vol. 18, no. 33, p. 1135, Oct. 2006.

[15] E. Drexler, C. Peterson, and G. Pergamit, “„Unbounding the Future: The nanotechnology revolution “, William Morrow and Company,” *Inc., New York*, 1991.

[16] R. K. Soong, “Powering an Inorganic Nanodevice with a Biomolecular Motor,” *Science*, vol. 290, no. 5496, pp. 1555–1558, 2000.

[17] S. Balasubramaniam and J. Kangasharju, “Realizing the internet of nano things: Challenges, solutions, and applications,” *Computer*, vol. 46, no. 2, pp. 62–68, Feb. 2013.

[18] B. Atakan and O. Akan, “Carbon nanotube-based nanoscale ad hoc networks,” *IEEE Communications Magazine*, vol. 48, no. 6, pp. 129–135, 2010.

[19] J. J. Lehtomäki, A. O. Bicen, and I. F. Akyildiz, “On the nanoscale electromechanical wireless communication in the VHF band,” *IEEE Transactions on Communications*, vol. 63, no. 1, pp. 311–323, 2015.

[20] B. Atakan and O. B. Akan, “Carbon Nanotube Sensor Networks,” *IEEE NanoCom2009*, 2009.

[21] I. F. Akyildiz, J. M. Jornet, and M. Pierobon, “Nanonetworks,” *Communications of the ACM*, vol. 54, no. 11, p. 84, 2011.

[22] T. Nakano, T. Suda, M. Moore, R. Egashira, A. Enomoto, and K. Arima, “Molecular communication for nanomachines using intercellular calcium signaling,” in *2005 5th IEEE Conference on Nanotechnology*, 2005, vol. 2, pp. 665–668.

[23] I. F. Akyildiz, M. Pierobon, S. Balasubramaniam, and Y. Koucheryavy, “The internet of Bio-Nano things,” *IEEE Communications Magazine*, vol. 53, no. 3, pp. 32–40, Mar. 2015.

[24] I. F. Akyildiz, J. M. Jornet, and M. Pierobon, “Propagation models for nanocommunication networks,” in *IEEE EuCAP*, 2010, pp. 1–5.

[25] M. Moore *et al.*, “A design of a molecular communication system for nanomachines using molecular motors,” in *Pervasive Computing and Communications Workshops, 2006. PerCom Workshops 2006. Fourth Annual IEEE International Conference on*, 2006, p. 6 pp.-559.

[26] M. Ş. Kuran, H. B. Yilmaz, T. Tugcu, and B. Özerman, “Energy model for communication via diffusion in nanonetworks,” *Nano Communication Networks*, vol. 1, no. 2, pp. 86–95, 2010.

[27] J. M. Jornet and I. F. Akyildiz, “Graphene-Based Nano-Antennas for

Electromagnetic Nanocommunications in the Terahertz Band," in *Photonics and Nanostructures - Fundamentals and Applications*, 2012, vol. 10, no. 4, pp. 353–358.

[28] J. Weldon, K. Jensen, and A. Zettl, "Nanomechanical radio transmitter," *Physica Status Solidi (B) Basic Research*, vol. 245, no. 10, pp. 2323–2325, Oct. 2008.

[29] J. M. Jornet and I. F. Akyildiz, "Graphene-based plasmonic nano-transceiver for terahertz band communication," in *8th European Conference on Antennas and Propagation, EuCAP 2014*, 2014, vol. 31, no. 12, pp. 492–496.

[30] L. Ren *et al.*, "Carbon nanotube terahertz polarizer," *Nano Letters*, vol. 9, no. 7, pp. 2610–2613, 2009.

[31] S. Abadal, E. Alarcón, A. Cabellos-Aparicio, M. Lemme, and M. Nemirovsky, "Graphene-enabled wireless communication for massive multicore architectures," *IEEE Communications Magazine*, vol. 51, no. 11, pp. 137–143, 2013.

[32] I. F. Akyildiz, W. Su, Y. Sankarasubramaniam, and E. Cayirci, "Wireless sensor networks: A survey," *Computer Networks*, vol. 38, no. 4. pp. 393–422, 2002.

[33] A. K. Geim and K. S. Novoselov, "The rise of graphene," *Nature Materials*, vol. 6, no. 3, pp. 183–191, Mar. 2007.

[34] K. S. Novoselov *et al.*, "Electric field in atomically thin carbon films," *Science*, vol. 306, no. 5696, pp. 666–669, 2004.

[35] I. Akyildiz and J. Jornet, "The Internet of nano-things," *IEEE Wireless Communications*, vol. 17, no. 6, pp. 58–63, 2010.

[36] L. A. Ponomarenko *et al.*, “Chaotic dirac billiard in graphene quantum dots,” *Science*, vol. 320, no. 5874, pp. 356–358, 2008.

[37] R. Bennewitz *et al.*, “Atomic scale memory at a silicon surface,” *Nanotechnology*, vol. 13, no. 4, pp. 499–502, Aug. 2002.

[38] S. S. P. Parkin, M. Hayashi, and L. Thomas, “Magnetic domain-wall racetrack memory,” *Science*, vol. 320, no. 5873, pp. 190–194, 2008.

[39] M. Ternes, C. P. Lutz, C. F. Hirjibehedin, F. J. Giessibl, and A. J. Heinrich, “The force needed to move an atom on a surface,” *Science*, vol. 319, no. 5866, pp. 1066–1069, 2008.

[40] M. D. Stoller, S. Park, Z. Yanwu, J. An, and R. S. Ruoff, “Graphene-Based ultracapacitors,” *Nano Letters*, vol. 8, no. 10, pp. 3498–3502, 2008.

[41] L. Ji *et al.*, “Multilayer nanoassembly of Sn-nanopillar arrays sandwiched between graphene layers for high-capacity lithium storage,” *Energy & Environmental Science*, vol. 4, no. 9, p. 3611, 2011.

[42] Z. L. Wang, “Towards self-powered nanosystems: From nanogenerators to nanopiezotronics,” *Advanced Functional Materials*, vol. 18, no. 22, pp. 3553–3567, 2008.

[43] S. Xu, B. J. Hansen, and Z. L. Wang, “Piezoelectric-nanowire-enabled power source for driving wireless microelectronics.,” *Nature communications*, vol. 1, no. 7, p. 93, 2010.

[44] Z. L. Wang and W. Wu, “Nanotechnology-enabled energy harvesting for self-powered micro-/nanosystems,” *Angewandte Chemie - International Edition*, vol. 51, no. 47, pp. 11700–11721, 2012.

[45] I. Dakua and N. Afzulpurkar, “Piezoelectric Energy Generation and Harvesting

at the Nano-Scale: Materials and Devices," *Nanomaterials and Nanotechnology*, vol. 3, p. 21, 2013.

[46] J. M. Jornet and I. F. Akyildiz, "Joint energy harvesting and communication analysis for perpetual wireless nanosensor networks in the terahertz band," *IEEE Transactions on Nanotechnology*, vol. 11, no. 3, pp. 570–580, 2012.

[47] M. Donohoe, S. Balasubramaniam, B. Jennings, and J. M. Jornet, "Powering In-Body Nanosensors With Ultrasounds," *IEEE Transactions on Nanotechnology*, vol. 15, no. 2, pp. 151–154, 2016.

[48] M. Dragoman and M. Aldrigo, "Graphene rectenna for efficient energy harvesting at terahertz frequencies," *Applied Physics Letters*, vol. 109, no. 11, pp. 113105–104313, Sep. 2016.

[49] C. R. Yonzon, D. A. Stuart, X. Zhang, A. D. McFarland, C. L. Haynes, and R. P. Van Duyne, "Towards advanced chemical and biological nanosensors - An overview," *Talanta*, vol. 67, no. 3. pp. 438–448, 2005.

[50] R. C. Stampfer *et al.*, "Fabrication of single-walled carbon-nanotube-based pressure sensors," *Nano Letters*, vol. 6, no. 2, pp. 233–237, 2006.

[51] P. Bondavalli, P. Legagneux, and D. Pribat, "Carbon nanotubes based transistors as gas sensors: State of the art and critical review," *Sensors and Actuators, B: Chemical*, vol. 140, no. 1. pp. 304–318, 2009.

[52] Y. Ohno, K. Maehashi, and K. Matsumoto, "Chemical and biological sensing applications based on graphene field-effect transistors," *Biosensors and Bioelectronics*, vol. 26, no. 4, pp. 1727–1730, 2010.

[53] I. Llatser, C. Kremers, A. Cabellos-Aparicio, E. Alarcón, and D. N. Chigrin, "Comparison of the resonant frequency in graphene and metallic nano-

antennas," in *AIP Conference Proceedings*, 2012, vol. 1475, pp. 143–145.

[54] I. Llatser, C. Kremers, A. Cabellos-Aparicio, J. M. Jornet, E. Alarcón, and D. N. Chigrin, "Scattering of terahertz radiation on a graphene based nanoantenna," in *AIP Conference*, 2011, no. 1398, pp. 144–146.

[55] J. C. Reed, H. Zhu, A. Y. Zhu, C. Li, and E. Cubukcu, "Graphene-enabled silver nanoantenna sensors," *Nano Letters*, vol. 12, no. 8, pp. 4090–4094, Aug. 2012.

[56] C. Feuillet-Palma, Y. Todorov, A. Vasanelli, and C. Sirtori, "Strong near field enhancement in THz nano-antenna arrays," *Scientific Reports*, vol. 3, no. 1, p. 1361, 2013.

[57] I. Llatser *et al.*, "Radiation characteristics of tunable graphennas in the terahertz band," in *Radioengineering*, 2012, vol. 21, no. 4, pp. 946–953.

[58] S. Li, L. Da Xu, and S. Zhao, "The internet of things: a survey," *Information Systems Frontiers*, vol. 17, no. 2, pp. 243–259, 2015.

[59] K. Yang, A. Pellegrini, M. O. Munoz, A. Brizzi, A. Alomainy, and Y. Hao, "Numerical analysis and characterization of THz propagation channel for body-centric nano-communications," *IEEE Transactions on Terahertz Science and Technology*, vol. 5, no. 3, pp. 419–426, May 2015.

[60] J. M. Jornet and I. F. Akyildiz, "The internet of multimedia Nano-Things," *Nano Communication Networks*, vol. 3, no. 4, pp. 242–251, 2012.

[61] J. M. Dubach, D. I. Harjes, and H. A. Clark, "Fluorescent ion-selective nanosensors for intracellular analysis with improved lifetime and size," *Nano Letters*, vol. 7, no. 6, pp. 1827–1831, 2007.

[62] A. Afsharinejad, A. Davy, B. Jennings, and C. Brennan, "Performance analysis of plant monitoring nanosensor networks at THz frequencies," *IEEE Internet of*

Things Journal, vol. 3, no. 1, pp. 59–69, 2016.

[63] A. Afsharinejad, A. Davy, and B. Jennings, "Dynamic channel allocation in electromagnetic nanonetworks for high resolution monitoring of plants," *Nano Communication Networks*, vol. 7, pp. 2–16, Mar. 2016.

[64] J. M. Jornet and I. F. Akyildiz, "Channel modeling and capacity analysis for electromagnetic wireless nanonetworks in the terahertz band," *IEEE Transactions on Wireless Communications*, vol. 10, no. 10, pp. 3211–3221, 2011.

[65] S. Luryi, J. M. Xu, and A. Zaslavsky, "Future Trends in Microelectronics: Up the Nano Creek," *Future Trends in Microelectronics: Up the Nano Creek*, vol. 27, no. 4, pp. 1–459, 2007.

[66] P. Avouris, Z. Chen, and V. Perebeinos, "Carbon-based electronics," *Nature Nanotechnology*, vol. 2, no. 10, pp. 605–615, Oct. 2007.

[67] RajJain, "'Channel Models: A Tutorial', WiMAX Forum AATG," *WiMAX Forum*, pp. 1–21, 2007.

[68] N. Moraitis and P. Constantinou, "Indoor channel measurements and characterization at 60 GHz for wireless local area network applications," *IEEE Transactions on Antennas and Propagation*, vol. 52, no. 12, pp. 3180–3189, Dec. 2004.

[69] A. F. Molisch, "Ultrawideband propagation channels-theory, measurement, and modeling," *IEEE Transactions on Vehicular Technology*, vol. 54, no. 5, pp. 1528–1545, Sep. 2005.

[70] M. Tamagnone, J. S. Gómez-Díaz, J. R. Mosig, and J. Perruisseau-Carrier, "Analysis and design of terahertz antennas based on plasmonic resonant

graphene sheets," *Journal of Applied Physics*, vol. 112, no. 11, pp. 114915–214102, 2012.

[71] P. Alonso-González *et al.*, "Controlling graphene plasmons with resonant metal antennas and spatial conductivity patterns," *Science*, vol. 344, no. 6190, pp. 1369–1373, 2014.

[72] G. W. Hanson, "Dyadic Green's functions and guided surface waves for a surface conductivity model of graphene," *Journal of Applied Physics*, vol. 103, no. 6, pp. 29902–114915, Mar. 2008.

[73] J. M. Jornet and I. F. Akyildiz, "Graphene-based Plasmonic Nano-Antenna for Terahertz Band Communication in Nanonetworks," *IEEE Journal on Selected Areas in Communications*, vol. 31, no. 12, pp. 685–694, Dec. 2013.

[74] I. F. Akyildiz and J. M. Jornet, "Realizing Ultra-Massive MIMO (1024×1024) communication in the (0.06-10) Terahertz band," *Nano Communication Networks*, vol. 8, pp. 46–54, 2016.

[75] M. Rosenau da Costa, O. V. Kibis, and M. E. Portnoi, "Carbon nanotubes as a basis for terahertz emitters and detectors," *Microelectronics Journal*, vol. 40, no. 4–5, pp. 776–778, 2009.

[76] C. Rutherglen and P. Burke, "Nanoelectromagnetics: Circuit and electromagnetic properties of carbon nanotubes," *Small*, vol. 5, no. 8, pp. 884–906, Apr. 2009.

[77] R. S. Liu, K. W. Fan, Z. Zheng, and P. Sinha, "Perpetual and fair data collection for environmental energy harvesting sensor networks," *IEEE/ACM Transactions on Networking*, vol. 19, no. 4, pp. 947–960, Aug. 2011.

[78] R. Piesiewicz *et al.*, "Short-range ultra-broadband terahertz communications:

Concepts and perspectives," *IEEE Antennas and Propagation Magazine*, vol. 49, no. 6, pp. 24–39, Dec. 2007.

[79] J. Y. Lee and S. N. Hwang, "A high-gain boost converter using voltage-stacking cell," *Transactions of the Korean Institute of Electrical Engineers*, vol. 57, no. 6, pp. 982–984, 2008.

[80] T. Kürner and S. Priebe, "Towards THz communications - Status in research, standardization and regulation," *Journal of Infrared, Millimeter, and Terahertz Waves*, vol. 35, no. 1, pp. 53–62, Jan. 2014.

[81] R. Wang, J. Q. Yao, D. G. Xu, J. L. Wang, and P. Wang, "The physical theory and propagation model of THz atmospheric propagation," *Journal of Physics: Conference Series*, vol. 276, no. 1, p. 12223, Feb. 2011.

[82] "IEEE 802.15.thz WPAN Interest Group." [Online]. Available: http://www.ieee802.org/15/pub/IGthzOLD.html.

[83] J. Y. Lee and S. N. Hwang, "A high-gain boost converter using voltage-stacking cell," *Transactions of the Korean Institute of Electrical Engineers*, vol. 57, no. 6, pp. 982–984, 2008.

[84] C. Jastrow *et al.*, "Wireless digital data transmission at 300 GHz," *Electronics Letters*, vol. 46, no. 9, p. 661, 2010.

[85] H. J. Song *et al.*, "Terahertz wireless communication link at 300 GHz," in *Proceedings - 2010 IEEE International Topical Meeting on Microwave Photonics, MWP 2010*, 2010, pp. 42–45.

[86] S. Priebe, C. Jastrow, M. Jacob, T. Kleine-Ostmann, T. Schrader, and T. Kürner, "Channel and propagation measurements at 300 GHz," *IEEE Transactions on Antennas and Propagation*, vol. 59, no. 5, pp. 1688–1698, May 2011.

[87] S. Kim and A. G. Zajic, “A path loss model for 300-GHz wireless channels,” in *2014 IEEE Antennas and Propagation Society International Symposium (APSURSI)*, 2014, pp. 1175–1176.

[88] A. Afsharinejad, A. Davy, B. Jennings, S. Rasmann, and C. Brennan, “A path-loss model incorporating shadowing for THz band propagation in vegetation,” in *2015 IEEE Global Communications Conference, GLOBECOM 2015*, 2015, pp. 1–6.

[89] A. Afsharinejad, A. Davy, B. Jennings, and C. Brennan, “An initial path-loss model within vegetation in the THz band,” *2015 9th European Conference on Antennas and Propagation, EuCAP 2015*. pp. 1–5, 2015.

[90] A. Afsharinejad, A. Davy, and M. Naftaly, “Variability of Terahertz Transmission Measured in Live Plant Leaves,” *IEEE Geoscience and Remote Sensing Letters*, vol. 14, no. 5, pp. 636–638, 2017.

[91] J. F. Federici, J. Ma, and L. Moeller, “Review of weather impact on outdoor terahertz wireless communication links,” *Nano Communication Networks*, vol. 10, pp. 13–26, Dec. 2016.

[92] J. Kokkoniemi, J. Lehtomauki, and M. Juntti, “Frequency domain scattering loss in THz band,” in *2015 Global Symposium on Millimeter-Waves, GSMM 2015*, 2015, pp. 1–3.

[93] J. Kokkoniemi, J. Lehtomaki, K. Umebayashi, and M. Juntti, “Frequency and time domain channel models for nanonetworks in terahertz band,” *IEEE Transactions on Antennas and Propagation*, vol. 63, no. 2, pp. 678–691, Feb. 2015.

[94] J. Kokkoniemi, J. Lehtomauki, M. Juntti, J. Lehtomäki, and M. Juntti, *Energy*

Detection in THz Nanonetworks in Scattering Environment. New York, New York, USA: ACM Press, 2015, pp. 1–6.

[95] A. Moldovan, M. A. Ruder, I. F. Akyildiz, and W. H. Gerstacker, "LOS and NLOS channel modeling for terahertz wireless communication with scattered rays," in *2014 IEEE Globecom Workshops, GC Wkshps 2014*, 2014, pp. 388–392.

[96] I. Llatser, A. Mestres, S. Abadal, E. Alarcon, H. Lee, and A. Cabellos-Aparicio, "Time-and frequency-domain analysis of molecular absorption in short-range terahertz communications," *IEEE Antennas and Wireless Propagation Letters*, vol. 14, pp. 350–353, 2015.

[97] K. Yasuko and S. Takamasa, "Terahertz-wave propagation model," *Journal of the National Institute of Information and Communications Technology*, vol. 55, no. 1, pp. 73--77, 2008.

[98] S. Priebe, M. Kannicht, M. Jacob, and T. Kurner, "Ultra broadband indoor channel measurements and calibrated ray tracing propagation modeling at THz frequencies," *Journal of Communications and Networks*, vol. 15, no. 6, pp. 547–558, Dec. 2013.

[99] F. Sheikh, M. El-Hadidy, and T. Kaiser, "Terahertz band: Indoor ray-tracing channel model considering atmospheric attenuation," in *IEEE Antennas and Propagation Society, AP-S International Symposium (Digest)*, 2015, vol. 2015–Octob, pp. 1782–1783.

[100] Y. Choi, J. W. Choi, and J. M. Cioffi, "A geometric-statistic channel model for THz indoor communications," *Journal of Infrared, Millimeter, and Terahertz Waves*, vol. 34, no. 7–8, pp. 456–467, Aug. 2013.

[101] C. Han, A. O. Bicen, and I. F. Akyildiz, “Multi-ray channel modeling and wideband characterization for wireless communications in the terahertz band,” *IEEE Transactions on Wireless Communications*, vol. 14, no. 5, pp. 2402–2412, 2015.

[102] K. Yang *et al.*, “Characterising skin-based nano-networks for healthcare monitoring applications at THz,” in *IEEE Antennas and Propagation Society, AP-S International Symposium (Digest)*, 2015, vol. 2015–Octob, pp. 199–200.

[103] Q. H. Abbasi, A. Sani, A. Alomainy, and Y. Hao, “On-body radio channel characterization and system-level modeling for multiband OFDM ultra-wideband body-centric wireless network,” *IEEE Transactions on Microwave Theory and Techniques*, vol. 58, no. 12 PART 1, pp. 3485–3492, Dec. 2010.

[104] Q. H. Abbasi, A. Sani, A. Alomainy, and Y. Hao, “Numerical characterization and modeling of subject-specific ultrawideband body-centric radio channels and systems for healthcare applications,” *IEEE Transactions on Information Technology in Biomedicine*, vol. 16, no. 2, pp. 221–227, Mar. 2012.

[105] X. Yang *et al.*, “On the sparse non-parametric model for body-centric ultra-wideband channel,” in *2014 31th URSI General Assembly and Scientific Symposium, URSI GASS 2014*, 2014, pp. 1–4.

[106] A. Brizzi, A. Pellegrini, L. Zhang, and Y. Hao, “Statistical path-loss model for on-body communications at 94 GHz,” *IEEE Transactions on Antennas and Propagation*, vol. 61, no. 11, pp. 5744–5753, Nov. 2013.

[107] K. Sayrafian-Pour, W.-B. Yang, J. Hagedorn, J. Terrill, and K. Y. Yazdandoost, “A statistical path loss model for medical implant communication channels,” in *2009 IEEE 20th International Symposium on Personal, Indoor and Mobile*

Radio Communications, 2009, pp. 2995–2999.

[108] Y. Hao, A. Brizzi, R. Foster, M. Munoz, A. Pellegrini, and T. Yilmaz, "Antennas and propagation for body-centric wireless communications: Current status, applications and future trend," in *2012 IEEE International Workshop on Electromagnetics: Applications and Student Innovation Competition, iWEM 2012*, 2012, pp. 1–2.

[109] P. Hall, Y. Hao, and S. L. Cotton, "IEEE Transactions on Antennas and Propagation Announces Special Issue on Antennas and Propagation for Body-Centric Wireless Communications," *IEEE Antennas and Propagation Magazine*, vol. 50, no. 2. p. 148, 2008.

[110] S. L. Cotton, R. D'Errico, and C. Oestges, "A review of radio channel models for body centric communications," *Radio Science*, vol. 49, no. 6, pp. 371–388, Jun. 2014.

[111] K. Yang, A. Alomainy, and Y. Hao, "In-vivo characterisation and numerical analysis of the THz radio channel for nanoscale body-centric wireless networks," in *2013 USNC-URSI Radio Science Meeting (Joint with AP-S Symposium), USNC-URSI 2013 - Proceedings*, 2013, pp. 218–219.

[112] K. Yang, A. Pellegrini, A. Brizzi, A. Alomainy, and Y. Hao, "Numerical analysis of the communication channel path loss at the THz band inside the fat tissue," in *2013 IEEE MTT-S International Microwave Workshop Series on RF and Wireless Technologies for Biomedical and Healthcare Applications, IMWS-BIO 2013 - Proceedings*, 2013, pp. 1–3.

[113] K. Yang, Q. H. Abbasi, K. Qaraqe, A. Alomainy, and Y. Hao, "Body-centric nano-networks: EM channel characterisation in water at the terahertz band,"

2014 Asia-Pacific Microwave Conference, no. March. pp. 531–533, 2014.

[114] E. Zarepour, M. Hassan, C. T. Chou, and M. Ebrahimi Warkiani, "Characterizing terahertz channels for monitoring human lungs with wireless nanosensor networks," *Nano Communication Networks*, vol. 9, pp. 43–57, 2016.

[115] P. Wang, J. M. Jornet, M. G. Abbas Malik, N. Akkari, and I. F. Akyildiz, "Energy and spectrum-aware MAC protocol for perpetual wireless nanosensor networks in the Terahertz Band," *Ad Hoc Networks*, vol. 11, no. 8, pp. 2541–2555, 2013.

[116] E. Zarepour, M. Hassan, C. Chou, and A. Adesina, "Electromagnetic Wireless Nanoscale Sensor Networks," in *Emerging Communication Technologies Based on Wireless Sensor Networks*, CRC Press, 2016, pp. 143–178.

[117] I. T. Javed and I. H. Naqvi, "Frequency band selection and channel modeling for WNSN applications using simplenano," in *IEEE International Conference on Communications*, 2013, pp. 5732–5736.

[118] H. Guo, P. Johari, J. M. Jornet, and Z. Sun, "Intra-Body Optical Channel Modeling for in Vivo Wireless Nanosensor Networks," *IEEE Transactions on Nanobioscience*, vol. 15, no. 1, pp. 41–52, 2016.

[119] J. M. Jornet and I. F. Akyildiz, "Channel Capacity of Electromagnetic Nanonetworks in the Terahertz Band," *2010 IEEE International Conference on Communications*, pp. 1–6, 2010.

[120] L. S. Rothman *et al.*, "The HITRAN2012 molecular spectroscopic database," *Journal of Quantitative Spectroscopy and Radiative Transfer*, vol. 130, pp. 4–50, 2013.

[121] J. M. Jornet and I. F. Akyildiz, "Femtosecond-long pulse-based modulation for

terahertz band communication in nanonetworks," *IEEE Transactions on Communications*, vol. 62, no. 5, pp. 1742–1754, 2014.

[122] A. Grami, *Wireless Communications*. Cambridge University Press, 2016.

[123] V. EC, *Transmission of information in a T-terminal discrete memoryless channel*, vol. 40, no. 3. University of California, 1969.

[124] E. C. Van Der Meulen, "Three-Terminal Communication Channels," *Advances in Applied Probability*, vol. 3, no. 1, pp. 120–154, 1971.

[125] T. M. Cover and A. A. El Gamal, "Capacity Theorems for the Relay Channel," *IEEE Transactions on Information Theory*, vol. 25, no. 5, pp. 572–584, Sep. 1979.

[126] J. N. Laneman, D. N. C. Tse, and G. W. Wornell, "Cooperative diversity in wireless networks: Efficient protocols and outage behavior," *IEEE Transactions on Information Theory*, vol. 50, no. 12, pp. 3062–3080, 2004.

[127] L. Ghabeli and M. R. Aref, "The asymmetric Gaussian parallel relay network," in *2010 Australian Communications Theory Workshop, AusCTW 2010*, 2010, pp. 77–80.

[128] G. Kramer and A. J. van Wijngaarden, "On the white Gaussian multiple-access relay channel," in *Information Theory, 2000. Proceedings. IEEE International Symposium on*, 2000, p. 40 EP.

[129] M. Gastpar and M. Vetterli, "On the capacity of wireless networks: the relay case," in *Proceedings.Twenty-First Annual Joint Conference of the IEEE Computer and Communications Societies*, 2002, vol. 3, no. c, pp. 1577–1586.

[130] P. Gupta and P. R. Kumar, "Towards an information theory of large networks: An achievable rate region," *IEEE Transactions on Information Theory*, vol. 49,

no. 8, pp. 1877–1894, Aug. 2003.

[131] S. Balasubramaniam and P. Lio', "Multi-hop conjugation based bacteria nanonetworks," *IEEE Transactions on Nanobioscience*, vol. 12, no. 1, pp. 47–59, Mar. 2013.

[132] A. Einolghozati, M. Sardari, and F. Fekri, "Relaying in diffusion-based molecular communication," in *IEEE International Symposium on Information Theory - Proceedings*, 2013, pp. 1844–1848.

[133] X. Wang, M. D. Higgins, and M. S. Leeson, "Relay analysis in molecular communications with time-dependent concentration," *IEEE Communications Letters*, vol. 19, no. 11, pp. 1977–1980, Nov. 2015.

[134] M. Pierobon, J. M. Jornet, N. Akkari, S. Almasri, and I. F. Akyildiz, "A routing framework for energy harvesting wireless nanosensor networks in the Terahertz Band," *Wireless Networks*, vol. 20, no. 5, pp. 1169–1183, Jul. 2014.

[135] H. Yu, B. Ng, and W. K. G. Seah, "Forwarding Schemes for EM-based Wireless Nanosensor Networks in the Terahertz Band," in *Proceedings of the Second Annual International Conference on Nanoscale Computing and Communication - NANOCOM' 15*, 2015, pp. 1–6.

[136] F. Moshir and S. Singh, "Ultrafast pulsed THz communication," in *IEEE International Symposium on Personal, Indoor and Mobile Radio Communications, PIMRC*, 2014, vol. 2014–June, pp. 348–353.

[137] F. Moshir and S. Singh, "Modulation and rate adaptation algorithms for terahertz channels," *Nano Communication Networks*, vol. 10, pp. 38–50, Dec. 2016.

[138] J. Kokkoniemi, J. Lehtomäki, and M. Juntti, "A discussion on molecular

absorption noise in the terahertz band," *Nano Communication Networks*, vol. 8, pp. 35–45, Jun. 2015.

[139] J. M. Jornet, "Low-weight error-prevention codes for electromagnetic nanonetworks in the Terahertz Band," *Nano Communication Networks*, vol. 5, no. 1–2, pp. 35–44, 2014.

[140] T. Himsoon, W. Su, and K. J. R. Liu, "Differential transmission for amplify-and-forward cooperative communications," *IEEE Signal Processing Letters*, vol. 12, no. 9, pp. 597–600, 2005.

[141] Q. Zhao and H. Li, "Differential modulation for cooperative wireless systems," *IEEE Transactions on Signal Processing*, vol. 55, no. 5 II, pp. 2273–2283, 2007.

[142] T. Wang, A. Cano, G. B. Giannakis, and J. N. Laneman, "High-performance cooperative demodulation with decode-and-forward relays," *IEEE Transactions on Communications*, vol. 55, no. 7, pp. 1427–1438, 2007.

[143] A. Sharma, V. Singh, T. L. Bougher, and B. A. Cola, "A carbon nanotube optical rectenna," *Nature Nanotechnology*, vol. 10, no. 12, pp. 1027–1032, 2015.

[144] M. N. Gadalla, M. Abdel-Rahman, and A. Shamim, "Design, Optimization and Fabrication of a 28.3 THz Nano-Rectenna for Infrared Detection and Rectification," *Scientific Reports*, vol. 4, p. 4270, 2014.

[145] Z. Zhu, S. Joshi, S. Grover, and G. Moddel, "Graphene geometric diodes for terahertz rectennas," *Journal of Physics D: Applied Physics*, vol. 46, no. 18, p. 185101, 2013.

[146] L. R. Varshney, "Transporting information and energy simultaneously," in *IEEE International Symposium on Information Theory - Proceedings*, 2008, pp.

1612–1616.

[147] P. Grover and A. Sahai, “Shannon meets tesla: Wireless information and power transfer,” in *IEEE International Symposium on Information Theory - Proceedings*, 2010, pp. 2363–2367.

[148] A. A. Nasir, X. Zhou, S. Durrani, and R. A. Kennedy, “Relaying protocols for wireless energy harvesting and information processing,” *IEEE Transactions on Wireless Communications*, vol. 12, no. 7, pp. 3622–3636, 2013.

[149] X. Zhou, R. Zhang, and C. K. Ho, “Wireless information and power transfer: Architecture design and rate-energy tradeoff,” *IEEE Transactions on Communications*, vol. 61, no. 11, pp. 4754–4767, Nov. 2013.

[150] Q. H. Abbasi, M. Ur-Rehman, K. Qaraqe, A. Alomainy, and M. U. Rehman, *Advances in Body-Centric Wireless Communication: Applications and State-of-the-art*. The Institution of Engineering and Technology, 2016.

[151] F. Dressler and S. Fischer, “Connecting in-body nano communication with body area networks: Challenges and opportunities of the Internet of Nano Things,” *Nano Communication Networks*, vol. 6, no. 2, pp. 29–38, 2015.

[152] G. Piro, K. Yang, G. Boggia, N. Chopra, L. A. Grieco, and A. Alomainy, “Terahertz Communications in Human Tissues at the Nanoscale for Healthcare Applications,” *IEEE Transactions on Nanotechnology*, vol. 14, no. 3, pp. 404–406, 2015.

[153] M. A. Hanson *et al.*, “Body area sensor networks: Challenges and opportunities,” *Computer*, vol. 42, no. 1, pp. 58–65, Jan. 2009.

[154] Q. H. Abbasi, H. El Sallabi, N. Chopra, K. Yang, K. A. Qaraqe, and A. Alomainy, “Terahertz Channel Characterization Inside the Human Skin for

Nano-Scale Body-Centric Networks," *IEEE Transactions on Terahertz Science and Technology*, vol. 6, no. 3, pp. 427–434, 2016.

[155] T. Binzoni, A. Vogel, A. H. Gandjbakhche, and R. Marchesini, "Detection limits of multi-spectral optical imaging under the skin surface," *Physics in Medicine and Biology*, vol. 53, no. 3, pp. 617–636, Feb. 2008.

[156] M. N. Gadalla and A. Shamim, "28.3THz bowtie antenna integrated rectifier for infrared energy harvesting," in *European Microwave Week 2014: Connecting the Future, EuMW 2014 - Conference Proceedings; EuMC 2014: 44th European Microwave Conference*, 2014, pp. 652–655.

[157] Z. Zhu, S. Joshi, and G. Moddel, "High performance room temperature rectenna IR detectors using graphene geometric diodes," *IEEE Journal on Selected Topics in Quantum Electronics*, vol. 20, no. 6, pp. 70–78, 2014.

[158] C. Balocco *et al.*, "Room-temperature operation of a unipolar nanodiode at terahertz frequencies," *Applied Physics Letters*, vol. 98, no. 22, 2011.

[159] M. Dragoman, M. Aldrigo, A. Dinescu, D. Dragoman, and A. Costanzo, "Towards a terahertz direct receiver based on graphene up to 10 THz," *Journal of Applied Physics*, vol. 115, no. 4, pp. 44307–114915, Jan. 2014.

[160] M. Donohoe, B. Jennings, J. M. Jornet, and S. Balasubramaniam, "Nanodevice Arrays for Peripheral Nerve Fascicle Activation Using Ultrasound Energy-Harvesting," *IEEE Transactions on Nanotechnology*, vol. 16, no. 6, pp. 919–930, Nov. 2017.

[161] J. M. Jornet, "A joint energy harvesting and consumption model for self-powered nano-devices in nanonetworks," in *IEEE International Conference on Communications*, 2012, pp. 6151–6156.

[162] G. Piro, G. Boggia, and L. A. Grieco, “On the design of an energy-harvesting protocol stack for Body Area Nano-NETworks,” *Nano Communication Networks*, vol. 6, no. 2, pp. 74–84, 2015.

[163] J. Liu, P. Fei, J. Zhou, R. Tummala, and Z. L. Wang, “Toward high output-power nanogenerator,” *Applied Physics Letters*, vol. 92, no. 17, 2008.

[164] D. Pech *et al.*, “Ultrahigh-power micrometre-sized supercapacitors based on onion-like carbon,” *Nature Nanotechnology*, vol. 5, no. 9, pp. 651–654, 2010.

[165] Y. Chen, R. Shi, W. Feng, and N. Ge, “AF Relaying with Energy Harvesting Source and Relay,” *IEEE Transactions on Vehicular Technology*, vol. 66, no. 1, pp. 874–879, 2017.

[166] Y. H. Suh and K. Chang, “A high-efficiency dual-frequency rectenna for 2.45- and 5.8-GHz wireless power transmission,” *IEEE Transactions on Microwave Theory and Techniques*, vol. 50, no. 7, pp. 1784–1789, Jul. 2002.

[167] J.-P. Fleurial, “Thermoelectric power generation materials: technology and application opportunities,” *Journal of the Minerals, metals and materials society*, vol. 61, no. 4, pp. 79–85, Apr. 2009.

[168] W. C. Brown, “Optimization of the Efficiency and Other Properties of the Rectenna Element,” in *MTT-S International Microwave Symposium Digest*, 1976, vol. 76, pp. 142–144.

[169] J. A. Hagerty, F. B. Helmbrecht, W. H. McCalpin, R. Zane, and Z. B. Popović, “Recycling ambient microwave energy with broad-band rectenna arrays,” *IEEE Transactions on Microwave Theory and Techniques*, vol. 52, no. 3, pp. 1014–1024, Mar. 2004.

[170] J. O. McSpadden, T. Yoo, and K. Chang, “Theoretical and experimental

investigation of a rectenna element\nfor microwave power transmission," *IEEE Transactions on Microwave Theory and Techniques*, vol. 40, no. 12, pp. 2359–2366, 1992.

[171] B. Strassner and K. Chang, "Microwave power transmission: Historical milestones and system components," *Proceedings of the IEEE*, vol. 101, no. 6, pp. 1379–1396, Jun. 2013.

[172] R. L. Bailey, "A Proposed New Concept for a Solar-Energy Converter," *Journal of Engineering for Power*, vol. 94, no. 2, p. 73, Apr. 1972.

[173] J. C. Fletcher and R. L. Bailey, "Electromagnetic wave energy converter." US Patent No.3,760,257, 18-Sep-1972.

[174] A. M. Marks, "Device for conversion of light power to electric power." US Patent No.4,445,050, 24-Apr-1981.

[175] G. H. Lin, R. Abdu, and J. O. M. Bockris, "Investigation of resonance light absorption and rectification by subnanostructures," *Journal of Applied Physics*, vol. 80, no. 1, pp. 565–568, 1996.

[176] C. L. Nehl, H. Liao, and J. H. Hafner, "Optical properties of star-shaped gold nanoparticles," *Nano Letters*, vol. 6, no. 4, pp. 683–688, 2006.

[177] H. Wang, D. W. Brandl, F. Le, P. Nordlander, and N. J. Halas, "Nanorice: A hybrid plasmonic nanostructure," *Nano Letters*, vol. 6, no. 4, pp. 827–832, 2006.

[178] P. Muhlschlegel, "Resonant Optical Antennas," *Science*, vol. 308, no. 5728, pp. 1607–1609, 2005.

[179] Z. Ma and G. A. E. Vandenbosch, "Systematic full-wave characterization of real-metal nano dipole antennas," *IEEE Transactions on Antennas and Propagation*, vol. 61, no. 10, pp. 4990–4999, Oct. 2013.

[180] M. Tamagnone, J. S. Gómez-Díaz, J. R. Mosig, and J. Perruisseau-Carrier, "Reconfigurable terahertz plasmonic antenna concept using a graphene stack," *Applied Physics Letters*, vol. 101, no. 21, p. 214102, Nov. 2012.

[181] D. K. Kotter, S. D. Novack, and W. D. Slafer, "Solar nantenna electromagnetic collectors," in *Proc. Int. Conf. Energy Sust.*, 2008, pp. 1–7.

[182] H. Kazemi *et al.*, "First THz and IR characterization of nanometer-scaled antenna-coupled InGaAs/InP Schottky-diode detectors for room temperature infrared imaging," in *Proc. SPIE 6542, Infrared Technology and Applications XXXIII*, 2007, p. 65421J.

[183] T. W. Crowe, W. L. Bishop, D. W. Porterfield, J. L. Hesler, and R. M. Weikle, "Opening the terahertz window with integrated diode circuits," *IEEE Journal of Solid-State Circuits*, vol. 40, no. 10, pp. 2104–2109, Oct. 2005.

[184] J. Bean, B. Tiwari, G. H. Bernstein, P. Fay, and W. Porod, "Long-wave infrared detection using dipole antenna-coupled metal-oxide-metal diodes," *IEEE 2008 Silicon Nanoelectronics Workshop, SNW 2008*, vol. 27, no. 1, p. 11, 2008.

[185] J. Kraček, "Wireless Power Transmission," in *Design and Optimization of Passive UHF RFID Systems*, no. August, Boston, MA: Springer US, 2007, pp. 3–15.

[186] G. Moddel, "Will rectenna solar cells be practical?," in *Rectenna Solar Cells*, vol. 9781461437, New York, NY: Springer New York, 2014, pp. 3–24.

[187] S. Grover and G. Moddel, "Engineering the current-voltage characteristics of metal-insulator-metal diodes using double-insulator tunnel barriers," *Solid-State Electronics*, vol. 67, no. 1, pp. 94–99, 2012.

[188] A. Sharma, V. Singh, T. L. Bougher, and B. A. Cola, "A carbon nanotube

optical rectenna," *Nature Nanotechnology*, vol. 10, no. 12, pp. 1027–1032, 2015.

[189] Z. Zhu, S. Joshi, B. Pelz, and G. Moddel, "Overview of optical rectennas for solar energy harvesting," in *Proceedings of SPIE - The International Society for Optical Engineering*, 2013, vol. 8824, p. 88240O.

[190] S. Grover and G. Moddel, "Applicability of Metal/Insulator/Metal (MIM) diodes to solar rectennas," *IEEE Journal of Photovoltaics*, vol. 1, no. 1, pp. 78–83, Jul. 2011.

[191] B. M. Kale, "Electron Tunneling Devices In Optics," *Optical Engineering*, vol. 24, no. 2, pp. 242267–242267, 1985.

[192] F. J. González and G. D. Boreman, "Comparison of dipole, bowtie, spiral and log-periodic IR antennas," *Infrared Physics and Technology*, vol. 46, no. 5, pp. 418–428, 2005.

[193] A. Ferris, S. Garbarino, D. Guay, and D. Pech, "3D RuO2 Microsupercapacitors with Remarkable Areal Energy," *Advanced Materials*, vol. 27, no. 42, pp. 6625–6629, 2015.

[194] Z. Rong, M. S. Leeson, and M. D. Higgins, "Relay-assisted nanoscale communication in the THz band," *Micro & Nano Letters*, vol. 12, no. 6, pp. 373–376, Jun. 2017.

[195] E. Zarepour, M. Hassan, C. T. Chou, and A. A. Adesina, "Energy-Harvesting Nanosensor Networks: Efficient event detection.," *IEEE Nanotechnology Magazine*, vol. 10, no. 4, pp. 4–12, 2016.

[196] S. Hall, I. Z. Mitrovic, N. Sedghi, Y. C. Shen, Y. Huang, and J. F. Ralph, "Energy Harvesting Using THz Electronics," in *Functional Nanomaterials and*

Devices for Electronics, Sensors and Energy Harvesting, A. Nazarov, F. Balestra, V. Kilchytska, and D. Flandre, Eds. Cham: Springer International Publishing, 2014, pp. 241–265.

[197] Y. Chen, W. Feng, R. Shi, and N. Ge, "Pilot-Based Channel Estimation for AF Relaying Using Energy Harvesting," *IEEE Transactions on Vehicular Technology*, vol. 66, no. 8, pp. 6877–6886, 2017.

[198] L. Liu, R. Zhang, and K. C. Chua, "Wireless information transfer with opportunistic energy harvesting," *IEEE Transactions on Wireless Communications*, vol. 12, no. 1, pp. 288–300, Jan. 2013.

[199] L. Liu, R. Zhang, and K. C. Chua, "Wireless information and power transfer: A dynamic power splitting approach," *IEEE Transactions on Communications*, vol. 61, no. 9, pp. 3990–4001, Sep. 2013.

[200] C. Shen, W. C. Li, and T. H. Chang, "Wireless information and energy transfer in multi-antenna interference channel," *IEEE Transactions on Signal Processing*, vol. 62, no. 23, pp. 6249–6264, Dec. 2014.

[201] R. Zhang and C. K. Ho, "MIMO broadcasting for simultaneous wireless information and power transfer," *IEEE Transactions on Wireless Communications*, vol. 12, no. 5, pp. 1989–2001, May 2013.

[202] Z. Xiang and M. Tao, "Robust beamforming for wireless information and power transmission," *IEEE Wireless Communications Letters*, vol. 1, no. 4, pp. 372–375, Aug. 2012.

[203] B. K. Chalise, Y. D. Zhang, and M. G. Amin, "Energy harvesting in an OSTBC based amplify-and-forward MIMO relay system," in *ICASSP, IEEE International Conference on Acoustics, Speech and Signal Processing* -

Proceedings, 2012, pp. 3201–3204.

[204] A. M. Fouladgar and O. Simeone, "On the transfer of information and energy in multi-user systems," *IEEE Communications Letters*, vol. 16, no. 11, pp. 1733–1736, Nov. 2012.

[205] D. W. K. Ng, E. S. Lo, and R. Schober, "Energy-efficient resource allocation in multiuser OFDM systems with wireless information and power transfer," in *2013 IEEE Wireless Communications and Networking Conference (WCNC)*, 2013, pp. 3823–3828.

[206] S. Lee, R. Zhang, and K. Huang, "Opportunistic wireless energy harvesting in cognitive radio networks," *IEEE Transactions on Wireless Communications*, vol. 12, no. 9, pp. 4788–4799, Sep. 2013.

[207] K. Ishibashi, H. Ochiai, and V. Tarokh, "Energy harvesting cooperative communications," in *IEEE 23rd International Symposium on Personal, Indoor and Mobile Radio Communications - (PIMRC)*, 2012, pp. 1819–1823.

[208] I. Krikidis, S. Timotheou, and S. Sasaki, "RF energy transfer for cooperative networks: Data relaying or energy harvesting?," *IEEE Communications Letters*, vol. 16, no. 11, pp. 1772–1775, Nov. 2012.

[209] I. Krikidis, "Simultaneous information and energy transfer in large-scale networks with/without relaying," *IEEE Transactions on Communications*, vol. 62, no. 3, pp. 900–912, Mar. 2014.

[210] A. A. Nasir, X. Zhou, S. Durrani, and R. A. Kennedy, "Wireless-powered relays in cooperative communications: Time-switching relaying protocols and throughput analysis," *IEEE Transactions on Communications*, vol. 63, no. 5, pp. 1607–1622, May 2015.

[211] C. K. Ho and R. Zhang, "Optimal energy allocation for wireless communications with energy harvesting constraints," *IEEE Transactions on Signal Processing*, vol. 60, no. 9, pp. 4808–4818, 2012.

[212] G. Huang and W. Tu, "Optimal resource allocation in wireless-powered OFDM relay networks," *Computer Networks*, vol. 104, pp. 94–107, 2016.

[213] C. Zhong, H. A. Suraweera, G. Zheng, I. Krikidis, and Z. Zhang, "Wireless information and power transfer with full duplex relaying," *IEEE Transactions on Communications*, vol. 62, no. 10, pp. 3447–3461, Oct. 2014.

[214] A. N. Pal and A. Ghosh, "Ultralow noise field-effect transistor from multilayer graphene," *Applied Physics Letters*, vol. 95, no. 8, 2009.

[215] Y. Chen, "Energy-Harvesting AF Relaying in the Presence of Interference and Nakagami-m Fading," *IEEE Transactions on Wireless Communications*, vol. 15, no. 2, pp. 1008–1017, 2016.

[216] A. Goldsmith, *Wireless Communications*. Cambridge: Cambridge University Press, 2005.

[217] T. M. Cover and J. A. Thomas, *Elements of information theory*. Wiley-Interscience, 2006.

[218] S. T. Chung and A. J. Goldsmith, "Degrees of freedom in adaptive modulation: A unified view," *IEEE Transactions on Communications*, vol. 49, no. 9, pp. 1561–1571, 2001.

[219] S. Falahati, A. Svensson, T. Ekman, and M. Sternad, "Adaptive Modulation Systems for Predicted Wireless Channels," *IEEE Transactions on Communications*, vol. 52, no. 2, pp. 307–316, Feb. 2004.

[220] C. Y. Wong, R. S. Cheng, K. Ben Letaief, and R. D. Murch, "Multiuser OFDM

with adaptive subcarrier, bit, and power allocation," *IEEE Journal on Selected Areas in Communications*, vol. 17, no. 10, pp. 1747–1758, 1999.